Learning-Dependent Plasticity in the Adult Brain

Dissertation

To fulfil the requirements for the degree of

"Doctor of Philosophy" **(Ph.D.)**

Submitted to the Faculty of Medicine

Friedrich Schiller University, Jena

by Sidra Gull, MS

Born on 22.03.1983 in Gujranwala, Pakistan

"And among His Signs is the creation of the heavens and the earth and the diversity of your languages and colours. Indeed, in that are Signs for those of knowledge."

The Quran 30:22

Table of content

List of Abbreviations

ABC	Avidin-Biotin-Peroxidase-complex
Arc	Activity-regulated cytoskeleton-associated protein
ANOVA	Analysis of variance
Au1	Primary auditory cortex
BrdU	5′-Bromodeoxyuridine
BSA	Bovine serum albumin
°C	Centigrade
Cl	Chloride
Co	Contra
conc.	Concentration
CTR	Control
d	Days
DAB	3, 3'-Diaminobenzidine
DBM	Deformation-based morphometry
dist.	Distilled
FWE	Familywise error test
GFAP	Glial fibrillary acidic protein
g	Gram
GM	Gray matter
H	hydrogen
HCL	Hydrochloric acid
Ip	Ipsi
lr	Large
LEnt	Lateral entorhinal cortex
LTP	Long-term potentiation
MD	Monocular deprivation
me	Medium
msh	Mushroom
MRI	Magnetic resonance imaging
MTL	Medial temporal lobe
min	Minute

ml	Milliliter
µl	Microlitter
µm	Micrometer
N	Normal
OKR	Optokinetic response
ns	Non-significant
#	Number
PBS	Phosphate-buffered saline
PFA	Paraformaldehyde
K$^+$	Potassium
PML	Paramedian lobule
%	Percentage
Pr	Primary
S100ß	S100 calcium-binding protein B
Sec	Secondary
sm	Small
Na	Sodium
sp	Spiny
TBS	Tris-buffered saline
TBS-T	Tris-buffered saline- Triton X-100
uncorr	Uncorrected
USA	United states of America
VA	Visual acuity
V1B	Primary binocular visual cortex
V2L	Secondary visual cortex
H$_2$O	Water

Summary

Magnetic resonance imaging (MRI) -based morphometry is one of the most promising methods for non-invasive detection learning purposes plastic brain areas in the human field. The approach is based on the structure-function relationship: for every functional change there is a structural change, and vice versa. The structural changes in contrast to the functional changes are generally slightly delayed and significantly prolonged. Plastic areas can therefore be detected by MRI also at rest (in the absence of active learning process) and independent of acute brain activity over time. However, the exact nature of cellular processes underlying learning induced GM swelling is unknown. Studies with adult animals have demonstrated learning-related transient swelling of astrocytes and explaining the same pattern as observed in learning associated transient GM changes seen by MRI. On this basis, we hypothesized astrocytic enlargement as a major underlie mechanism to produce these GM volume changes. To test this hypothesis, we combined monocular deprivation (MD) based perceptual learning with longitudinal tracking of GM macro-structure changes *in-vivo* by MRI and deformation-based morphometry (DBM) accompanied by microscopic analyses of astrocytic and neuronal features in albino Wistar rats.

MD resulted in enhanced sensitivity of the optokinetic response (OKR) of the undeprived eye that was monitored using an optometer. To search for the areas of the brain mainly involved in this sensory adaptation, T2-weighted brain magnetic resonance images were acquired longitudinally at baseline and 3, 7 and 10 days following MD (male Wistar rats, 2 months) and processed by DBM. The changes in astrocytic morphology, neuronal activity, synaptic plasticity, spine pool and genesis of neurons, glia as well as blood vessels were analysed by using immunohistochemistry (GFAP, Arc, S100ß, BrdU) and Golgi impregnation approaches.

We observed that over a period of 10d, MD enhanced the functioning of the un-deprived eye that was monitored by measuring the OKR sensitivity (in terms of visual acuity [VA] and contrast sensitivity). The OKR response of the undeprived eye increased rapidly during the first 3 days of MD and stabilized around day 8. Temporal volume changes were observed in the visual cortex, lateral entorhinal cortex (LEnt) and cerebellum. The visual areas showed the initial swelling followed by the late shrinkages. In cerebellum, a delayed late swelling was observed. However, the best

correlation of the learning curve (increase in VA/day) was found with the time course of volume changes in LEnt that transiently swelled. We selected LEnt for elucidating the cellular substrates of GM volumetric changes. Using cross-sectional microscopic analyses, we observed an elevated Arc expression (immunohistochemistry), an enhanced spine pool (both immatured and matured spines) (Golgi impregnation) and significantly enlarged but morphologically simple astrocytes (immunohistochemistry with GFAP) during GM swelling at the 3rd day of MD that was further accompanied by a reduced density of astrocytes and newly born nuclei. The swelling in LEnt was reversed towards the baseline until the 10th day of MD. The Arc expression, density and hypertrophy of astrocytes also reversed to baseline along with GM but the spine pool of matured spines persisted. Besides, we observed that the volume changes in astrocytes occurred parallel to GM and explained 60% contribution, signifying astrocytic hypertrophy as the main underlie factor for the morphometry based GM swelling. Moreover, we did not see any increase in the density of newly born nuclei and astrocytes suggesting, that neuronal, glial as well as angio-genesis did not contribute in the DBM based swelling. Therefore, by showing a significant correlation between Arc expression, astrocytic enlargement, and DBM signal in the entorhinal cortex, these results fill the tremendous gap in our current understanding of the cellular substrates of morphometry based structural changes. Overall our study showed glial hypertrophy as the major cellular mechanism underlying these structural changes. Future studies are needed to analyze the reason of astrocytic enlargement as well as demonstrate the results of this study, is lateral entorhinal cortex crucially involved in the processing of visual signals.

Zusammenfassung

Magnetresonanztomographie (MRT)-basierte Morphometrie ist eine der aussichtsvollsten Methoden zur nicht-invasiven Detektion lernrelevanter plastischer Hirnareale im humanen Bereich. Die Herangehensweise basiert auf dem Struktur-Funktions-Zusammenhang: jede funktionelle Veränderung geht mit einer strukturellen Veränderung einher und umgekehrt. Dabei sind die Strukturveränderungen im Gegensatz zu den funktionellen Veränderungen generell leicht zeitverzögert und deutlich langanhaltender. Plastische Areale können daher mittels MRT auch in Ruhephasen außerhalb des aktiven Lernprozesses und unabhängig von akuter Hirnaktivität im Zeitverlauf detektiert werden. Es ist derzeitig jedoch unklar, auf welchen zellulären Prozessen diese makroskopischen Strukturveränderungen basieren. Ältere tierexperimentelle Studien zeigten lernbedingte Schwellungen der Astrozyten. Die hohe Anzahl der Astrozyten und das Ausmaß deren Schwellung machen einen direkten Zusammenhang mit den MRT-basierten Signalen sehr wahrscheinlich. Die hier vorgelegte Studie fokussiert daher auf die Detektion makroskopisch plastischer Hirnareale während „visual-perception learning" und auf die Analyse der zugrunde liegenden zellulären Prozesse auf mikroskopischer Ebene.

Als Lernmodell fungierte der Verschluss eines Auges („monocular deprivation", MD) bei jungen adulten Wistar-Ratten. Optometrische Messungen zeigten eine sprunghafte Verbesserung der Sehschärfe des offenen Auges in den ersten 3 Tagen nach MD und eine Stabilisierung der erhöhten Sehschärfe nach 8 Tagen („visual perception learning"). Temporäre zerebrale Strukturveränderungen wurden an repetitiv generierten T2-gewichteten MRT-Aufnahmen mittels Deformations-basierter Morphometrie 3, 7 und 10 Tage nach MD detektiert. Visuelle Areale zeigten dabei initiale Schwellungen gefolgt von späten Schrumpfungen. Im Zerebellum zeigte sich eine verzögerte späte Schwellung. Die beste Korrelation mit der Lernkurve fand sich jedoch im lateralen entorhinalen Kortex, welcher initial anschwillt und sein Volumen nach Stabilisierung der erhöhten Sehschärfe re-normalisiert. Cross-sektionale mikroskopische Analysen zeigten hier eine transient erhöhte Expression des Plastizitäts-Markers Arc (Immunhistochemie). Weiterhin zeigte sich ein transient erhöhter Spine-Pool (Golgi-Impregnation) wobei initial vornehmlich die Anzahl unreifer Spines zunimmt. Das Ganze ging mit einer territorialen Vergrößerung und Hypertrophie der Astrozyten einher (Golgi-Impregnation) wobei deren Zytoskelett degradiert (GFAP-

Immunhistochemie). Als Ausdruck einer transienten Gewebeschwellung nahm die Zelldichte transient ab. Wir konnten keine Bildung neuer Zellen detektieren (BrdU-Labeling). Nach Stabilisierung der erhöhten Sehschärfe und Normalisierung des Kortexvolumens re-normalisierte sich auch die Dichte und das Volumen der Astrozyten. Demgegenüber war ein leicht erhöhter Pool stabiler Spines persistierend. Finale Modellrechnungen ergaben, dass die Hypertrophie der Astrozyten rund 60 % der makroskopischen MRT-basierten Gewebeschwellung erklärt.

Die hier vorgelegte Arbeit belegt somit erstmals eine Schlüsselposition der Astrozyten bei der Generierung lernbedingter lokaler Schwellungen des Gehirns und unterstreicht deren Signifikanz bei Lernprozessen. Weitere Studien sind erforderlich, um den Grund der Astrozytenschwellung zu analysieren. Weiterhin belegen die Ergebnisse dieser Studie, dass der laterale entorhinale Kortex entscheidend an der Verarbeitung visueller Signale beteiligt ist.

1. Introduction

According to the Symmorphosis concept, living organisms are thought to be designed economically and their structural design is matched to functional demand (Weibel et al., 1991) even body organs of individual members of the same species get modified according to their usage. For instance, the brain regions which are extensively used grow enlarged over time that can be observed using magnetic resonance imaging (MRI). For example, hippocampus is considered to be involved in the spatial navigation and it was shown that London cab drivers who needed to often navigate unusual routs, had larger posterior hippocampus relative to controls from the general population (Maguire et al., 2000) and to London bus drivers matched for stress levels and driving experience (Maguire et al., 2006). Similarly, the professional musicians who extensively learned and practiced complex motor and auditory skills since childhood and throughout their career showed an increase in the gray matter (GM) volume in the motor, auditory, and visual–spatial brain regions when compared with amateur musicians and non-musicians (Gaser and Schlaug, 2003). Similarly, GM changes were also found in correlation with professional experience in mathematicians (Aydin et al., 2007), with second-language proficiency (Mechelli et al., 2004) and meditators (Luders et al., 2009). But this use dependant enlargement of a particular region involved in the specific function of interest seems to appear over a longer period of practicing in contrast to learning associated enlargements that appear just 7 days after starting learning (Driemeyer et al., 2008). However, cross-sectional studies cannot provide any causal evidence for the learning-associated structural plasticity in the adult human brain.

Learning is a highly dynamic process and there is an overwhelming evidence to indicate that for each new learning event, there is some required and sufficient change in the nervous system that supports learning (Cooper, 2005; Hebb, 1949; Kandel, 2001). However, longitudinal studies with learning have shown that learning associated GM swelling is transient in nature (Boyke et al., 2008; Draganski et al., 2004; Draganski et al., 2006; Driemeyer et al., 2008; Taubert et al., 2010). Draganski et al. (2004) found that learning a complex visuomotor task (juggling) for a period of 3 months during which the participants had learned to sustain a three-ball cascade for at least a minute, induced task-specific transient GM changes in the medial temporal

visual area (also known as V5). No changes were observed in the control group that did not engage in the juggling. The extent of these GM changes in the jugglers reduced during a subsequent 3-month period in which they did not practice juggling. To analyze the time course of these volume changes the same experiment was repeated with another young cohort (Driemeyer et al., 2008), but with shorter scanning intervals. They observed similar changes in V5 just after 7 days of juggling practice. Interestingly, the observed changes were larger in the initial learning phase than during continued training. The former two studies involved students in their early twenties; Boyke et al. (2008) repeated the experiments with an elderly cohort, revealing the same structural neuroplasticity, although attenuated by a lower juggling performance of this group. Moreover, temporal structural GM changes in the sensorimotor related regions and prefrontal cortex have been observed just after 90 minutes of practicing (distributed over 2 weeks) of a complex balancing task (Taubert et al., 2010). Interestingly, the structural changes in sensorimotor related regions were highly transient and started disappearing until the 5th week of training (after 360 minutes of practice) while the structural changes in the prefrontal cortex were continuously increased during 6 weeks (540 minutes) of training. This distinct temporal dynamics of structural GM changes indicated that learning is a complex brain function operating at different time scales in different networks of the brain. Additionally, these results indicate that functionally relevant structural brain alterations can be induced by relatively brief periods of learning. Therefore, there is a need of employing a non-invasive longitudinal approach for the detailed and precise characterization of the GM changes over the entire period of learning. Morphometric investigations using high-resolution MRI is a promising means to investigate the structure–function relations characteristic of the brain for plasticity associated learning processes (May, 2011).

MRI depends on the absorbance specificity of anatomical nuclei for the electromagnetic radiation of a specific frequency dependent upon the magnetic field strength they experience and images are then created on the basis of the three-dimensional distribution of these nuclei (Mietchen and Gaser, 2009). Morphometry based approaches like deformation based morphometry (DBM) can be employed to analyze MRI scans. The principle of DBM is to warp the second scan to the baseline scan by introducing high-dimensional deformations. Next, the differences between

both images are encoded in the deformations applied for the warp. These deformations can then be used to calculate volume changes by using non-linear algorithms (Gaser et al., 2001). In contrast to other morphometry approaches, DBM allows the detection of the structural differences independent of sharp tissue borders (Gaser et al., 2012).
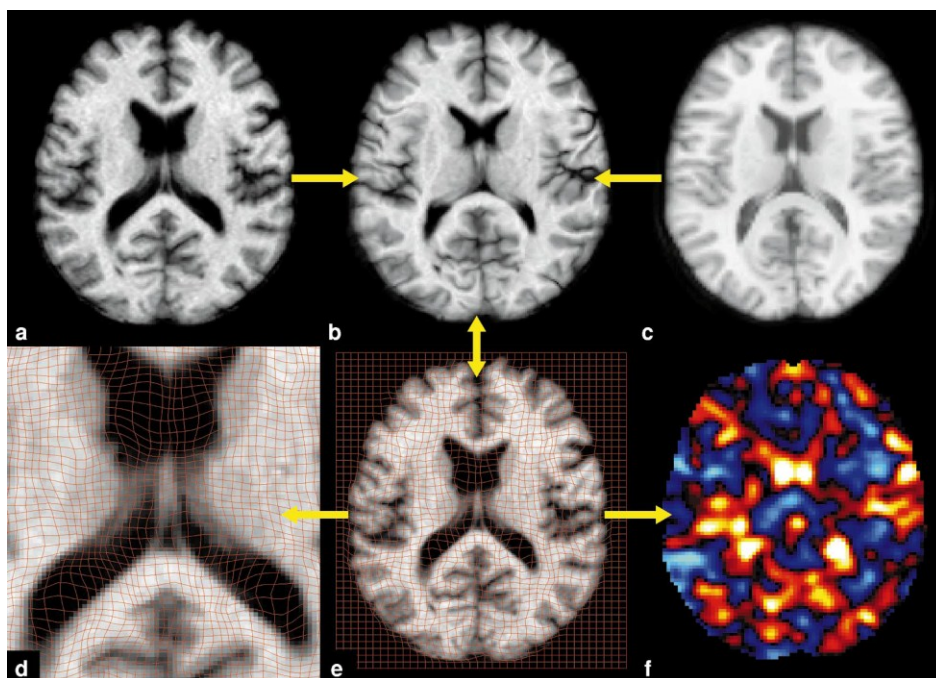

Fig. 1: Steps of analysis in deformation.

An example is shown for a single subject in one axial slice. The single object brain (image a) has been corrected for orientation and overall size to the template brain (c). Nonlinear normalization removes most of the anatomical differences between the two brains by introducing local deformations to the object brain, which then (b) looks as similar as possible to the template. Note that these slices only represent two-dimensional information, whereas the method actually works in three dimensions. Image (e) shows the deformations applied to the object brain by a deformed grid and a magnification of the ventricles is displayed in (d). Analysis for DBM can be either multivariate using these x-y-z displacements of the entire 3-D deformation field or univariate using the local Jacobian determinant as a derivative of the field (f) (Gaser et al., 2001).

Besides in human, MRI based morphometry has been employed to analyze learning associated structural plasticity in animals. Quallo et al. (2009) analyzed the volume changes in the brain of adult macaque monkeys by using structural MR images collected before (2 measurements), during (3 measurements), and after (1 measurement) learning to use a rake to retrieve food. Monkeys received intensive

training each day over a period of 21 days. The learning-related changes were found in the right superior temporal sulcus and secondary somatosensory area. It has been found recently that five days of Morris water maze training (six trials per day) in mice resulted in the expansion of regional GM volume (Lerch et al., 2011).

Currently, the exact nature of cellular processes underlying the learning associated transient structural changes in the GM of the adult brain is not known. Based on the animal studies (Lerch et al., 2011) it is reasonable to assume that structural brain alterations are the consequences of multiple factors such as an increase in cell size, neural and glial genesis as well as spine density (May et al., 2007). Studies involving different learning paradigms have shown the rapid alterations in neurogenesis (Kee et al., 2007), synapse morphology and dendritic spine numbers (Fu and Zuo, 2011), astrocyte morphology (Kleim et al., 2007; Viola et al., 2009) and a change in the neuronal activity pattern(Carpenter-Hyland et al., 2010; Okuno, 2011).

Neurogenesis

The hippocampal formation produces new neurons throughout adulthood in many vertebrates, from birds to primates (Barnea and Nottebohm, 1994; Bayer, 1982; Gould et al., 1997; Kempermann et al., 1997). It is hypothesized that these newly synthesized neurons are involved in the learning and memory (Barnea and Nottebohm, 1994; Gould et al., 1999b). Neurogenesis was found to be enhanced during environmental enrichment (Kempermann et al., 1997; Nilsson et al., 1999), spatial learning (Barnea and Nottebohm, 1994; Kee et al., 2007; Kempermann and Gage, 2002) and exercise (van Praag et al., 1999). However, Gould et al. (1999a) have shown that neurogenesis only contributes in the hippocampal dependent learning task.

Spine density

Spines encompass the postsynaptic portion of glutamatergic synapses and have highly diverse structures (Kasai et al., 2010). The cytoskeleton of dendritic-spines is composed of the actin filaments which are highly motile and serve as a fundamental mechanism for plasticity. Spines are the major sites for structural plasticity of excitatory neuronal circuits. A typical spine consists of the bulby head and thin neck. Spines originate from small protrusions and filopodia on dendrites (Knott et al., 2006; Nagerl et al., 2007; Ziv and Smith, 1996). The generation of these protrusions

and filopodia may be influenced by activity (Matsumoto-Miyai et al., 2009; Richards et al., 2005) however, the process of spine generation tends to be spontaneous and pseudo-random, unlike the process of activity-dependent spine enlargement, which is synapse-specific (Kasai et al., 2010). Newly generated spines are small while older spines tend to be large (Hofer et al., 2009; Yasumatsu et al., 2008; Zito et al., 2009). The spine head volume varies over a wide range (0.005-1μm^3) and reflects the strength of the synapse. The expression level of functional postsynaptic AMPA receptors is proportional to the spine-head volume (Kasai et al., 2010). The spine-head enlargement or shrinkage (or elimination) can be induced by certain patterns of repetitive stimulation. This volume change accompanies a long-term functional plasticity of the glutamatergic synaptic transmission, including long-term potentiation (LTP) and long-term depression (LTD) (Lang et al., 2004; Okamoto et al., 2004; Zhou et al., 2004). Thus, newly generated spines are small and represent "silent synapses" that are the potential sites for LTP and enlargement. This activity dependent enlargement of stimulated spines is rapid and occurs at the level of single spines and represents the formation of a new functional connection with fast AMPA receptors. Hence, a newly generated spine, the physical embodiment of a 'silent synapse,' works as a seed for such a connection (Kasai et al., 2010). Unlike spine enlargement, which occurs over a short time period, activity induced spine generation occurs 0.5–1 hour after stimulation (Engert and Bonhoeffer, 1999; Maletic-Savatic et al., 1999; Nagerl et al., 2004).

Studies with animals have shown that learning is associated with an increase in synapse and spine density. Synaptogenesis and associated changes in the dendritic spines can be formed over the periods of minutes to hours (Fu and Zuo, 2011; Holtmaat and Svoboda, 2009; Johansen-Berg et al., 2012). A large body of literature has shown that environmental enrichment can also increase the number of synapses and dendritic spines per neuron in adult animals (Briones et al., 2004; Jones et al., 1997; Kozorovitskiy et al., 2005). Specific forms of training like motor skill learning induces increase in synapse number in higher-order brain regions involved in motor learning, such as motor cortex (Kleim et al., 2002; Kleim et al., 1996) and cerebellum (Anderson et al., 1994; Black et al., 1990; Kleim et al., 1998; Kleim et al., 1997). Recently, Keifer et al. (2015) claimed that increases in the dendritic spine density may partially explained the learning-induced GM structural changes.

Astrocytes

Astrocytes are the most numerous subtypes of glial cells within the central nervous system (CNS) and it appears that the ratio of astrocytes to neurons increases with increasing complexity of the CNS. The term astrocyte was introduced by Lenhossek (1893) to describe the star-shaped neuroglial cells (Jacobson, 1993). The cell body of a typical astrocyte accounts for only 2% of its total volume whilst the larger cell processes constitute 58%. The very fine thin processes which account for 40% of the cell volume are highly mobile (Hirrlinger et al., 2004). The cytoskeleton of an astrocyte is composed of intermediate filaments, microtubules and microfilaments (Haseleu et al., 2013). Three intermediate filament proteins may be found in the astrocytes: nestin, vimentin, and glial fibrillary acidic protein (GFAP). Nestin and vimentin are main intermediate filament proteins in the immature astroglial cells, whereas the maturing and adult astrocytes contain vimentin and GFAP (Eliasson et al., 1999a). Intermediate filaments are present only in the cell body and larger cellular processes but absent in the fine processes (Theodosis et al., 2008), where microfilaments (actin) mainly build up the cytoskeleton (Haseleu et al., 2013). Astrocytes are responsible for maintaining potassium (K^+) homeostasis during the neuronal firing. A brief increase in the neuronal activity results in a transient increase in K^+ efflux from the neuron to the extra cellular space (ECS) (Ballanyi et al., 1987; Dietzel et al., 1989; Macvicar et al., 2002). Effective clearance of K^+ is essential for normal brain function otherwise it will enhance neuronal excitability and increase the probability of epileptic episodes and major sink of excess ECS-K^+ is the surrounding astrocytes (Lux et al., 1986; Somjen, 2004). Additionally, astrocytes are considered the essential partners in the synapse formation, synaptic transmission, and plasticity (Eroglu and Barres, 2010). Astrocytes secrete synaptogenic molecule such as apolipoprotein E (Goritz et al., 2005; Mauch et al., 2001), thrombospondins (Christopherson et al., 2005; Risher and Eroglu, 2012) and hevin (Kucukdereli et al., 2011) that instruct the synapse formation and development (Clarke and Barres, 2013). But these synapses are silent (lacking AMPA receptors) and to convert the silent synapses into functional synapses, astrocytes further secrete glypicans (Allen et al., 2012). Several studies have suggested complementary experience-driven changes in the glial and synaptic morphology. For instance, the housing of rats in a complex environment resulted in an increase in synapse number (Briones et al., 2004) that was further found to be associated with glial cell proliferation(Altman and Das, 1964),

increased surface density of GFAP positive astrocytic processes (Jones et al., 1996; Sirevaag and Greenough, 1991) and increased astrocytic ensheathing of synapses (Jones and Greenough, 1996). Using a motor learning paradigm Anderson and colleagues (1994) demonstrated that the increased synapse number was accompanied by a proportional increase in the volume of astrocyte per Purkinje cell, that persisted only during the learning period (Kleim et al., 2007). Further, an enhanced complexity in the astrocytic morphology was observed in mice following 8 weeks of housing in enriched cages (Viola et al., 2009). Astrocytes are also considered to be involved in the elimination of neuronal debris and synapses. Phagocytosis by astrocytes has been reported in response to glioma (Lantos, 1974), trauma (al-Ali and al-Hussain, 1996; Bechmann and Nitsch, 1997) and during the developmental axon death (Berbel and Innocenti, 1988).

Change in neuronal activity pattern

The capacity of neural networks to store and utilize the new experience and learning associated information depends on the pattern of neuronal activity. Learning and behavior associated studies have shown increased neuronal activity in learning relevant areas as assessed by the expression of the immediate-early gene Arc. Arc stands for activity-regulated cytoskeleton-associated protein, also termed as Arg 3.1 (Okuno, 2011) whose mRNA is rapidly transcribed and targeted to the dendrites of neurons as they engage in the information processing and storage (Gusev et al., 2005). Arc is a dual marker and its expression is measured to assess the enhanced neuronal activation (Guzowski et al., 1999) and synaptic plasticity (Gao et al., 2010; Hayashi et al., 2012; Shepherd et al., 2006). In rats and mice, Arc mRNA and protein induction has been observed in the specific brain areas during exploration of new environments (Guzowski et al., 1999; Ramirez-Amaya et al., 2005), performance of the behavioural tasks that induced the formation of new spatial memory, fear-conditioning memory (Barot et al., 2009) and olfactory memory (Desgranges et al., 2010) as well as several types of operant learning (Carpenter-Hyland et al., 2010; Guzowski et al., 2001; Kelly and Deadwyler, 2003; Rapanelli et al., 2010).

Hypothesis of the study

The underlying GM changes may be heterogeneous depending on the factors such as time after the onset of learning, its consequent temporal dynamics (reversible or permanent) and on the brain regions involved. For Instance, the medical students

memorizing extensively for 3 months for an intermediate exam were found to exhibit bilaterally increased GM volume in the hippocampus (Draganski et al., 2006), a brain region where neurogenesis takes place in adults (Kempermann et al., 1997) while in learning-associated studies where GM changes were seen just after a week of training in the cortex, neurogenesis as a promising cellular correlate seems suspicious because it might take up months for the stem cells to differentiate into the neurons (Cummings et al., 2005). Instead, the rapidly-evolving structural brain alterations are more likely to be related to the fast adjusting neural systems, such as spine and synapse turnover (Holtmaat et al., 2005; Lendvai et al., 2000; Xu et al., 2009) and morphological changes in the astrocytes (Kleim et al., 2007). To support this assumption, it was demonstrated that new dendritic spines can evolve within one hour after learning (Engert and Bonhoeffer, 1999; Maletic-Savatic et al., 1999; Nagerl et al., 2004). Recently, Keifer et al. (2015) described that increase in the dendritic spine density may partially explain the learning-induced GM structural change. Additionally, the morphological changes in astrocytes also seem a promising cellular correlate as astrocytes show substantial volume changes within seconds (Ostby et al., 2009) while neurons maintained their volume when GM swelled and shrank (Andrew et al., 2007). Kleim et al. (2007) reported that 3-4 month-old rats subjected to acrobatic learning showed the hypertrophy of astrocytes that only persisted during the period of learning explaining the same pattern as observed in the learning associated transient GM changes seen by MRI-morphometry (Boyke et al., 2008; Draganski et al., 2004; Driemeyer et al., 2008). On the basis of this correlation, we hypothesized astrocytic enlargement as a major underlie factor to produce the learning associated GM volume expansion.

2. Aims of study

Learning induces the transient GM structural plasticity that persists only during the period of learning and can be detected by using MRI-morphometric approaches. However, to date the cellular underpinnings of learning associated transient macrostructural plasticity in the GM of adult brain are enigmatic. The experiments with rats have shown transient hypertrophy of astrocytes during acrobatic learning (Kleim et al., 2007), explaining the same pattern as observed in learning associated transient GM changes seen by MRI (Draganski et al., 2004; Draganski et al., 2006; Driemeyer et al., 2008). On the basis of this correlation, we hypothesized astrocytic enlargement as a major underlie mechanism to produce learning associated GM volume changes. To check this hypothesis we have performed a study by combining the monocular deprivation (MD) based perceptual learning with longitudinal MRI measurements complemented by microscopic analyses.

Monocular deprivation (MD) is a highly acceptable experimental model to study the neuroplasticity (Wiesel and Hubel, 1965) that leads to visual perceptual learning to adapt with monocular vision. Perceptual learning is defined as an increase in the ability to extract information from the environment (Gibson, 1969) and following MD represented by enhancement of the optokinetic response (OKR) sensitivity (measured as visual acuity [VA] and contrast sensitivity] threshold through the undeprived eye. The OKR sensitivity can be longitudinally monitored by using a visual optometer (Greifzu et al., 2011; Lehmann and Löwel 2008; Prusky et al., 2006)

The main aims of our study are as follows:

1. Establishment of strategies firstly to induce the perceptual learning associated plasticity in the brain using MD and secondly to longitudinally detect the complete profile of this plasticity using MRI and DBM analysis.

2. Cross-sectional analyses to explicate the cellular basis of morphometry based learning associated transient structural plasticity following MD. Although we assume astrocytic enlargement as the major cellular mechanism underlying structural plasticity of GM, we have decided to check all other possible factors like spine density, Arc expression, astrocytic morphological changes

and neuronal, glial as well as angio-genesis to elucidate the complete microscopic profile of learning associated macrostructural plasticity.

3. Material and Methods

3.1. Animals

In this study 8 weeks old Wistar rats of the strain RccHan[TM]: WIST (Harlan Laboratories, Horst, Netherlands) were used. The animals were kept in the service unit for small rodents (SEC) of the Institute of Laboratory Animal Science (IVTK) of the University of Jena under specific pathogen-free (SPF) and constant conditions (22-24 °C, 70-80% humidity, 12-hour day / night cycle) with free access to food and water. In accordance with the Animal Protection Act, the rats were carried out in the cages of type IV (595 x 380 x 200 mm). The animal experiments were carried-out within the framework approved by the Thuringian State Office of Food Safety and Consumer Protection under the planned experiment one-compliance with the provisions and in coordination with the Animal Experiments Officer (TVA 02-24 / 11).

3.2. Study design

Test study

Test experiment was performed to establish the strategies for main longitudinal and cross-sectional studies. Rats were tested with visual optometer for two days to get the baseline measurements of visual acuity and contrast sensitivity. Next day, MD of the left eye for all the rats was performed. Rats were then tested for seven consecutive days with visual optometer and then sacrificed (Fig. 2).
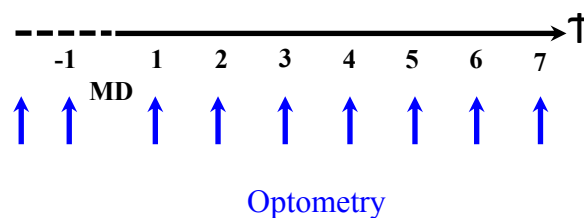

Fig. 2: The regimen for test study.
Following the two days baseline measurements with the visual optometer, MD of the left eye was performed. Afterwards, the optometry was performed for consecutive seven days. The rats were then sacrificed.

11

Longitudinal study

For longitudinal study, three different kinds of the strategies were employed.

In the first approach, MD and visual optometry were coupled with MRI and DBM analysis (MD-OPT-MRI). Following the two days' baseline visual optometry measurements of both eyes, baseline MRI was done. Afterwards, MD of the left eye for MD rats was performed on the same day. Following MD, MRI was performed at day 3, 7 and 10 and for rest of the days optometry for the undeprived right eye was
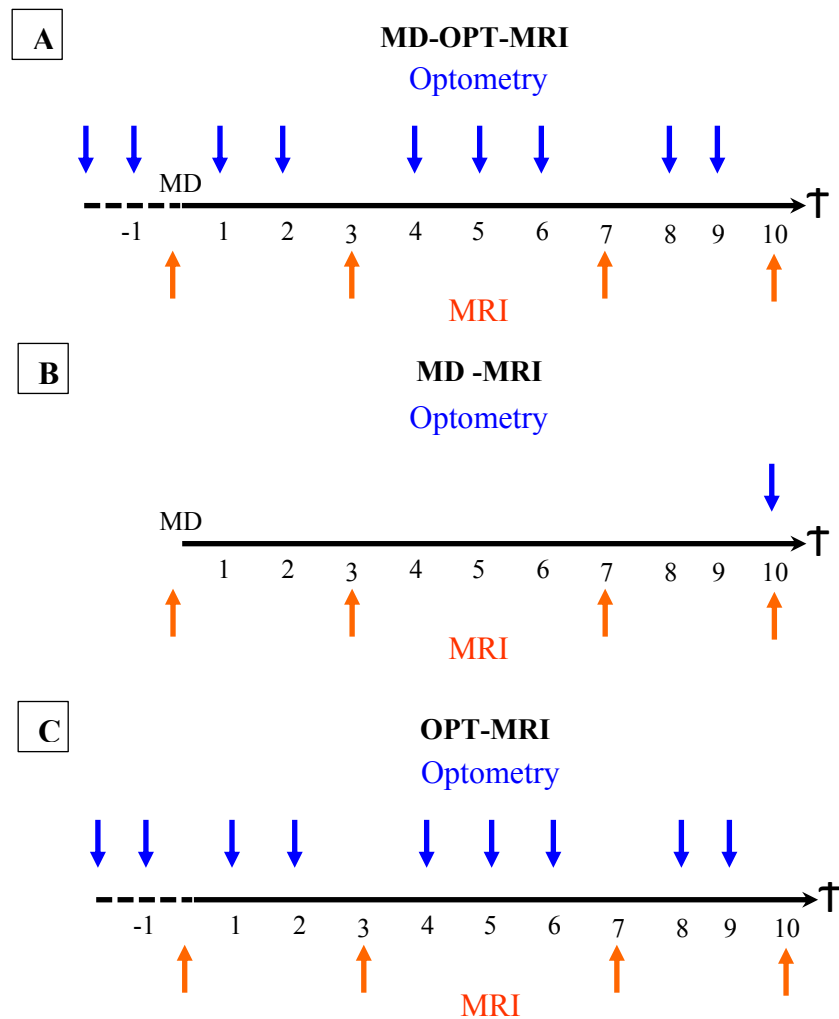

Fig. 3: The regimen for longitudinal study.

(A) (MD-OPT-MRI): Following the two days' baseline optometry, baseline MRI and MD of the left eye was done at the same day. Afterwards, MRI was performed at day 3, 7 and 10 while optometry was performed for 1, 2, 4, 5, 6, 8 and 9 day following MD. The rats were then sacrificed. (B) (MD-MRI): Baseline MRI and MD of left eye were done at the same day. Afterward, MRI was performed at day 3, 7 and 10. Optometry was performed at 10d of MD after last MRI. The rats were then sacrificed. (C) (OPT-MRI). Following two days' baseline optometry, baseline MRI was performed. Afterwards, MRI was performed at day 3, 7 and 10 while optometry was performed for 1, 2, 4, 5, 6, 8 and 9d after baseline MRI. Rats were then sacrificed.

done. Then rats were sacrificed (Fig. 3A).

For the second approach, we coupled MD with MRI and DBM analysis (MD-MRI). Following the baseline MRI, MD of the left eye for MD rats was performed at the same day. Following MD, MRI was performed at day 3, 7 and 10 and for rest of the days, rats stayed in the cages. In order to analyze the effect of MD (without daily optometry) on VA, after last MRI at 10d of MD, the optometry was performed to measure VA sensitivity of the undeprived right eye. Then, the left eye of all MD rats was re-opened and VA of the left eye was measured to calculate the enhancement as the baseline OKR of both eyes were found same in test study and first approach (MD-OPT-MRI) (Fig. 3B).

For the third approach, we coupled optometry with MRI and DBM analysis (OPT-MRI). Following the two days' baseline visual optometry measurements of both eyes, baseline MRI was done. Afterwards, MRI was performed at day 3, 7 and 10d following the baseline MRI and for rest of the days optometry for both eyes was done. Then rats were sacrificed (Fig. 3C).

For all three approaches, age-matched control rats were also measured with MRI but not tested for optometry.

Cross-sectional study

For cross-sectional studies, we included 2 groups of MD (MD-3d and MD-10d) along with control rats. For MD rats, after two days' baseline optometry, MD of the left eye was performed. Md-3d group was tested with optometer for 3days and sacrificed at 3d after optometry while Md-10d group was tested with optometer for 10days and then sacrificed at 10d of MD (Fig. 4) All the groups (MD-3d, MD-10d and Control) were sacrificed at the same age (72 days).
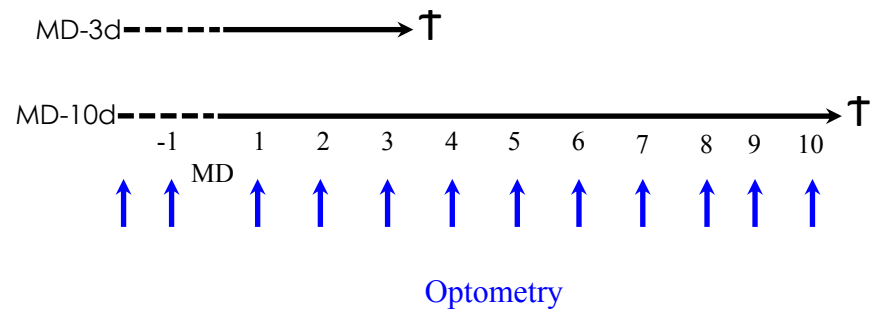
Fig. 4: The regimen for cross-sectionalstudy.
Following two days' baseline optometry, baseline MD of the left eye was done. Afterwards, MD-3d rats were tested with optometer for 3days and then sacrificed. MD-10d rats were tested with optometer for 10days and then sacrificed.

5′-Bromodeoxyuridine labeling study

In order to analyze the contribution of cell genesis in GM swelling seen by MRI at day 3 following MD, the proliferating cells were analyzed in MD-3d and control rats. To label the proliferating cells, thymidine analog 5′-bromodeoxyuridine (BrdU, Sigma-Aldrich, St Louis, MO, USA; 100 mg/kg body weight) dissolved in 0.9% saline was used. Both MD (n = 7) and control (n = 6) rats were injected with BrdU every 12 hours for 3 consecutive days. MD rats received the first injection immediately after the closing of the left eye (MD). These rats were sacrificed 12 hours after the last injection (Fig. 5).
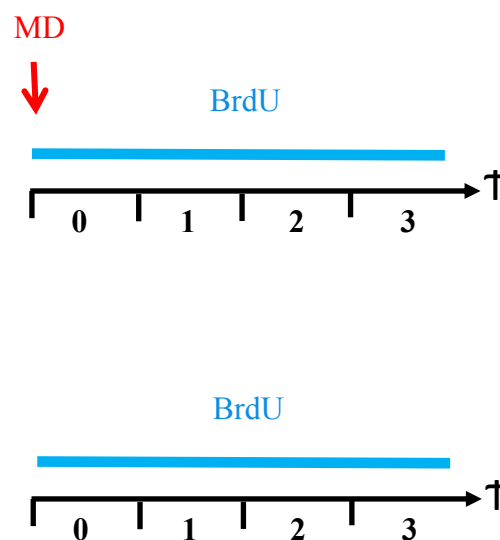

Fig. 5: 5′-Bromodeoxyuridine (BrdU) injection regimen to analyze.
(A) BrdU was injected immediately after MD (2daily 100 mg/kg BrdU injections, 12 hours apart). (B) The control rats (without MD) were also injected in the same manner. Rats were sacrificed 12 hours after the last injection (day 3).

3.3. Monocular deprivation (MD)

To induce the monocular deprivation (MD), we had closed the left eye of rats. For this purpose, each rat was first anesthetized by keeping it in the jar having Isoflurane (2.5%) and O_2: N_2O= 20:40 l\h (each 2bar). Then the unconscious rat was transferred on the operation table and its mouth was fixed in a pipe with a continuous supply of Isoflurane (2.5%) and O_2: N_2O= 20:40 l\h (each 2bar) to keep the rat unconscious. Afterwards, under dissecting microscope the antibiotic Polyspechan HC, N1 (Alcon) was applied on the left eye and the surrounding area was cleaned with disinfectant Softasept® N (B-Braun, Germany). The eye was sewn shut with stitches and rat was kept back in the cage. The stitches were checked every day and the rats which had opened their stitched eyes were excluded from the study.

3.4. Optometry

The visual acuity (VA) and contrast sensitivity (optokinetic response [OKR]) of rats were measured using visual optometer developed by Prusky et al. (2004).
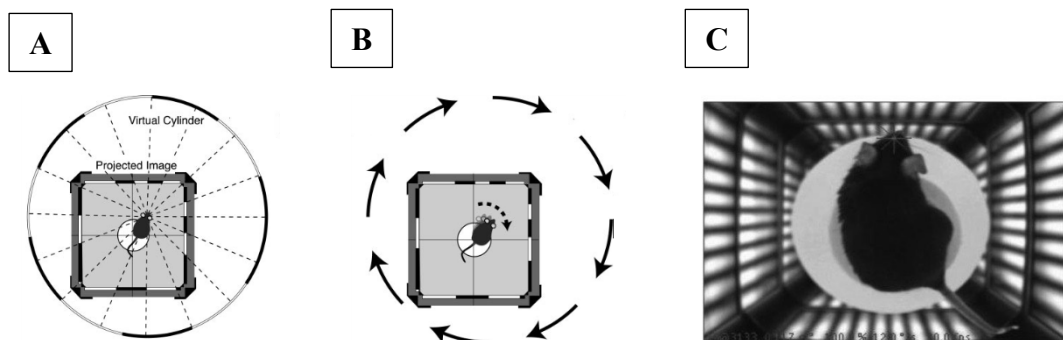
Fig. 6: Virtual geometry and optomotor.
(A) A virtual cylinder is projected in 3-D coordinate space on the monitors. The head of the animal centers the rotation of the cylinder. (B) When the cylinder is rotated, the animal tracks the drifting grating with head and neck movements. (C) A single-frame video camera image of the animal tracking the cylinder grating. The four-line crosshair is positioned between the eyes of the animal, and the coordinates are used to center the rotation of the cylinder (Prusky et al., 2004).

Baseline measurement

Rats were placed on the platform of the visual optometer individually and were allowed to move freely. The door of optometer was closed and the visual stimuli consisting of moving gratings (low spatial frequency and 100% contrast) were drawn on the walls of optometer. Rat moved its head and upper body parts slowly

(tracking), following the grating pattern on the screens. Then the value of spatial frequency (cyc/deg) was started increasing systematically with alternatively changing the direction of grating until the threshold reached (beyond this value no tracking). This threshold represented the visual acuity (VA). To measure the contrast sensitivity, the spatial frequency was set at 0.150 cyc/deg. When rat started tracking, the value of contrast was started decreasing with the sudden reversal of the direction of moving gratings until the threshold reached. This step was repeated for the spatial frequency values 0.150, 0.119, 0.89, 0.61, and 0.44 (cyc/deg) to measure the contrast sensitivity threshold. For each rat, two baseline measurements were taken.

Measurement following MD

Following MD, to measure the change in the visual acuity and contrast sensitivity, for the test experiment after MD, optometry was done for consecutive 7 days (Fig. 2). For longitudinal analysis, optometry was done according to the schedule presented in Fig. 3 i.e. the optometry was done at day 1, 2, 5, 6, 8 and 9 of MD and baseline MRI and no testing was done at day 3, 4, 7 and 10 because rats were transferred to another place for MRI. For cross-sectional analysis, two groups: MD-3d and MD-10d were included. Following MD, optometry was performed for consecutive 3 days for the MD-3d group while for consecutive 10 days for the MD-10d group (Fig. 4). On each day before starting, the eyes of all the rats with MD were checked very carefully. Then each MD rat was kept on the platform and tested for the visual acuity and contrast sensitivity threshold in the same way as described for the baseline measurement. As the left eye was closed, the tracking was only in the counter-clockwise direction. But the direction of the grating was changed alternatively to make sure that tracking was just in the response to movements of the grating.

3.5. Magnetic resonance Imaging (MRI)

To analyze the structural changes in the GM of rats during MD, MRI was performed according to the scheme presented in Fig. 3 i.e. the first measurement was taken before MD as a baseline MRI and afterwards 3 measurements were taken following MD for both MD as well as control rats with co-operation of Medical Physics Group of the Institute of Diagnostic and Interventional Radiology (IDIR) of the University Hospital Jena. For this purpose, a clinical 3T whole body scanner (MagnetomTIM Trio, Siemens Medical Solutions, Erlangen, Germany) equipped with a dedicated rat

head coil with a linearly polarized Litz coil volume resonator (Doty Scientific Inc., Columbia, SC, USA) was used as described previously (Herrmann et al., 2012).

Fig. 7: Photograph showing coil placement, immobilization of the animal head and anesthesia supply on clinical 3T whole body scanner.

The rat is fixed by a head mount on a small animal imaging platform. Inhalation anesthetics are supplied through the tubes on the far right directly to the rat's snout (Herrmann et al., 2012).
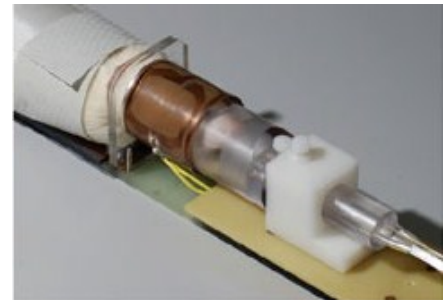
Briefly, freely breathing rats were anesthetized with isoflurane (1.7 % in oxygen, 1.5 l/min). T2-weighted images were obtained using a 3D SPACE (Sampling Perfection with Application-Optimized Contrasts Using Different Flip Angle Evolutions) sequence (Siemens Healthcare, Erlangen, Germany) with an isotropic resolution of 0.33 mm^3 (matrix 192×130×96, FoV 64×43×32 mm, bandwidth 145 Hz/px, TE/TR=352 ms/2500 ms, flip angle-mode 'T2var', echo spacing of 10.7 ms, turbo factor of 67 and Partial Fourier of 7/8 in both phase encode directions). While the CPC coil measurements were performed using three repetitions each consisting of two averages with a total acquisition time TA=42 min, the improved signal-to-noise ratio (SNR) performance of the Doty coil enabled a protocol with two repetitions (one average) with TA=14 min.

3.6. Deformation based morphometry (DBM)

The changes in the brain structure were analyzed by deformation-based morphometry (DBM) which warps subsequent MR images of individual datasets to match their baseline images by high-dimensional nonlinear registration (Gaser et al., 2012) with the MATLAB-based application package SPM8 (Wellcome Department of Imaging Neuroscience, United kingdom). The Jacobian determinant of the deformations was used to calculate the voxel-wise local volume changes with significance criteria: strong (with correction) and weak (without correction). During the DBM analysis, the stack of four three-dimensional T2-weighted MR images was generated per animal (MD: n=24; CTR: n=23; Figure 3). First measurement was performed immediately before MD to obtain an individual reference image. The

remaining three measurements followed sequentially 3, 7 and 10 days after MD. Next, the images generated after MD were warped onto their own reference image by high-dimensional nonlinear registration. This registration minimizes morphologic differences between each sequential image and the reference image and the information about these differences is coded in three separate deformation fields. Then we used the Jacobian determinant to calculate the local volume changes over time in relation to the first measurement. Finally, we tested the voxel-wise for spatio-temporal differences between MD- and control animals by using a repeated measure ANOVA. We applied a t-test to investigate an interaction between time and group by testing for an early volume increase in MD-animals relative to controls (MD-3d>MD-10d vs. CTR-3d<CTR-10d). Additionally, we tested in the contrary for MD-induced late evolving volume increases (MD-3d<MD-10d vs. CTR-3d>CTR-10d).

3.7. Immunohistochemistry

Transcardial perfusion

Rats were deeply anesthetized in a sealed jar containing isoflurane-soaked cotton balls. Afterward, rats were transferred to a plastic tray and fixed with clamps. For continuous anesthesia, a 50 ml tube (Eppendorf) containing isoflurane soaked paper towel was inverted at the nose of the rat. They were then transcardially perfused through the left cardiac ventricle using a peristaltic pump (35 ml/min) with 70 ml of phosphate-buffered saline (PBS, pH 7.4) followed by 280 mL of 4% paraformaldehyde (PFA)(Riedel de Häen). The brains were removed and post-fixed in the same fixative solution at 4°C overnight.

Cryoprotection

Brains were cryoprotected first in a 10% sucrose solution (4°C, 1day) and then in 30% sucrose solution in PBS at 4°C until they sank down. Next, brains were flash-frozen in -30°C methyl butane (Merck, Germany) and stored at -80°C.

Cutting of frozen sections

For immunohistochemical analysis, brains were sectioned with a cryostat (Leica 2000 R SM, Germany). The brains were frozen on the stage using Tissue-Tek (Sakura) and the temperature reached at -43 ° C within 10 minutes. Coronal sections of 40μm thickness were sectioned and collected in antifreeze solutions containing 30% ethylene glycol and 30% glycerol and stored at -20°C.

Immunohistochemical staining

For immunohistochemical analysis of BrdU (5′-Bromodeoxyuridine), S100ß (S100 calcium-binding protein B), GFAP (Glial fibrillary acidic protein) and Arc (activity-regulated cytoskeleton-associated protein), DAB (3, 3'-diaminobenzidine) staining was performed by avidin-biotin-peroxidase method (Figure 8). The detailed protocol for each immunogen is presented in the table (Tab.1). Briefly, free-floating 40μm thick coronal sections (Bregma approximately -5.04-6.12 mm) were washed overnight at 4°C. Next day, they were incubated in H_2O_2 (Merck, Germany) to inactivate endogenous peroxidises for 30min followed washing. Next, the blocking was done in normal serum from the species in which the secondary antibody was raised. After that, slices were incubated with primary antibody (BrdU, S100ß, GFAP, Arc) overnight at 4°C. Next day, after being washed, slices were re-blocked with same serum and then incubated in secondary antibody two hours followed by washing. Next, slices were incubated in AB-Reagent (Avidin-Biotin-Peroxidase-complex, prepared 30 min before) (Vectastain Elite ABC-Kit, Vectorlab, PK-6100, USA) and then washed. The slices were transferred to DAB solution (DAB-Tablet, Sigma D-4293, USA) and to develop the reaction H_2O_2 solution (H_2O_2-Tablet, Sigma U8879, USA) was added. Finally, the slices were washed and mounted on slides in Gelatine (Roth, Germany) and covered with Entellan (Merck, Germany) and coverslips and coded before quantitative analysis. Primary antibodies were as follows: BrdU (rat, AbD Serotec, USA), S100ß (rabbit, Synaptic system, Germany), GFAP (mouse, Chemicon, USA), Arc (guniea pig, Synaptic system, Germany) (Tab. 3).

Fig. 8: Schematic representation of the immunohistochemical detection by the avidin-biotin-peroxidase method.

At first, the primary antibody binds specifically to the antigen. Then primary antibody coupled to the secondary biotinylated antibody. Finally, the avidin binds with biotin-peroxidase (P) to make Avidin-Biotin-P complex. Peroxidases oxidize the associated 3, 3'-diaminobenzidine (DAB) to a brown phenazine polymer, H_2O_2 acts as an electron acceptor.

Tab. 1: Protocols for immunohistochemistry of each immunogen.

Steps	Arc	GFAP	S100ß	BrdU
Washing	5 x 15 min in TBS	6 x 10 min in TBS-T 2 (0.2% Triton X-100)	6 x 10 min in TBS-T2	6 x 15 min in TBS
Quenching of endogenous peroxidase (30 min at RT)	0.45% H_2O_2 in TBST 1	0.24% H_2O_2 in TBST 2	0.24% H_2O_2 in TBST 2	0.45% H_2O_2 in TBST 1
Washing	3 x 15 min in TBS	3 x 10 min in TBS-T 2	3 x 10 min in TBS-T 2	3 x 15 min in TBS
Denaturation (30 min at 37 °C)	-	-	-	2N HCL
pH Neutralisation (30 min at RT)	-	-	-	0.1M borate buffer (pH : 8.5)
Washing	-	-	-	2 x 15 min in TBS
Blocking (at RT)	30 min in TBS-Plus 1	2 h in TBS-Plus 2	2 h in TBS-Plus 2	30 min in TBS-Plus 1
Primary antibody (overnight at 4 °C)	Anti-Arc (guniea pig, Synaptic system) 1 : 500 in TBS-Plus 1	Anti-GFAP (mouse, Chemicon) 1 : 1000 in TBS-Plus 2	Anti-S100ß (rabbit, Synaptic system) 1 : 12000 in TBS-Plus 2	Anti-BrdU (rat, abD Serotec) 1 : 500 in TBS-Plus 1
Washing	3 x 15 min in TBS	4 x 10 min in TBS-T 2	4 x 10 min in TBS-T 2	3 x 20 min in TBS
Re-blocking (30 min at RT)	TBS-Plus 1	TBS-Plus 2	TBS-Plus 2	TBS-Plus 1
Secondary antibody (at RT)	Donkey anti- guniea pig (Jackson) 1 : 500 in TBS-Plus 1	Donkey anti- mouse (Jackson) 1 : 500 in TBS-Plus 2	Donkey anti- rabbit (Jackson) 1 : 500 in TBS-Plus 2	Donkey anti- rat (Jackson) 1 : 500 in TBS-Plus 1
Washing	3 x 10 min in TBS	4 x 10 min in TBS-T 2	4 x 10 min in TBS-T 2	3 x 10 min in TBS
AB- Reagent (1 hour at RT)	In TBS-T 1	in TBS-T 2	in TBS-T 2	in TBS-T 1
Washing	3 x 10 min in TBS	4 x 10 min in TBS-T 2	4 x 10 min in TBS-T 2	3 x 10 min in TBS
DAB reaction (10 min at RT)	In TBS-T 1	in TBS-T 2	in TBS-T 2	in TBS-T 1
Washing	3 x 10 min in TBS	4 x 10 min in TBS-T 2	4 x 10 min in TBS-T 2	3 x 10 min in TBS

Abbreviations for Tab.1: Arc: Activity-regulated cytoskeleton-associated protein, BrdU: 5′-Bromodeoxyuridine, DAB: 3, 3'-Diaminobenzidine, Sec.: Secondary, GFAP: Glial fibrillary acidic protein, HCL: hydrochloric acid, min: minute, PBS: Phosphate-buffered saline, Pr.: Primary, S100ß: S100 calcium-binding protein B, TBS: Tris-buffered saline, TBS-T: Tris-buffered saline- Triton X-100.

Tab. 2: Buffers used for immunohistochemistry.

Buffer	Recipe
TBS	26.44g HCl, 2.88g Tris-Ultra (Base), 18g NaCl, 2N HCL to adjust pH: 7.4, final volume 2000ml with dist. H_2O.
TBS-T 1	1X TBS, 0.1% Triton X-100
TBS-T 2	1X TBS, 0.2% Triton X-100
Citrate buffer	1.47g $Na_3C_6H_5O_7$ in 400ml dist. H_2O, 2N HCL to adjust pH: 6, 0.25ml Tween 20, final volume 500ml with dist. H_2O.
Borate buffer	*Stock I* (0.1 M Boric acid), *Stock II* (0.1M Sodiumtetraborat-decahydrat). 50ml of *Stock I* to 250ml of *Stock II* to adjust pH: 8.5.
TBS-Plus 1	1X TBS, 0.1% Triton X-100, 3% Normal donkey serum, 2% Bovine serum albumin (BSA), 2% Milk powder.
TBS-Plus 2	1X TBS, 0.2% Triton X-100, 3% Normal donkey serum.
AB reagent	50µl reagent A, 50µl reagent B, 2.5ml TBS-T.
DAB reagent	1 tablet DAB in 5ml TBS-T, 1 tablet H_2O_2 in 5ml TBS-T.
PBS	8g NaCl, 0.2g KCl, 1.44g NA_2HPO_4, 0.24g KH_2PO_4, 2N HCL to adjust pH: 7.4, final volume 1000ml with dist. H_2O.

Abbreviations: HCL, Hydrochloric acid, KCl: Potassium chloride, KH_2PO_4: Potassium dihydrogen phosphate, ml: milliliter, µl: microliter, N: Normal, NaCl: Sodium chloride, TBS: Tris-buffered saline, TBS-T: Tris-buffered saline- Triton X-100, DAB: 3, 3'-Diaminobenzidine, PBS: Phosphate-buffered saline.

Tab. 3: Antibodies used for immunohistochemistry.

Pri. Antibody	Source	Cat #	Company	Sec. Antibody	Source	Cat #	Company
Anti-BrdU	Rat	OBT0030CX	AbB Serotec, USA	**Anti-Rat Biotinylated**	Donkey	712-067-003	Jackson ImmunoResearch Laboratories, USA
Anti-S100ß	Rabbit	287003	Synaptic system, Germany	**Anti-Rabbit Biotinylated**	Donkey	711-065-152	Jackson ImmunoResearch Laboratories, USA
Anti-GFAP	Mouse	MAB360	Chemicon, USA	**Anti-mouse Biotinylated**	Donkey	715-065-151	Jackson ImmunoResearch Laboratories, USA
Anti-Arc	Guniea pig	156005	Synaptic system, Germany	**Anti-Gunie pig Biotinylated**	Donkey	706-065-148	Jackson ImmunoResearch Laboratories, USA

Abbreviations: Arc: Activity-regulated cytoskeleton-associated protein, BrdU: 5′-Bromodeoxyuridine, Sec.: Secondary, GFAP: Glial fibrillary acidic protein, Pr.: Primary, S100ß: S100 calcium-binding protein B.

3.8. Golgi-Cox Staining

The Golgi staining for neurons and astrocytes was performed using FD Rapid Golgi Stain™ kit (FD Neurotechnologies, USA). The neuronal staining was performed according to the manufacturer's instructions. Briefly, animals were decapitated by rodent guillotine following anesthetization in a sealed jar containing isoflurane-soaked cotton balls. Brains were immediately extracted and rinsed briefly in Milli-Q water to remove the blood from the surface. They were then immersed in the impregnation solution, made by mixing equal volumes of the Solutions A and B, and stored at room temperature for 2 weeks at 26°C in the dark. The impregnation solution was replaced next day. For astrocytes, we used FD Rapid Golgi Stain™ kit according to our own established protocol (Gull et al., 2015). Briefly, the isoflurane anesthetized rats were transcardially perfused with 4% PFA. The extracted brains were post-fixed for 4 days in the same fixative additionally containing 8% Glutaraldehyde. Afterwards, they were immersed in the impregnation solution, made by mixing equal volumes of Solutions A and B for 3 days at 26°C in the dark. The impregnation solution was replaced next day. After impregnation; for the both glial and neuronal staining, the impregnated brains were then transferred into Solution C and stored at 4ºC in the dark for 1 week. The solution was replaced after the first 24 hours of immersion. Next, these brains were flash-frozen in -30°C methyl butane and stored at -80°C. Afterwards, brains were then sliced (150μm/slice) using a cryostat (Leica CM3050 S, Germany) at -22°C and slices were collected on Superfrost Plus glass slides (Thermo Scientific, USA) with solution C and dried naturally at the room temperature. These slides were rinsed with Milli-Q water twice, 2 minutes each and then placed in a mixture consisting of 1 part solution D, 1 part solution E, and 2 parts Milli-Q water for 10 minutes. Then, they were rinsed in double Milli-Q water 2 times, and dehydrated in solutions of increasing ethanol concentration (50%, 70%, and 95%) for 4 minutes each and in the absolute ethanol for 16 minutes. Finally, they were cleared in xylene for 12 minutes before coverslipped in Entellan. The slides were then coded to make quantitative analysis blind.

3.9. Quantitative analysis of cell density

The density of BrdU[+,] S100ß[+] and Arc^{+} cells was calculated in MD-3d, MD-10d and control rats. The brain regions were selected according to "The rat brain in stereotaxic coordinates"(Paxinos and Watson, 2004). As previously described

(Raslan et al., 2014), analyses were performed using the Stereo Investigator software 8.1 (MicroBrightField [MBF], USA) and a microscope (Axioscope 2 mot plus, Zeiss, Germany) equipped with a motorized stage (Zeiss, Germany) and a CX 9000 digital camera (MBF, USA). Cell density (N_V) was estimated by applying optical fractionator method in two slices per animal with randomly placed dissectors. The regions of interest were outlined (Plan Neofluar 5x objective, Zeiss. Germany). For cell counting, a Plan Neofluar 40x objective (Zeiss) was used (Fig. 9) and the dissector size for BrdU$^+$, S100ß$^+$ and Arc$^+$ cells was used according to the Tab. 4.
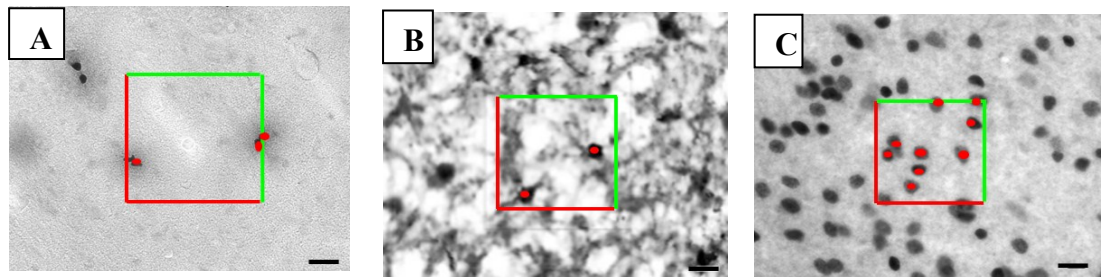
Fig. 9: Schematic representation of the strategy employed for measuring the cell density of BrdU$^+$ (A), S100ß$^+$ (B) and Arc$^+$ (C) cells.

The region of interest was constructed using Stereo Investigator under lower magnification (50X). Then a grid and frame of specific size were applied under higher magnification (400X). Next, the cells present inside and also intersecting with green lines of the frame were marked. The software then presented the number of marked cells that were exported to Microsoft Excel and numbers were used to calculate the density. Scale bars: A, B and C, 20μm.

Tab. 4: Sampling schemes used for cell counts.

Marker	Region	Grid (μm)	Counting frame (μm)	Disector height (μm)	Guard Zone (μm)
BrdU	LEnt	200 x 200	150 x 150	11	2
	Au1	200 x 200	150 x 150	11	2
S100ß	LEnt	100 x 100	65 x 65	11	2
	Au1	120 x 120	80 x 80	11	2
Arc	LEnt	100 x 100	60 x 60	11	2
	Au1	100 x 100	60 x 60	11	2

Abbreviations: Arc: Activity-regulated cytoskeleton-associated protein, BrdU: 5′-Bromodeoxyuridine, Au1: primary auditory cortex, BrdU: 5′-Bromodeoxyuridine, LEnt lateral entorhinal cortex, S100ß: S100 calcium-binding protein B.

3.10. Quantitative analysis of Spine density

The spines were quantified on the basal dendrites of pyramidal in MD-3days (n = 4 rats), MD-10days (n = 4 rats) and control (n = 5 rats). Since the density depends on the order of dendrites (Kassem et al., 2013), we have performed the analysis specifically from order 2 to 3 of basal dendrites. Golgi stained slides were analyzed on a light microscope (Axioskop 2 mot plus; Carl Zeiss, Germany equipped with MBF CX9000 digital camera). A 100X objective was used for spine analysis.
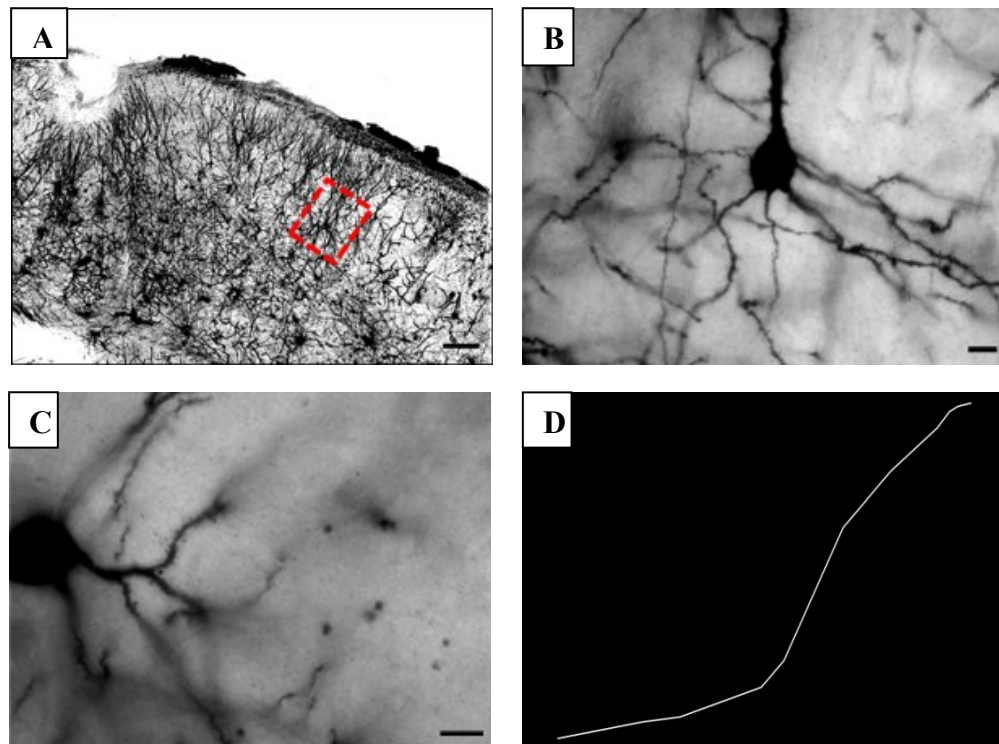
Fig. 10: Schematic representation of the strategy employed for quantification of spine density.

(A) The region of interest was selected using a 5X objective. (B) The basal dendrites of the pyramidal neurons were selected under the higher magnification 40X. (C) For quantification, a 100 X objective was used to manually count the spines in the selected segment (order 2-3 of a basal dendrite). (D) Afterward, the same segment was constructed using Neurolucida under 100X objective and the length of constructed segment was measured using Neurolucida Explorer and then the spine count was divided by the segment length to get the spine density of that segment. Scale bars: A, 100µm; B and C, 10µm.

Three neurons per hemisphere and three basal dendrites per neurons were selected. All the protrusions were counted as spines if they were in the direct contact with the dendritic shaft. Five types of spines were quantified: small ($\leq$ 1µm), medium (1-1.5µm), larger (1.5-4.5µm) on the basis of length and mushroom and spiny on the basis of shape (Fig. 11). The counting was done manually from second to third order dendrites (30-40µm) in Neurolucida 8 (MBF, USA) software. The length of the

selected segment was measured by Neurolucida Explorer (MBF, USA) (Fig. 10). Once the segment spines were counted, the number was divided by the length of the segments measured using Neurolucida Explorer, to get spine density of that segment.
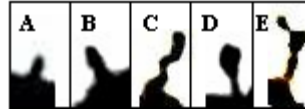
Fig. 11: Representative images of spines in different morphological categories.

(A) Small [$\leq$ 1µm], (B) Medium [1-1.5µm], (C) Larger [1.5-4.5µm], (D) Mushroom, (E) Spiny.

3.11. Quantitative analysis of astrocytic complexity

GFAP stained sections were used to quantify the morphology of astrocytes with a light microscope (Axioskop 2 mot plus; Carl Zeiss, Germany equipped with MBF CX9000 digital camera) in MD-3days, MD-10days and control rats (n = 6 rats/group). The analysis was performed only on the strictly stellate shaped astrocytes (with > 5primary branches). Seven astrocytes per hemisphere were included in the analysis. At first, the morphology of astrocytes was constructed using Neurolucida 8 (MBF, USA under 100X objective) and then Sholl's concentric circle method (Dall'Oglio et al., 2008; Sholl, 1953) was applied using Neurolucida Explorer (MBF, USA). In brief, the virtual circles with 3µm intervals were drawn
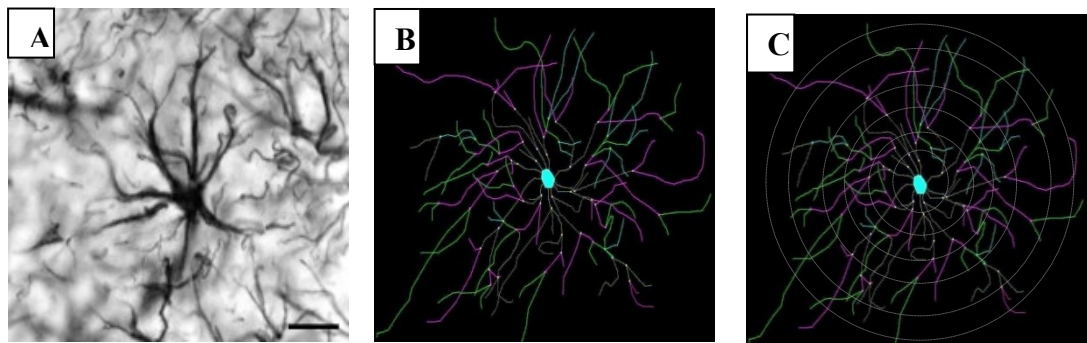
Fig. 12: Schematic representation of the strategy employed for Sholl method used for estimating the degree of astrocytic ramification.

(A) The stellate shaped GFAP stained astrocyte was selected. (B) The morphology of the selected astrocyte was constructed using Neurolucida software under a 100X objective. The Sholl analysis was then performed on the constructed astrocyte using Neurolucida explorer. (C) In Sholl analysis, virtual circles with 3µm intervals were drawn around the constructed astrocyte and the number of intersections of astrocytic processes with the virtual circles was quantified to get the information about the ramification and complexity

around each constructed astrocyte, and the number of intersections of astrocytic processes with each virtual circle was quantified that gives a measure of ramification and complexity of astrocytes (Fig. 12).

The primary processes quantification was done by counting the processes extending directly from the soma of the same astrocytes.

3.12. Quantitative analysis of astrocytic volume

To quantify the volume of astrocytes, Golgi stained sections were utilized. The images were taken on a light microscope (Axioskop 2 mot plus; Carl Zeiss, Germany equipped with MBF CX9000 digital camera) in MD-3days (n = 7 rats), MD-10days (n = 7 rats) and control (n = 5 rats). On average 30 astrocytes per hemisphere were selected for the analysis on the basis of their morphology as validated in the literature (Grosche et al., 2013; Ogata and Kosaka, 2002; Olude et al., 2015; Ranjan and Mallick, 2012). The selected astrocytes appeared as dense precipitates surrounded by highly complex and irregularly ramified processes. The volume accessed by single astrocyte (i.e., by its territory) was defined as the space over which the astrocyte processes extend, including the finest elaborations of the main branches (Grosche et al., 2013). To calculate the volume, three-dimensional z-stacks from Golgi-impregnated brain slices were obtained with a light microscope (Axioskop 2 mot plus; Carl Zeiss, Germany equipped with MBF CX9000 digital camera). The area of each astrocyte was calculated by using Image J. For this purpose, the stacks of individual astrocytes were loaded in Image J (http://rsb.info.nih.gov/ij/index.html)
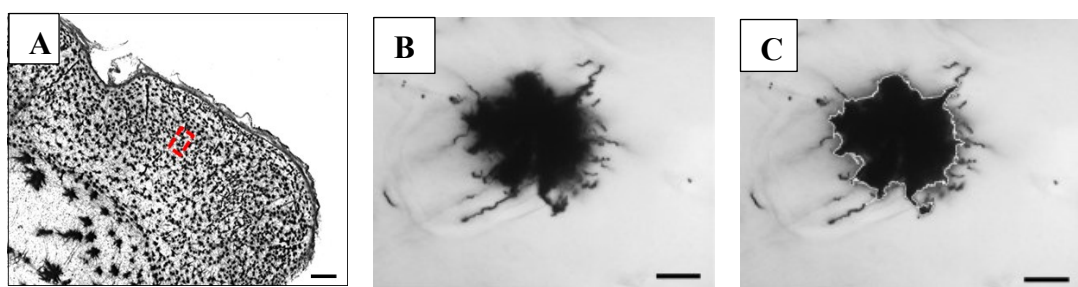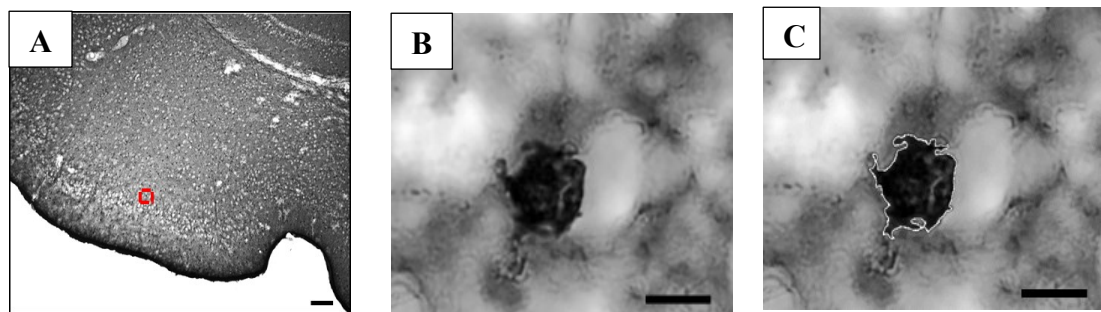

Fig. 13: Schematic representation of the strategy employed for the quantification of astrocytic volume.

(A) The region of interest was selected using a 5X objective. (B) The astrocytes were selected under the higher magnification 100X. Three-dimensional z-stacks from the selected astrocytes were obtained. (C) The stacks of individual astrocytes were loaded in the Image J and "Threshold" was applied. Threshold included only the densest part of the astrocytes and that area was delineated. Next, the volume was calculated by considering the delineated part as a virtual circle. Scale bars: A, 100μm; B and C, 10μm.

and processed by applying "Minimum Intensity Z-Projection" method. Then the image was scaled and "Threshold" was applied. Threshold included only the densest part of astrocytes and that area was delineated. Then the "Data window" represented the area in μm^3 (Fig. 13). This area was treated as a virtual circle and used to calculate the volume of an astrocyte (Grosche et al., 2013).

To quantify the volume of astroglial soma, S100ß stained slices were used and the analysis was performed in the same manner as described above for MD-3days (n= 6 rats), MD-10days (n= 6 rats) and control (n= 10 rats) (Fig. 14).

Fig. 14: Schematic representation of the strategy employed for the quantification of volume of astrocytic soma.

(A) The region of the interest was selected using a 5X objective. (B) The astrocytes with rounded soma were selected under the higher magnification with100X objective. Three-dimensional z-stacks from the selected astrocytes were obtained. (C) The stacks of the individual astrocytes were loaded in Image J and "Threshold" was applied. Threshold included only the densest part of astrocytic soma and that area was delineated. Next, the volume was calculated by considering delineated part as a virtual circle. Scale bars: A, 100μm; B and C, 10μm.

3.13. Estimation of the volume fraction of astrocytes

To calculate the volume fraction of astrocytes, Golgi staining data were combined with the S100ß$^+$ astrocyte counting data, and the influence of different staining techniques had to be ruled out. To calculate this factor, the area of 10 Golgi stained slices from control rats was measured and normalized to the area of the S100ß$^+$ slices from control rats. The subtraction from 100% results in the shrinkage of about 35%. Assuming that all the structures shrink to about the same degree, we included this factor for calculating the normalized volume of astrocytes (V_N). We first multiplied mean astrocyte territorial volume (V_M) of control rats by shrinkage factor and then added the resulting value (V_S) in V_M to calculate V_N.

$$V_S = V_M * 0.35$$

$$V_N = V_S + V_M$$

Next, we multiplied the normalized volume of astrocytes (V_N) with the density of astrocytes (N_V) (estimated by stereological counting S100ß$^+$), indicated the volume fraction of astrocytes (V_F).

$$V_F = V_N * N_V$$

3.14. Statistical analysis

Statistics were performed using Sigma plots and SPSS. The groups were compared by 1 way ANOVA (analysis of variance), 1-way repeated measures ANOVA on ranks, Familywise error (FEW) or by t-test when only two groups were compared. The inter-hemispheric comparison was done by paired t-test. Data were excluded only based on the out-layers analysis. Statistically significant values are indicated as follows: Non-significant (NS): $p > 0.05$; Significant: *$p < 0.05$ (among groups), $^{\$}p <$ 0.05 (between hemispheres).

3.15. Bregma and layer distribution

For all the microscopic analyses, we included lateral entorhinal cortex (LEnt) as a target region while primary auditory cortex (Au1) as a control region. The slices were selected from Bregma -5.00 to -6.00 according to "The rat brain in stereotaxic coordinates"(Paxinos and Watson, 2004). The layer distribution in LEnt was done according to "The Rat Nervous System" (outer layers: I, II, III occupy 65%, middle layer: IV occupies 5% and deeper layers: V, VI occupy 30%) (Witter and Amaral, 2004) while in Au1, outer layers (I, II, III) occupy 36%, middle layer (IV) occupies 13% and dipper layers (V, VI) occupy 51% area (Zille, 1985). The microscopic analyses for cross-sectional experiments were done bilaterally in layer II and III of LEnt   and   layer   III   and   IV   of   Au1.

4. Results

4.1. Optokinetic response of undeprived eye

Following MD, visual perceptual learning was accessed by measuring the OKR sensitivity of the undeprived eye. MD has produced large and statistically highly significant changes in the OKR sensitivity (measured as visual acuity [VA] and cross-sensitivity) through the undeprived right eye and the pattern of enhancement in OKR sensitivity was similar for all studies. Tab. 5 provides a summary of the statistical analysis, baseline VA and enhanced VA, duration of enhancement after an MD in days, *p* values of repeated-measures ANOVAs for the group, as well as references to figures. Tab. 6 provides a summary of the statistical analysis, baseline contrast sensitivity and enhanced contrast sensitivity, duration of enhancement after an MD in days, *p* values of repeated-measures ANOVAs for the group, as well as references to figures.

Test study

For test study, we characterized the effect of 7d of MD on VA and contrast sensitivity. No change was observed through both eyes before MD (baseline measurements). After MD, OKR sensitivity started increasing for undeprived eye and stabilized till day 6 to 7 of MD. The maximum enhancement was observed till day 3 and then the speed of increase slowed down and ultimately stopped (Fig. 15).
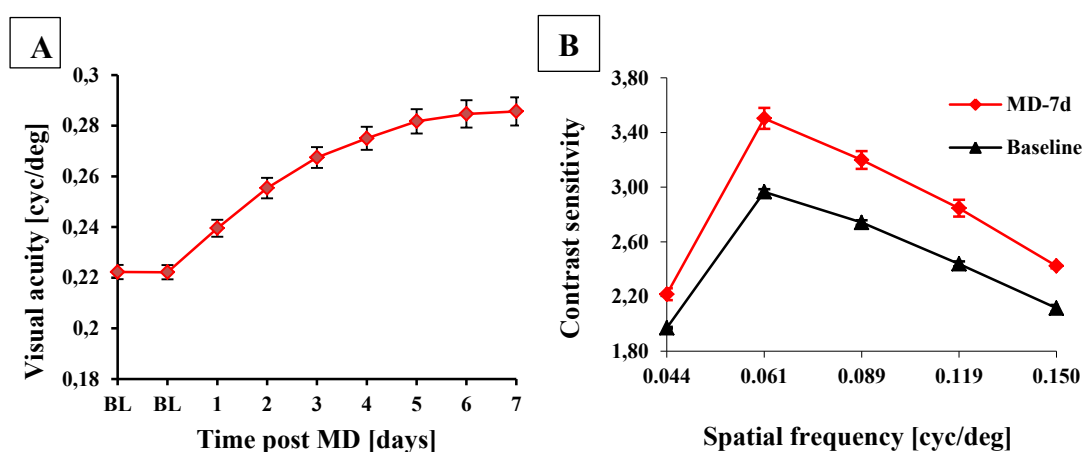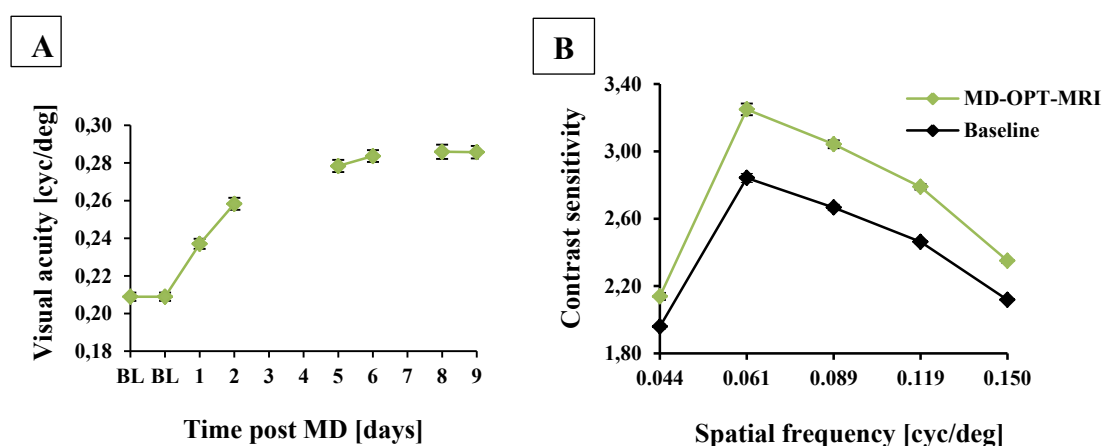

Fig. 15: Effect of 7d MD on OKR sensitivity.

(A) Visual acuity through undeprived right eye was increased gradually and reached a maximum over 6 to 7d of MD. (B) Effect of MD on contrast sensitivity was similar: sensitivity increased from baseline over 7d of MD. Data represented as mean ± SEM.

Longitudinal study

For longitudinal study, three different kinds of strategies were employed. For the first approach, we characterized the effect of MD on VA and contrast sensitivity with daily testing with optometer (MD-OPT-MRI) (Fig. 3A). The baseline measurement for both eyes was stable. Following MD, optometry was performed at day 1, 2, 5, 6, 8 and 9. After MD, OKR sensitivity started increasing for undeprived eye and stabilized till day 8 of MD. The maximum enhancement was observed till day 3 and then the speed of increase slowed down and ultimately stopped (Fig. 16).

Fig. 16: Effect of MD and daily optometry on OKR sensitivity (MD-OPT-MRI).
(A) Visual acuity through undeprived right was increased gradually and reached a maximum over 8d of MD. Gaps indicate the time points where no measurement was performed. (B) Effect of MD on contrast sensitivity was similar: sensitivity increased from baseline over 9d of MD (as no measurement was performed at 10d of MD). Data represented as mean ± SEM.

For the second approach, we characterized the effect of MD on VA sensitivity without daily testing with optometer (MD-MRI). Optometry was performed to measure VA sensitivity of undeprived right eye at 10d of MD (Fig. 3B). Then, the left eye of all MD rats was re-opened and VA of left eye was measured to calculate the change in VA of undeprived right eye as the baseline OKR of both eyes were found same in test study and first approach (MD-OPT-MRI) and a significant increase in VA of undeprived right eye was observed (Fig. 17).

**Fig. 17: Effect of MD without daily optometry on VA sensitivity (MD-MRI).**

Visual acuity through undeprived right eye was increased from baseline over 10d of MD. Data represented as mean ± SEM
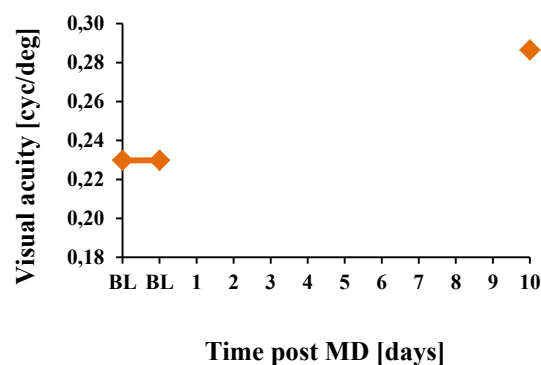
Further, it was observed that the VA increase following MD was significantly more when MD was coupled with daily optometry (Fig. 18).

Fig. 18: Effect of daily optometry on visual acuity enhancement following MD.

The increase in the visual acuity through undeprived right eye with daily optometry (MD-OPT-MRI, n=24) was 37% and without optometry (MD-MRI, n=10) was 24%. Optometry has significantly enhanced the VA increase following MD. (*p = <0.001, Mann-Whitney Rank Sum Test).
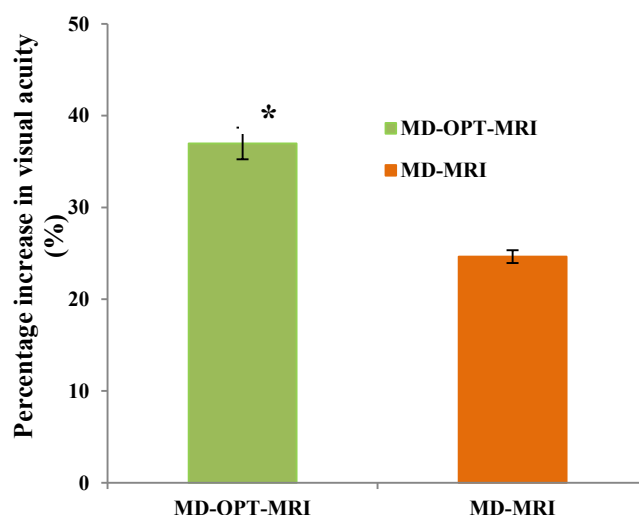
For the third approach, we characterized the effect of daily testing with optometer on VA and contrast sensitivity without MD (OPT-MRI). The baseline measurement for both eyes was stable. Following baseline MRI, the optometry was performed at day 1, 2, 5, 6, 8 and 9 (Fig. 3C). No enhancement in OKR sensitivity was observed for any eye over the entire period. Data represented as taking a mean of both eyes. (Fig. 19)
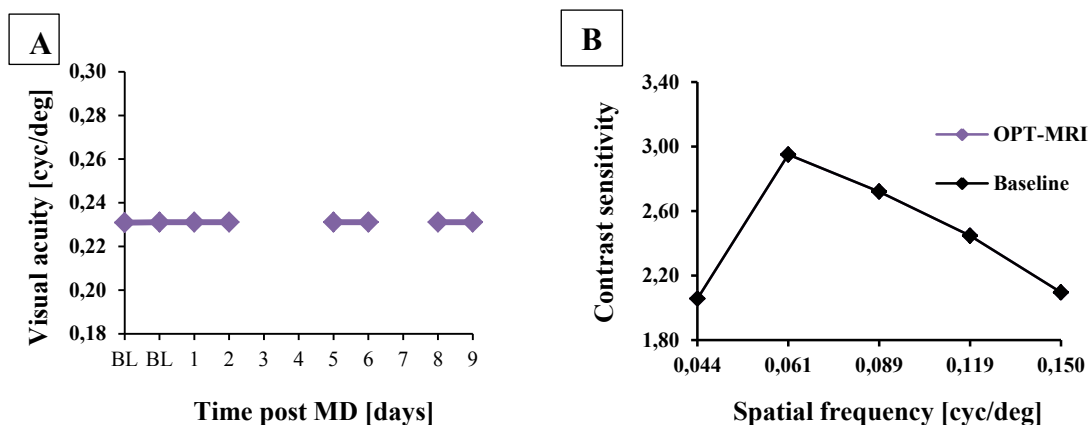
Fig. 19: Effect of daily optometry on OKR sensitivity (OPT-MRI).

(A) Mean of visual acuity through both eyes was remained unchanged after daily optometry. Gaps indicate the time points where no measurement with optometer was performed. (B) The effect of daily optometry on mean contrast sensitivity was similar: no change in sensitivity was observed relative to baseline over 9d of study. Data represented as mean ± SEM.

Cross-sectional study

For cross-sectional study, we have included two groups of MD i.e. MD-3d and MD-10d where the effect of MD on OKR sensitivity was observed for 3 and 10days time duration successively (Fig. 4). No change in baseline measurements was seen. After MD, an enhanced VA and contrast sensitivity was observed for the entire period of MD for MD-3d rats (Fig. 20) and for MD-10d rats, the enhancement in OKR was
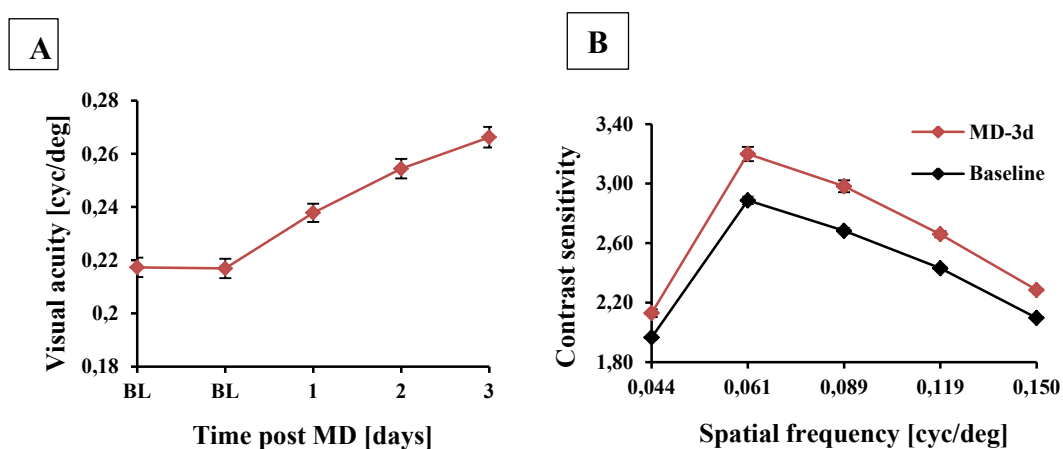
Fig. 20: Effect of 3d MD on OKR sensitivity.

(A) Visual acuity through undeprived right eye was increased gradually over 3d of MD. (B) Effect of MD on contrast sensitivity was similar: sensitivity increased from baseline over 3d of MD. Data represented as mean ± SEM.

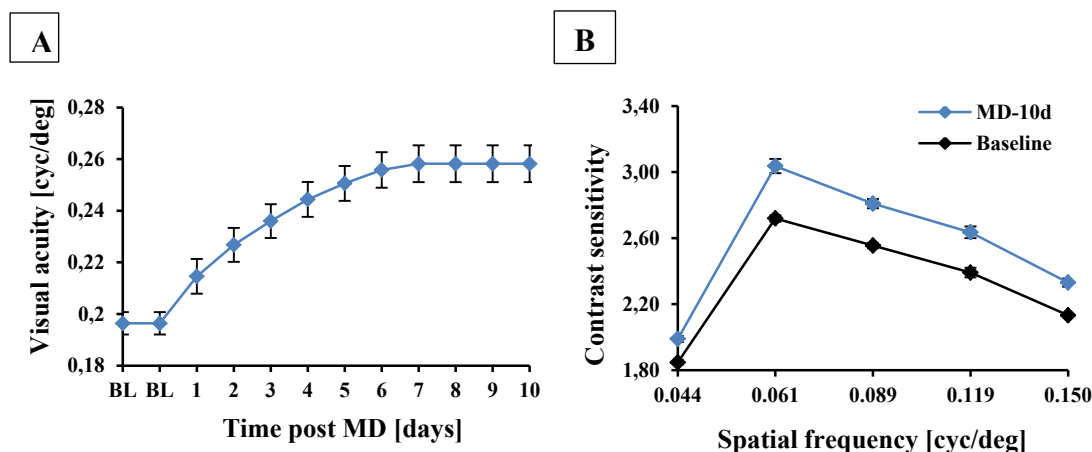33

stabilized till day 6 to 7 of MD (Fig. 21).

Fig. 21: Effect of 10d MD on OKR sensitivity.

(A) Visual acuity through undeprived right eye was increased gradually and reached a maximum over 6 to 7d of MD. (B) Effect of MD on contrast sensitivity was similar: sensitivity increased from baseline over 10d of MD. Data represented as mean ± SEM.

Time course for change in OKR sensitivity following MD

Overall we have observed 22-37% enhancement in VA and 8-17% increase in contrast sensitivity of undeprived right eye depending on the duration (3-10days). The increase in contrast sensitivity also depended on spatial frequency value used for contrast sensitivity measurement and the least enhancement was observed for bordered spatial frequencies (0.150 and 0.44 cyc/deg). For cross-sectional experiments (test study for 7days and MD-10d), we observed maximum OKR sensitivity increase (20% in VA and 10% in contrast sensitivity) during initial 3days. Afterward, the enhancement slowed down and ultimately OKR threshold became stable till 7d. During longitudinal study (MD-OPT-MRI), we found an increase of 37% in VA and on average 12% in contrast sensitivity following MD. Since optometry was skipped for 3, 7 and 10d, a slightly different pattern of increase in OKR sensitivity was observed. The maximum enhancement in OKR sensitivity was observed for initial 2days (24% in VA and 7% increase in contrast sensitivity) and OKR threshold became stable till 8d.

4.2. Structural brain changes detected by DBM

To screen for MD-induced macro-structural brain plasticity, MR images were analyzed by DBM. We observed similar structural changes for MD-OPT-MRI and

MD-MRI groups, so we have pooled the data as MD group. Similarly, the structural profile OPT-MRI group matched with control rats and was pooled together as controls. For MD rats, we have found the temporal volume changes in the left primary binocular visual cortex (V1B), right secondary visual cortex (V2L), left lateral entorhinal cortex (LEnt) and right paramedian lobule (PML) (Fig. 22B; data are presented as percentage volume changes in MD-animals normalized to the mean of controls) (Tab. 7). The left LEnt showed transient GM swelling (6%) which recovered to baseline at the end of the observation period. A similar dynamic was found in the left V1B (6%). However, the early GM swelling in V1B shifted into late shrinkage (3.7%). A late GM shrinkage was also found in the right V2L (2.8%). In contrast to the patterns in LEnt, V1B and V2L, we have observed late GM swelling in the left cerebellar PML (4.8%) (Fig. 22C).

4.3. Correlation of DBM and optokinetic response.

The daily increase in VA represents the rate of visual perception learning (Fig. 22A). In order to find out a correlation between learning rate and brain structural changes, the difference in percentage volume changes between MD and controls (% points) was plotted against the learning rate. We observed that the temporal pattern of volume change observed in LEnt is in best accordance with the rate of visual perception learning. The swelling appeared during visual acuity improvement whereas it reversed to baseline level as soon as the visual acuity reached the maximal value. No shrinkage, which possibly represents a secondary manifestation of sensory deprivation in the visual areas, was observed in LEnt (Fig. 22D). Therefore, we selected the LEnt for further cross-sectional analyses. Additionally, we included primary auditory cortex (Au1) as a control region for each cross-sectional analysis.
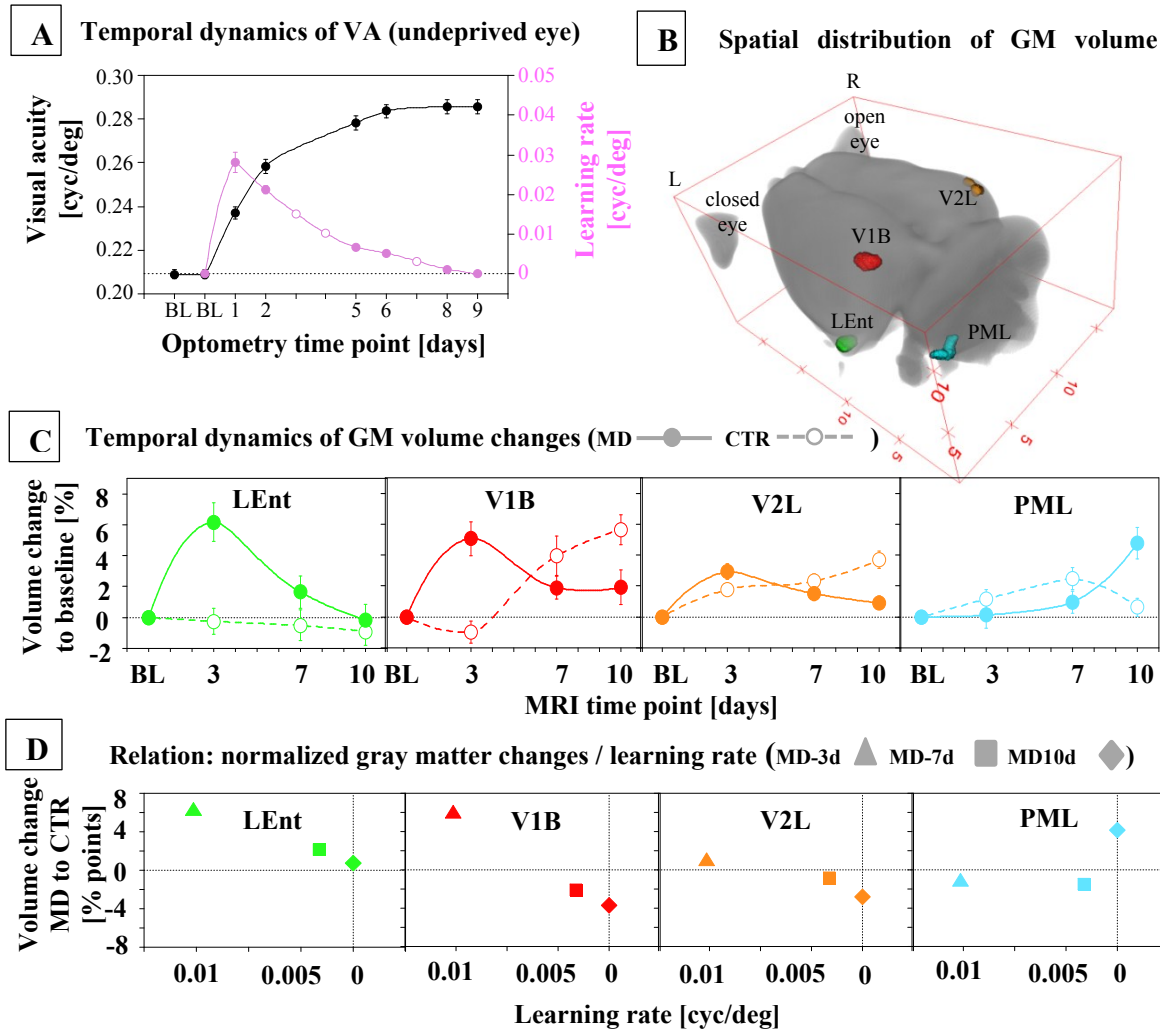
A Temporal dynamics of VA (undeprived eye)

B Spatial distribution of GM volume

C Temporal dynamics of GM volume changes (MD —●— CTR --○--)

D Relation: normalized gray matter changes / learning rate (MD-3d ▲ MD-7d ■ MD10d ◆)

Fig. 22: DBM and learning results.

(A) Learning results: The visual acuity (VA) threshold of undeprived right eye was significantly increased over the period of MD ($p < 0.001$, 1-way repeated measures ANOVA on ranks, Tukey HSD). The Learning rate (daily increase in VA threshold) was maximum at day 1 following MD and then gradually decreased. (B) DBM analysis indicates the volume changes in the ipsilateral lateral entorhinal cortex (LEnt), primary visual cortex (V1B) paramedian lobule (PML) and contralateral secondary visual cortex (V2L) to closed eye in MD rats. (d) The temporal dynamics of GM volume changes during MD shows in MD rats (n = 24): at 3d a significant transient expansion in LEnt and V1B relative to baseline and aged match control rats (n = 23); at 10d a significant expansion in PML relative to baseline and controls, a tendency of increased volume in LEnt and significant shrinkage in V1B and V2L with respect to control rats ($p < 0.05$, one way ANOVA, FWE). (D) When normalized GM changes (difference in volume of MD and control rats) were plotted against learning rate, a positive correlation at all-time points (MD-3, 7 and 10) was seen only for LEnt.

4.4. Density of newly born nuclei and matured astrocytes

Given the assumption that angio as well as neuron/glial genesis may contribute to the volume expansion detected with DBM, we addressed this question using 5′-Bromodeoxyuridine (BrdU) labelled nuclei of newly born cells which were counted to analyze the proliferation in control (n = 6) and MD-3d (n = 7). Although no significant difference was found between the groups for LEnt of each hemisphere but a trend towards the reduction in the density of newly born cells was observed in ipsilateral LEnt of MD-3d rats (p = 0.16, student t-test), (Fig. 23A), (Tab. 8) supporting the observation that volume changes in GM affect the cell density (Vernon et al., 2014). No such trends had been seen in Au1 (Fig. 23B) (Tab. 8).

Fig. 23: Effect of MD on newly born nuclei.

Graphs present the density of BrdU$^+$ cells in monocularly deprived (MD-3d: n=7) and control (CTR: n=6) rats in ipsi (Ip) and contralateral (Co) LEnt (A) and Au1 (B). No significant difference was seen between the groups (p > 0.4, student t-test) and among the hemispheres (p = > 0.5, paired t-test) for both LEnt and Au1 but a trend towards reduction in density of newly born nuclei was observed in ipsilateral LEnt of MD-3d rats. Data represented as mean ± SEM.
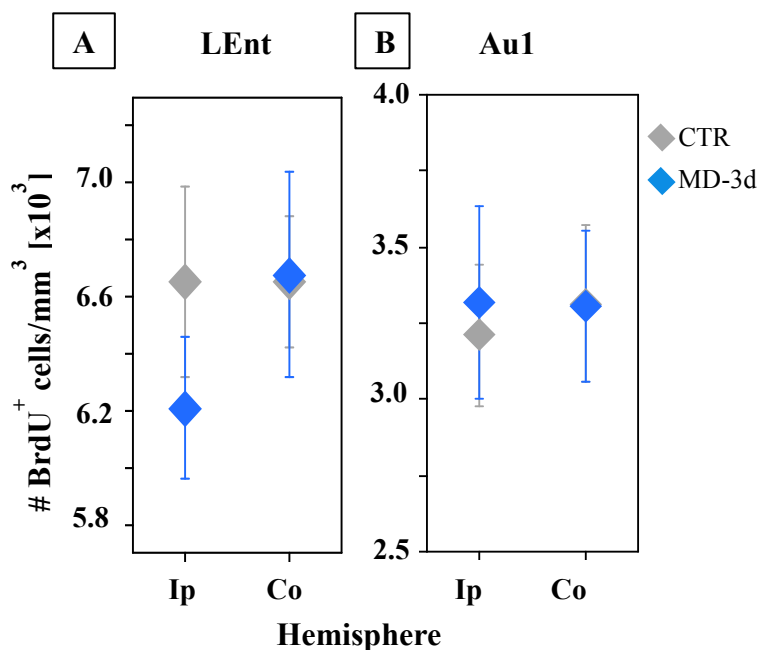

For additional confirmation, we then applied the analogous approach for analyzing the astrocytic density using S100ß stained astrocytes. The density was compared in LEnt and Au1 of each hemisphere among control (n = 10), MD-3d (n = 5) and MD-10d (n = 6) rats. In ipsilateral LEnt, counting revealed that the mean density of astrocytes (number of astrocytes per mm³) in control rats was 35309.3 ± 516.6, in MD-3d was 33566.4 ± 920.4 and in MD-10d was 35431.2 ± 492.7. A significant reduction in density was observed in MD-3d rats relative to both control and MD-

10d rats ($p < 0.05$, Student t-test) (Fig. 24A) (Tab. 9), No such changes had been seen in Au1 (Fig. 24B) (Tab. 9).

Fig. 24; Effect of MD on S100ß⁺ astrocytes.

Graphs present the density of S100ß⁺ astrocytes in monocularly deprived (MD) and control (CTR) rats in ipsi (Ip) and contralateral (Co) LEnt (A) and Au1 (B). A significant reduction in density of S100ß⁺ astrocytes was observed in ipsilateral LEnt in MD-3d rats (n=5) relative to both control (n=10) and MD-10d rats (n=6) ($p < 0.05$, Student t-test). Data represented as mean ± SEM.
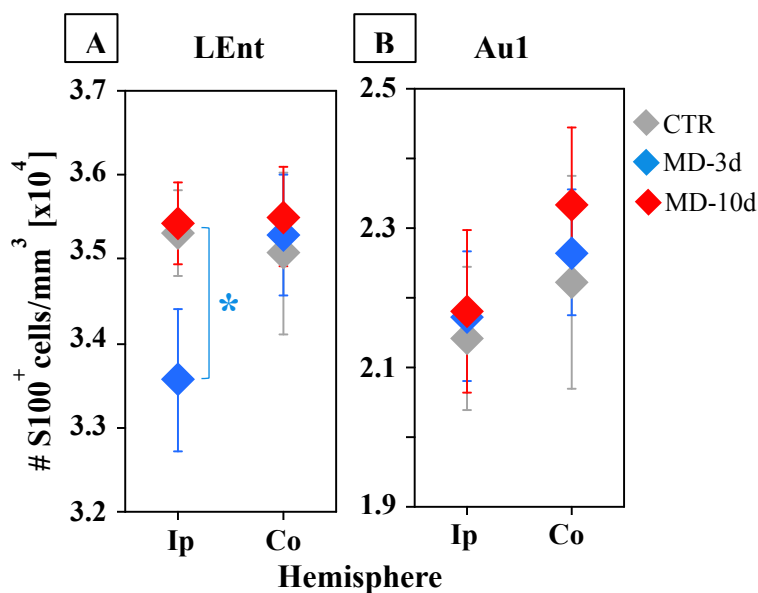
This reduction in the density of BrdU⁺ and S100ß⁺ cells reflects the morphometry based volume expansion at the histological level in LEnt.

## 4.5. Density of matured and immatured spines

Golgi stained neurons were used to determine the quantitative changes in the densities of small, medium, large, mushroom and spiny spines along the second and third orders of basal dendrites of pyramidal neurons in the outer layer (II/III) of LEnt and middle layers (III/IV) of AU1 cortex in MD-3days (n= 4 rats), MD-10days (n= 4 rats) and control (n= 5 rats). The analysis was performed on 3 basal dendrites/neuron and 3 neurons/rat. Once the branch order was determined for basal dendrite, the spine count for each type was carried out separately at higher magnification (using 100X objective).

In ipsilateral LEnt, a significant increase in the density of the medium, large, mushroom and spiny spines was seen in both MD-3d and MD-10d groups ($p < 0.01$, 1-way ANOVA, Tukey HSD). The medium spines were increased significantly for

both MD groups ($p < 0.001$, 1-way ANOVA, Tukey HSD) but in MD- 3d rats the density was more than MD-10days rats ($p < 0.05$, 1-way ANOVA, Tukey HSD). The density of small spines was increased significantly in MD-3d ($p < 0.001$, 1-way ANOVA, Tukey HSD) but not in MD-10d rats ($p = 0.14$, 1-way ANOVA, Tukey HSD). No significant change in density was observed for any type of spines among the groups for right LEnt ($p > 0.3$, 1-way ANOVA, Tukey HSD) (Tab. 10). The group-wise inter-hemispheric comparison revealed the same pattern of increase in spine density in MD-3d as well as in MD-10d rats ($p < 0.05$, Paired t-test) (Fig. 27), (Tab. 12). The overall increase in spine density was 57% in MD-3d and 30% in MD-10d and 52% enhanced spine pool consisting on matured spines persisted (Fig. 25, 26D).

Fig. 25: Percentage change in spine density of MD rates relative to control rats.

Spine density in control (CTR) is equivalent to 100%, in MD-3d group 157% and in MD-10d group 130%. The increase in spine density was 57% in MD-3d group and 30% in MD-10d relative to CTR.
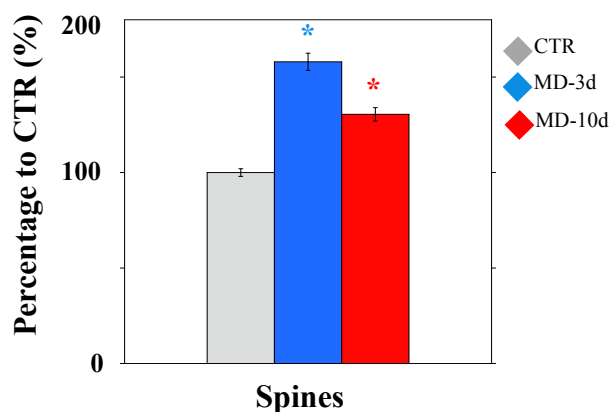
The spine density in Au1 cortex was neither significantly changed among the groups (MD-3days vs MD 10-days vs Control) ($p > 0.1$, 1-way ANOVA, Tukey HSD) nor between the hemispheres (Left vs Right) ($p > 0.1$, Paired t-test) within individual groups (Fig. 27), (Tab. 11, 12).
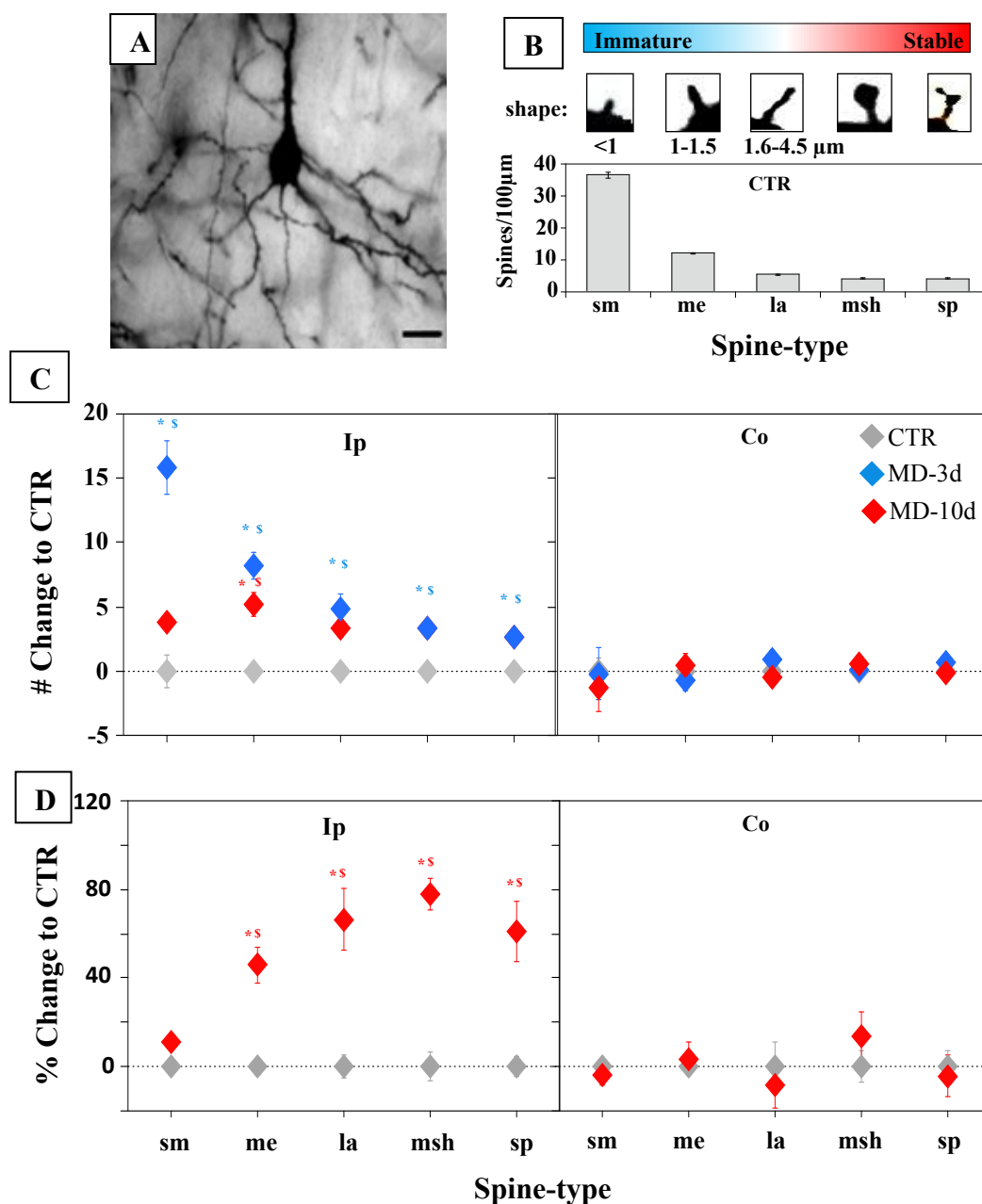
Fig. 26: Effect of MD on spine density of basal dendrites of pyramidal neurons in LEnt.

Golgi-stained neurons were used for estimating the changes in spine density. (A) Photomicrograph of a Golgi-stained pyramidal neuron. The analysis was performed on 2nd and 3rd orders of basal dendrites. Scale bar: 20µm. (B) Spine characterization in control rats. Graph presents the density of different types of spines. CTR (control), sm (small), md (medium), large (la), msh (mushroom), sp (spiny). (C) Graph presents the change in the density (#: number of spines per 100µm) of different types of spines in monocularly deprived (MD) rats relative to CTR rats (The density of spines in CTR is taken equivalent to 0). (D) Graph presents the percentage (%) change in density of different types of spines in MD-10d rats with respect to CTR rats. Graphs (C) and (D) indicate that the shift in the density of immatured (Sm) spines was transient while matured and stable spines stayed permanently (MD-3d: n=4, MD-3d: n=4, Control: n=5; 3 neurons/animal; 3 dendrites/neuron (*$p < 0.05$, one-way ANOVA, Tukey HSD. $^{\$}p < 0.05$ ipsi- vs. contralateral, paired t-test). Data represented as mean ± SEM.
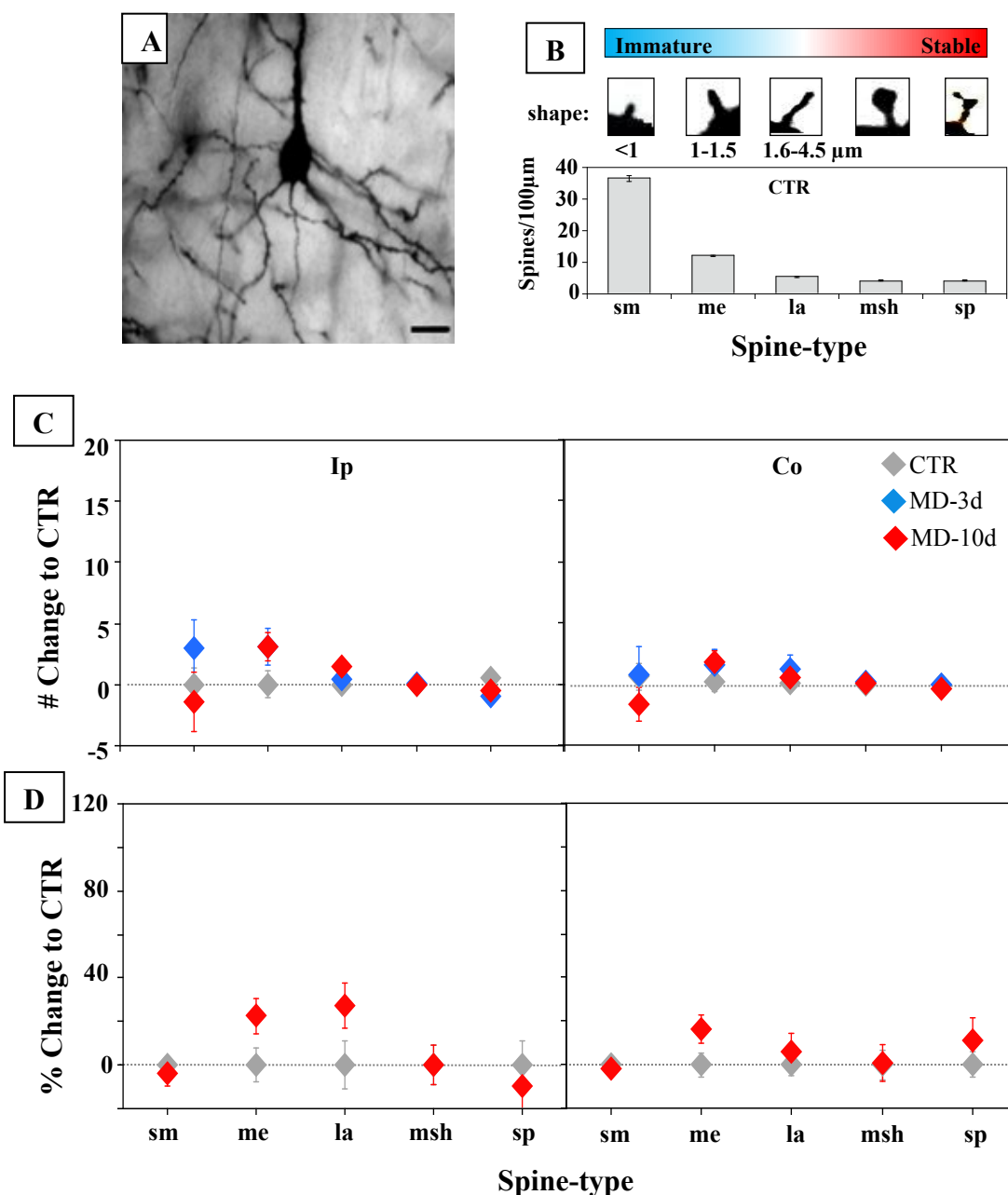
40

Fig. 27: Effect of MD on spine density of basal dendrites of pyramidal neurons in Au1.

Golgi-stained neurons were used for estimating the changes in spine density. (A) Photomicrograph of a Golgi-stained pyramidal neuron. The analysis was performed on 2nd and 3rd orders of basal dendrites. Scale bar: 20µm. (B) Spine characterization in control rats. Graph presents the density of different types of spines. CTR (control), sm (small), md (medium), large (la), msh (mushroom), sp (spiny). (C) Graph presents the change in the density (#: number of spines per 100µm) of different types of spines in monocularly deprived (MD) rats relative to CTR rats (The density of spines in CTR is taken equivalent to 0). (D) Graph presents the percentage (%) change in density of different types of spines in MD-10d rats with respect to CTR rats. Graphs (C) and (D) indicate no significant change in density of immatured (Sm) and matured and stable spines in Au1 (MD-3d: n=4, MD-3d: n=4, Control: n=5; 3 neurons/animal; 3 dendrites/neuron (*$p > 0.1$, one-way ANOVA, Tukey HSD. $^{\$}p > 0.1$ ipsi- vs contralateral, paired t-test). Data represented as mean ± SEM.

4.6. Morphological changes in astrocytes

We quantified and compared the morphology of astrocytes by Sholl analysis (Dall'Oglio et al., 2008; Sholl, 1953; Viola et al., 2009) using GFAP stained astrocytes in LEnt and Au1 of both hemispheres of control, MD-3d and MD-10d groups (n = 42 Astrocytes from 6 rats/each group). For Ipsilateral LEnt, the quantification revealed that the mean number of intersections (a measure of complexity) in control rats was 18.8 ± 0.4, in MD-3d was 16.1 ± 0.4 and in MD-10d was 21.4 ± 0.5. Statistical analysis indicated that the complexity of astrocytes is significantly reduced in MD-3d rats but enhanced in MD-10days rats ($p < 0.001$, 1-way ANOVA, Tukey HSD). No change was observed among the groups for contralateral hemisphere ($p > 0.1$, 1-way ANOVA, Tukey HSD). Besides, a group-wise inter-hemispheric comparison also confirmed the reduced complexity in MD-3d and increased complexity in MD-10d rats ($p < 0.001$, Paired t-test) (Fig. 28A, C) (Tab. 13).

The astrocytic complexity in Au1 cortex was neither significantly changed among the groups (MD-3days vs MD-10days vs Control) ($p > 0.3$, 1-way ANOVA, Tukey HSD) nor between the hemispheres ($p > 0.2$, Paired t-test) (Left vs Right) within individual groups (Fig. 28B, D) (Tab. 13).

In order to check that the change in complexity of astrocytes was either due to primary or ramified processes, the mean number of primary processes was also quantified employing the same GFAP stained astrocytes. No significant changes were observed in mean number of primary processes among the groups ($p > 0.3$, 1-way ANOVA, Tukey HSD) and also between the hemispheres within individual group ($p > 0.2$, Paired t-test) (Tab. 14) for both LEnt (Fig. 28E) and Au1(Fig. 28F) .
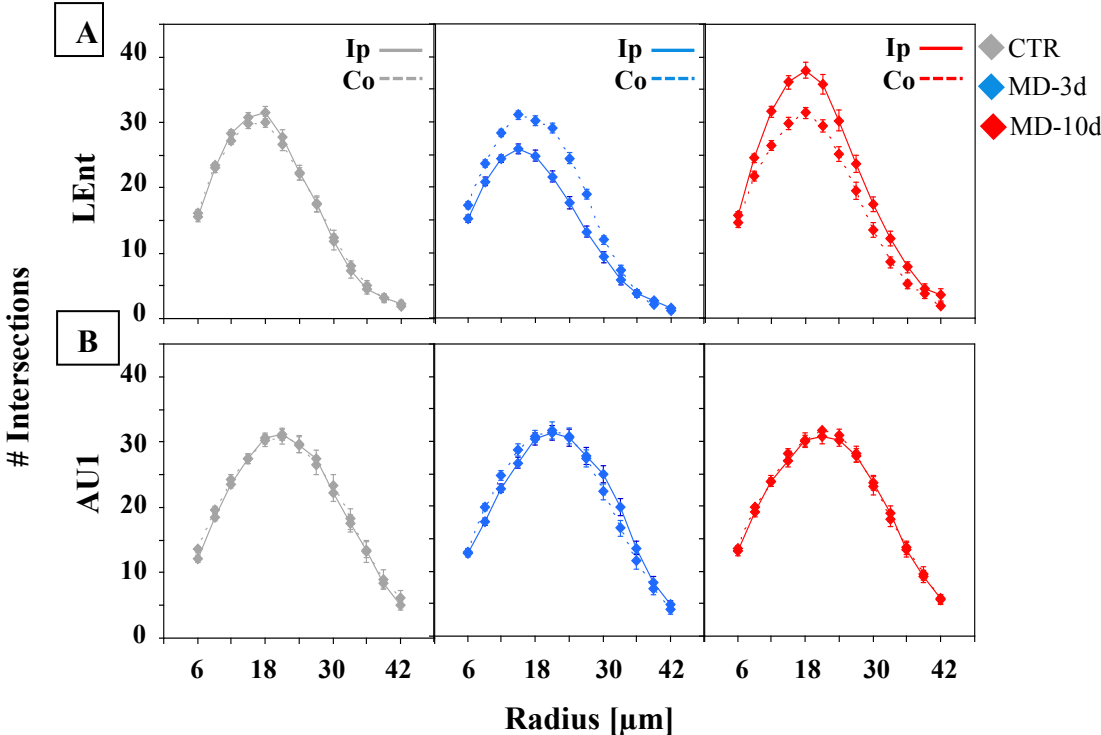
Fig. 28: Effect of MD on the morphology of astrocytes.

The complexity of astrocytic cytoskeleton was analyzed by performing the Sholl analysis on glial fibrillary acidic protein (GFAP) stained astrocytes in LEnt (lateral entorhinal cortex) and Au1 of Ip (ipsilateral) and Co (contralateral) hemispheres. Graphs (A) number of intersections (C) mean number of intersections present that in ipsilateral LEnt complexity of astrocytic cytoskeleton was reduced in MD-3d but increased in MD-10d (n=42 astrocytes from 6 rats/each group. *$p < 0.001$, one-way ANOVA, Tukey HSD. ${}^{\$}p < 0.001$ ipsi- vs contralateral, paired t-test. Graphs (B) number of intersections (D) mean number of intersections in Au1. Graphs (E) and (F) presents number of primary processes of the same astrocytes used for Sholl anaysis in LEnt and Au1 respectively. No significant change was seen among the groups and (*$p > 0.3$, one way ANOVA, Tukey HSD) and between hemispheres (${}^{\$}p > 0.2$ ipsi- vs. contralateral paired t-test) for both LEnt and Au1. Data represented as mean ± SEM.
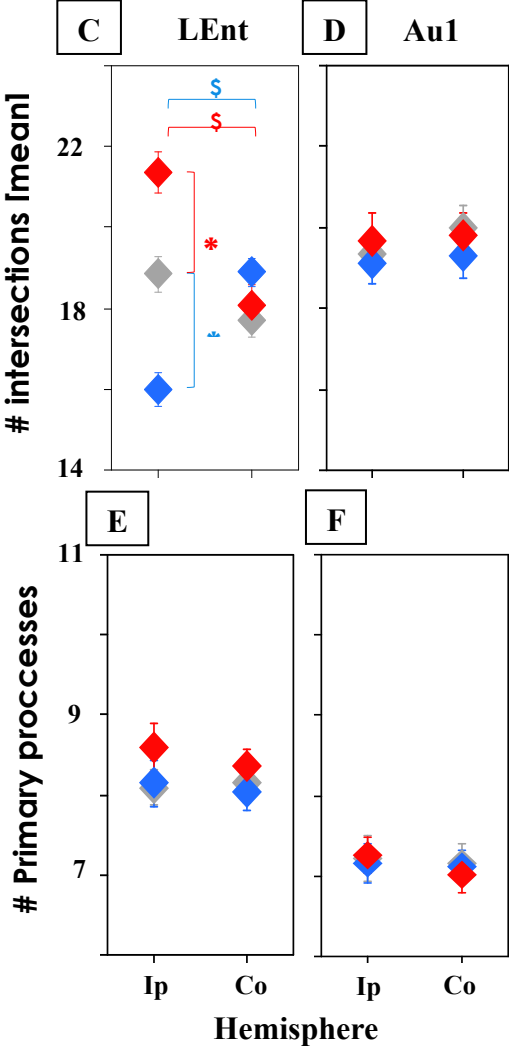
4.7. Enlargement of astrocytes

The volume of astrocytes was measured and compared bilaterally in LEnt of control (n = 5), MD-3d (n = 7) and MD-10d (n = 7) rats using Golgi-impregnated astrocytes. For ipsilateral LEnt, the mean volume in control rats was 1534.7 ± 65.8, in MD-3d was 2305.2 ± 50.2 and MD-10d was 1706.7 ± 36. The volume of astrocytes was found to be increased in ipsilateral LEnt by 50% in MD-3d and 11% in MD-10d rats ($p < 0.001$, 1-way ANOVA, Tukey HSD). No significant change was observed among the groups in contralateral hemisphere ($p > 0.5$, 1-way ANOVA, Tukey HSD). The enlargement of astrocytes in LEnt in both Md-3d and 10d was further validated via group-wise inter-hemispheric comparison ($p < 0.01$, Paired t-test) (Fig. 29A) (Tab. 15).

**Fig. 29: Effect of MD on the volume of astrocytes.**
Golgi stained astrocytes were used to analyze the volume of individual astrocytes. Graphs present the mean volume of astrocytes in monocularly deprived (MD) and control (CTR) rats in ipsi (Ip) and contralateral (Co) LEnt (b) and Au1 (c). The volume of astrocytes in ipsilateral LEnt in Md-3d (n=7) was significantly increased in comparison to both MD-10d (n=7) and control (n=5) (*$p < 0.001$, one way ANOVA, Tukey HSD. $^{\$}p$ <0.01 ipsi- vs contralateral; paired t-test). No significant difference was seen for Au1 (*$p > 0.1$, one-way ANOVA, Tukey HSD. $^{\$}p > 0.2$ ipsi- vs. contralateral; paired t-test). Data represented as mean $\pm$ SEM.
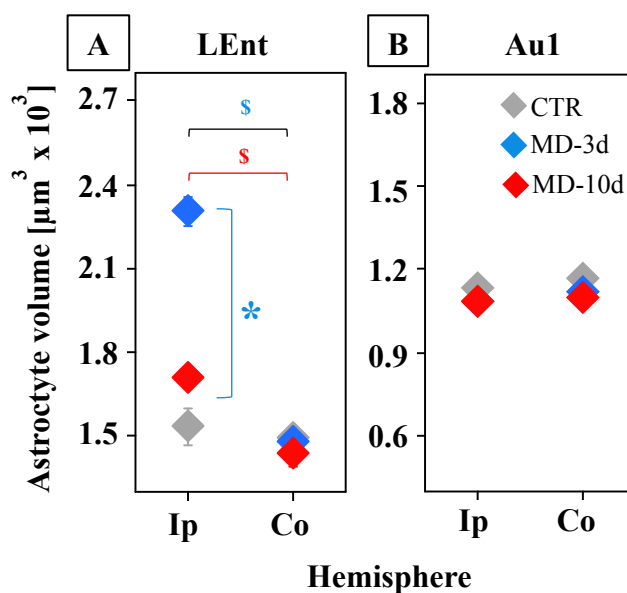
Next, we assessed the swelling of astrocytic soma using S100ß stained slices in LEnt and Au1 of both hemispheres. In ipsilateral LEnt mean volume of the soma was 330.81 ± 6.31 for control rats (n = 10), 383.94 ± 16.59 for MD-3d (n = 5) and 327.20 ± 9.57 for MD-10d (n = 6) rats. The data indicates 19.5% increase in MD-3d rats ($p < 0.01$, 1-way ANOVA, Tukey HSD). No increase was seen in MD-10d rats and also for contralateral LEnt ($p > 0.1$, 1-way ANOVA, Tukey HSD) (Fig. 30A) (Tab. 16). Additional group-wise inter-hemispheric comparison also fortified significant enlargement of astrocytic cell body in MD-3d rats ($p = 0.001$, Paired t-test).

Fig. 30: Effect of MD on the volume of astrocytic soma.

S100ß stained astrocytes were employed to analyze the volume of astrocytic soma. Graph presents the volume of astrocytic soma in monocularly deprived (MD) and control (CTR) rats in ipsi (ip) and contralateral (co) hemispheres of LEnt (A) and Au1 (B). The volume of astrocytic soma in ipsilateral LEnt in Md-3d (n=5) was significantly increased relative to MD-10d (n=6) and control (n=10) (*$p < 0.01$, one way ANOVA, Tukey HSD. $^{\$}p = 0.001$ ipsi- vs. contralateral; paired t-test). No significant difference was seen for Au1 (*$p > 0.7$, one way ANOVA, Tukey HSD. $^{\$}p > 0.4$ ipsi- vs contralateral; paired t-test). Data represented as mean ± SEM.
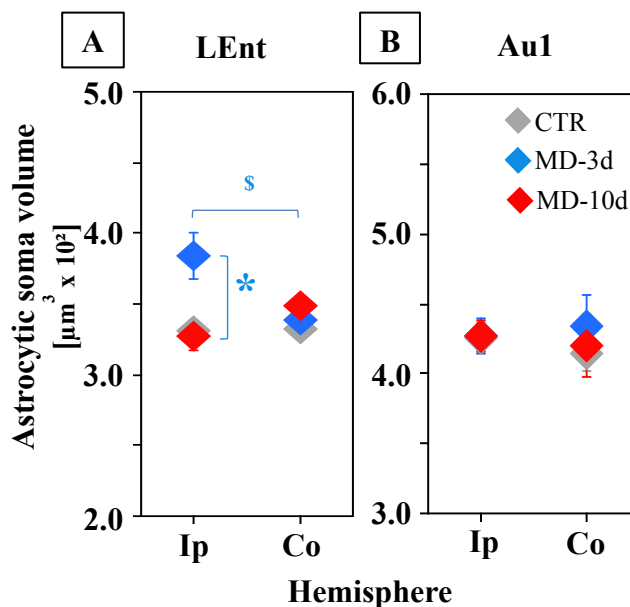

Further in Au1 cortex, the volume of astrocytes and astrocytic soma was neither significantly changed among the groups (MD-3days vs MD-10days vs Control) ($p > 0.1$, 1-way ANOVA, Tukey HSD) nor between the hemispheres (Left vs Right) ($p > 0.2$, Paired t-test) within individual groups (Fig. 29, 30B) (Tab. 15, 16).

4.8. Arc expression

The Arc expression was measured by quantifying the density of Arc^{+} cells for estimation of neuronal activation (Guzowski et al., 1999) and synaptic plasticity (Gao et al., 2010; Hayashi et al., 2012; Shepherd et al., 2006). We have compared the density of Arc[+] in LEnt and Au1 of each hemisphere among control (n = 8), MD-3d (n = 5) and MD-10d (n = 5) rats. Quantification revealed the mean number of Arc^{+} cells in ipsilateral LEnt in control rats was 90454.5 ± 5409.1, in MD-3d was 114520.2 ± 2717.3 and in MD-10d was 93013.5 ± 4352.3. The number of Arc^{+} cells in MD-3d group was significantly increased in the ipsilateral hemisphere ($p < 0.05$, 1-way ANOVA, Tukey HSD) while no significant changes were observed in the contralateral hemisphere and in MD-10d group ($p > 0.2$, 1-way ANOVA, Tukey HSD) (Fig. 31A) (Tab. 17). An additional group-wise inter-hemispheric comparison confirmed increased Arc-expression in MD-3d rats ($p = 0.036$, Paired t-test).

45

Fig. 31: Effect of MD on density of Arc[+].

Graphs present the density of Arc^{+} cells in monocularly deprived (MD) and control (CTR) rats in ipsi (Ip) and contralateral (Co) of LEnt (A) and Au1 (B). The Density of Arc^{+} cells was significantly increased in ipsilateral LEnt of MD-3d rats (n=5) with respect to MD-10d (n=5) and Control (n=8) rats (*p < 0.01, one-way ANOVA, Tukey HSD. $^{\$}p$ < 0.05 ipsi- vs. contralateral; paired t-test). No significant difference was seen for Au1 (*p > 0.8, one way ANOVA, Tukey HSD. $^{\$}p$ > 0.2 ipsi- vs contralateral; paired t-test). Data represented as mean ± SEM.
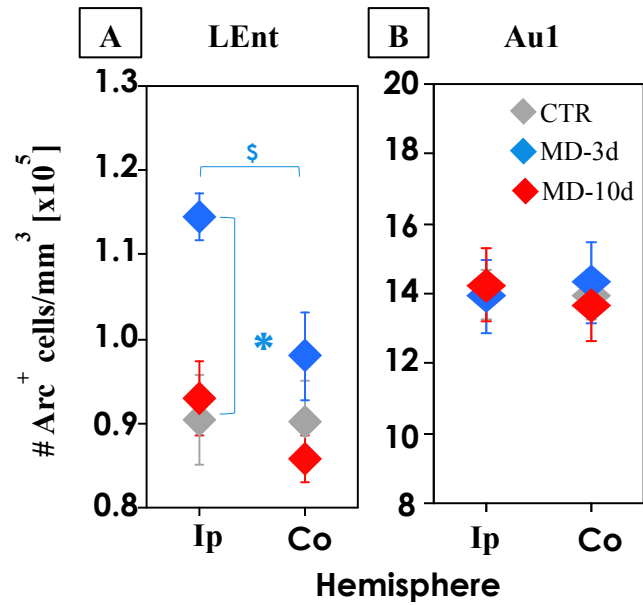
For Au1, no significant changes had been seen in Arc^{+} cells among the groups (p > 0.8, 1-way ANOVA, Tukey HSD) and also between the hemispheres (p > 0.2, Paired t-test) (Fig. 31B) (Tab. 17).

4.9. Correlation of DBM and astrocytic enlargement

While DBM and microscopic analysis of astrocytic enlargement provide a compelling evidence for changes in the brain structure after MD, we sought to further quantify the relationship between DBM and astrocytic enlargement. For this purpose, we first multiplied the mean astrocyte territorial volume (V_M) of control rats (1534.7 μm³, Tab.15) by shrinkage factor (0.35, Section 3.13) and then added the resulting value (V_S) in V_M to calculate the normalized volume of astrocytes (V_N).

$$V_N = V_S + V_M$$

$$V_N = (1534.7 * 0.35) + 1534.7 = 2072 \ \mu m^3 = 2.072 \times 10^{-6} \ mm^3/cell$$

Next, we multiplied the normalized volume of astrocytes (V_N) with the density of astrocytes (N_V) (estimated by stereological counting S100ß[+], 35309.3 cells/mm³, Tab. 9) to quantify the volume fraction of astrocytes (V_F).

$$V_F = V_N * N_V$$

$$V_F = 35309.3 \text{ cells/mm}^3 * 2.072 \text{ x } 10^{-6} \text{ mm}^3/\text{cell} = 0.073$$

The estimated volume fraction of astrocytes in LEnt was 7.3%. Fifty percent increase in astrocytic volume can produce 3.65% swelling in overall volume of LEnt (Fig. 32).
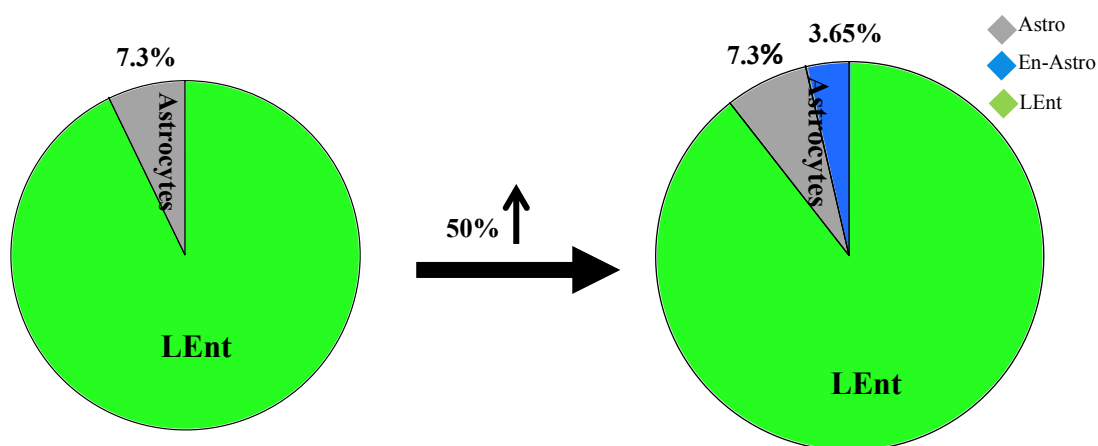
Fig. 32: volume fraction of astrocytes in LEnt.

Astrocytes (Astro) were found to occupy 7.3% volume of LEnt. 50% increase in astrocytic territory (En-Astro) could produce 3.65% increase in the volume of LEnt.

Via DBM analysis, we have found 6.1% swelling in LEnt and astrocytic enlargement contributed 60% to produce this GM swelling (Fig. 33).

Fig. 33: Contribution of astrocytic enlargement in GM swelling of LEnt.

The enlargement of astrocytic territory (En-Astro) contributed 60% to produce GM swelling in LEnt detected by MRI-DBM analysis at 3rd of MD.
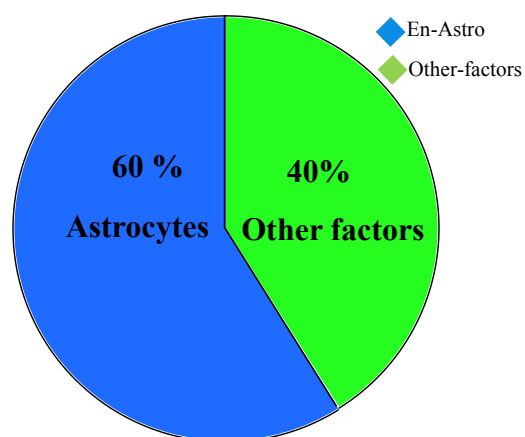
5. Discussion

Monocular deprivation (MD) complemented by MRI and microscopic analyses enabled us to characterize and relate the structural and functional basis of perceptual learning. We found that MD of left eye resulted in visual perception learning of undeprived right eye [measured as an increase in visual acuity (VA) and contrast sensitivity (Greifzu et al., 2011; Lehmann and Löwel, 2008; Prusky et al., 2006)] and temporal volume changes in the visual cortex (V1B, V2L), medial temporal lobe (Lateral entorhinal cortex [LEnt]) and cerebellum (paramedian lobule [PML]). Additionally, it was observed that the learning curve (increase in VA/day) correlated positively only with the time course of volume changes in the medial temporal lobe (MTL) at all-time points, suggesting MTL as a chief brain network for adaptation from binocular to monocular perception. Since the structural and functional brain reorganizations are assumed to be closely linked at every level and the events at neuronal and synaptic level are considered as functional hallmarks of learning, our data revealed astrocytes as the key structural determinant of learning.

Learning and memory are assumed to be registered and stored in the form of functional and structural changes in synaptic efficiency (Black et al., 1990; Hebb, 1949; Kleim et al., 1996). This processing is achieved through several mechanisms that involve generation of coincident rhythmic activity (Huerta and Lisman, 1993), long-term potentiation (LTP) (Whitlock et al., 2006), remodeling of synaptic networks (Chklovskii et al., 2004) and growth of new spines (Yuste and Bonhoeffer, 2001). Spines encompass the postsynaptic portion of glutamatergic synapses (Kasai et al., 2010). Spines are highly dynamic, their generation, turnover and stabilization depend on the sensory input (Comery et al., 1996). An increasing body of evidences specifies the structural rearrangements of spines following exposure to different experiences and learning paradigms (Comery et al., 1996; Keifer et al., 2015; Lamprecht et al., 2006; Lee et al., 2007; Leuner et al., 2003; O'Malley et al., 2000) that complement with synapse formation (Holtmaat et al., 2005; Okabe et al., 2001). A newly generated spine, the physical embodiment of a 'silent synapse,' works as a seed for connection between neurons (Kasai et al., 2010) and repetitive stimuli strengthens these connections and results in maturation and enlargement of spines (De Roo et al., 2008) while the rarely stimulated spines are pruned or eliminated

over time (Holtmaat and Svoboda, 2009; Zhou et al., 2004). Our data support these findings by showing an enlarged pool of both immatured and matured spines during the initial phase but only of matured spines on the later phase of MD (Fig. 26), confirming that stable connections are long lasting (Holtmaat and Svoboda, 2009; Holtmaat et al., 2005; Yasumatsu et al., 2008). However due to technical limitations, we could not analyze the turnover at individual spine level. Recently, it has been shown that dendritic spine density may be the cellular mechanism that underlies the learning associated changes in GM that was detected by voxel-based morphometry (Keifer et al., 2015). But, learning induced structural changes are transient in nature and persist only during the period of learning (Boyke et al., 2008; Draganski et al., 2004; Draganski et al., 2006; Driemeyer et al., 2008; Taubert et al., 2010). If spine rearrangement is the basis of these structural changes in brain, then it must set back to baseline parallel to GM. To answer this question, we quantified spine density during GM swelling and also when it reversed to baseline and an increased spine pool was seen at both time points. However, the density was significantly increased during swelling and only 48% of the enhanced spine pool reversed along with GM (Fig. 25). Since the major part of enhanced spine pool persisted after the reversal of GM swelling, suggesting that spine rearrangement may contribute to but is not necessarily a major cause of morphometry based structural changes.

Carpenter-Hyland et al., (2010) showed an increased Arc expression only in the learning relevant area in rats that had just learned the tone detection task and emphasized Arc as an intrinsic factor of learning. Our results support and augment these findings by showing an elevated Arc expression only in the target region (LEnt) in MD rats (Fig. 31). Additionally, it was observed that enhancement in Arc expression was only restricted during swelling and no change in expression was seen when GM reversed back to baseline, pointing out a strong correlation of Arc expression with learning associated structural changes. Arc is a marker for enhanced neuronal activation (Guzowski et al., 1999) as well as synaptic plasticity (Gao et al., 2010; Hayashi et al., 2012; Shepherd et al., 2006). Astrocytes are considered essential partners in the maintenance of neuronal activity (Pellerin, 2005; Simard and Nedergaard, 2004; Zagami et al., 2005) synapse formation, synaptic transmission, and plasticity (Eroglu and Barres, 2010). To carry out these diverse tasks, astrocytes rely on their elaborate architecture and undergo morphological

changes during synaptic plasticity (Bernardinelli et al., 2014; Hawrylak et al., 1993; Klintsova et al., 1995; Perez-Alvarez et al., 2014) and neuronal activation (Ostby et al., 2009; Ransom et al., 1985). We confirmed these findings by showing temporal astrocytic enlargement analogous to Arc expression. Additionally, it was seen that astrocytic enlargement occurred in parallel to GM structural changes. We observed that increase in the astrocytic volume (astrocytic territory) was ≈50% during swelling and ≈11% when GM set back near to baseline level (Fig. 29). Besides, astrocytes were found to occupy approximately 7.3% of the volume of the EC, a figure consistent with previous estimates of cortex, (Genoud et al., 2006; Jones and Greenough, 1996; Thomas et al., 2012) . Notably, 50% increase in the 7.3% volume fraction can produce 3.65% swelling (Fig. 32). By MRI and DBM, we have found 6.1% swelling in the LEnt (Fig. 22C), hence enlargement of astrocytes explains 60% contribution (Fig. 33), signifying astrocytic hypertrophy underlie the main contributor for the learning associated GM structural changes seen by MRI and DBM and follows from the results by Kleim et al. (2007) who showed hypertrophy of astrocytes only during the period of motor learning but not 28 days later. Astrocytic enlargement might be the outcome of 2 factors (i) swelling following neuronal activation (Ostby et al., 2009) (ii) formation of the new processes to ensheath the newly formed synapses (Viola et al., 2009). Additionally at 10th day of MD, about 0.7% swelling in LEnt still persisted and the 11% enlargement in astrocytes explains this swelling. Astrocytes are star-shaped glia and the soma of a typical astrocyte accounts for only 2% of its total volume whilst the processes (primary, ramified and thin) represent rest (Wolff J, 2004). Around 20% swelling in the astrocytic soma was also observed during the significant GM swelling (Fig. 30), explaining the 40% enlargement of astrocytes during GM swelling. This swelling of cell body may explain the functional relevance of astrocytes during enhanced neuronal activation (as represented by our Arc data, Fig. 31). Astrocytes are responsible for maintaining K^+ homeostasis during neuronal firing. A brief increase in neuronal activity results in a transient increase in K^+ efflux from the neuron to the extra cellular space (ECS) (Ballanyi et al., 1987; Dietzel et al., 1989; Macvicar et al., 2002). The effective clearance of K^+ is essential for normal brain functioning otherwise it will enhance neuronal excitability and increase the probability of epileptic episodes and major sink of excess ECS- K^+ is the surrounding astrocytes (Lux et al., 1986; Somjen, 2004). This influx of potassium is accompanied by anions (Walz and Hertz, 1983) and

causes the set-up of an osmolarity gradient that drives the water from the ECS into the astrocytes (Ransom et al., 1985; Walz and Hinks, 1985) and leads to the astrocytic swelling (Macvicar et al., 2002; Ostby et al., 2009). The astrocytic enlargement may also be contributed by the cytoskeleton monomers, increased expression of synaptogenic molecule that instruct the synapse formation and development (Clarke and Barres, 2013) such as apolipoprotein E (Goritz et al., 2005; Mauch et al., 2001), thrombospondins (Christopherson et al., 2005; Risher and Eroglu, 2012) and hevin (Kucukdereli et al., 2011). However, these synapses are silent (lacking AMPA receptors) and to convert the silent synapses into the functional synapses, astrocytes further secrete glypicans (Allen et al., 2012). As no swelling in the soma was seen after the reversal of GM, so persistent enlargement in EC may solely be due to the formation of new processes, further confirmed by the enhanced ramification of astrocytes analyzed by the cytoskeleton-based Sholl analysis that revealed morphologically simple astrocytes during GM swelling but more complexed after reversal, suggesting astrocytic plasticity during GM volume changes (Fig. 28).

According to the, "tripartite synapse concept" astrocytes are an integral part of synapses (Ho et al., 2011) and enhanced synaptic plasticity demands a counter ramification of astrocytic processes to ensheath the newly formed synapses. The ramification of astrocytic processes requires a reduction in the cytoskeleton content. Glial fibrillary acidic protein (GFAP) along with vimentin constitutes the major cytoskeleton entity of astrocytes (Bignami et al., 1972; Eliasson et al., 1999b; Eng et al., 1971) and gives stability to astrocytic processes (Pekny et al., 1999; Pekny and Wilhelmsson, 2006). GFAP exist as phosphorylated and de-phosphorylated forms in the astrocytes (Middeldorp and Hol, 2011; Rodnight et al., 1997). Only phosphorylated GFAP polymerize with vimentin to make the astrocytic cytoskeleton (Takemura et al., 2002). The phosphorylation of GFAP depends on the Ca^{2+} conc. of astrocyte (Rodnight et al., 1997; Vinade et al., 1997). During activation, neurons generate Ca^{2+} waves in the astrocytes locally (Perea and Araque, 2005; Theodosis et al., 2008) that would dephosphorylate GFAP (Rodnight et al., 1997) and make astrocytic processes flexible (Theodosis et al., 2008) to ramify to give rise the new processes for ensheathing the newly generated synapses and results in morphologically simple astrocytes due to the lack of cytoskeleton during the highly

synaptic period (Missler et al., 1994). After stabilization of neuronal activity, GFAP would rephosphorylate (Rodnight et al., 1997) and polymerize with vimentin to make the cytoskeleton of newly formed astrocytic processes and result in morphologically complex astrocytes (Viola et al., 2009) (Fig. 34). Our data confirm these observations by showing the morphologically simple GFAP stained astrocytes during the neuronal activation and synaptic plasticity but more complexed when the plasticity was over and this complexity is attributed by formation of the ramified processes as no change had been seen in the number of primary processes which directly emerged out of the soma (Fig. 28). . Perez-Alvarez et al. (2014) also showed the structural rearrangements of astrocytic processes during the enhanced synaptic activity. However due to technical limitations, we could analyze only GFAP stained
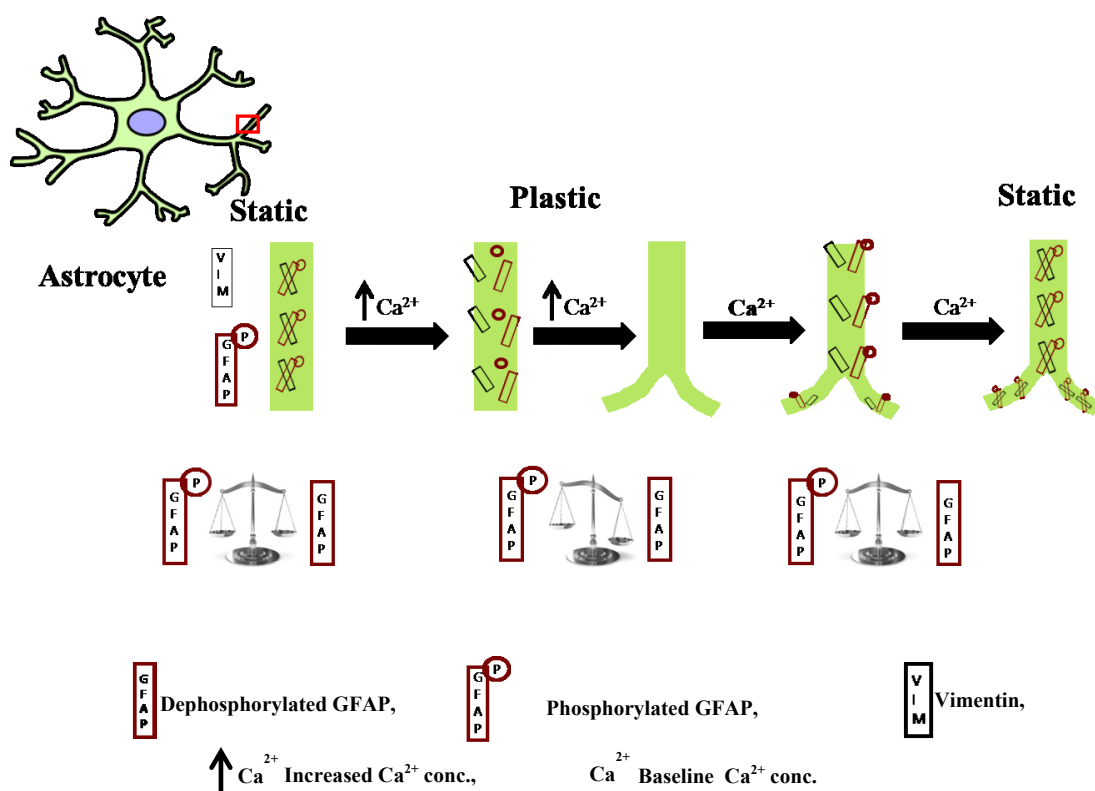

Fig. 34: A proposed model for cytoskeleton plasticity during the ramification of astrocytic processes.

Ca^{2+} regulates the dynamic equilibrium between the phosphorylated and dephosphorylated state of GFAP which in turn determine the cytoskeleton stability. Increased Ca^{2+} concentration (conc.) during enhanced synaptic plasticity leads to dephosphorylation of GFAP which results in deploymerization of intermediate filaments (Vimentin and GFAP). Consequently, astrocytic processes lack cytoskeleton and become flexible to ramify. When synaptic plasticity is over and Ca^{2+} conc. reverses to baseline, GFAP starts phosphorylating and polymerizing with vimentin to form the cytoskeleton entity of newly formed processes which ensheath the recently generated synapses.

astrocytic processes and the magnification of light microscope did not allow us to extend our analysis to the fine astrocytic processes which are in contact with synapses

Learning is also thought to be regulated by neurogenesis in the adult mammalian brain. Accumulating evidence implies that promotion or suppression of hippocampal neurogenesis could correspond with improvement or impairment in learning and memory performances, respectively (Feng et al., 2001; Kempermann et al., 1997; Shors et al., 2002). For instance, enriched environment enhanced neurogenesis (Kempermann et al., 1997), which was paralleled by better spatial learning performance in the Morris water maze task (MWM) in rats (Bruel-Jungerman et al., 2005; Nilsson et al., 1999) as well as in mice (Iso et al., 2007). van Praag et al. (1999) reported that 3-month-old female C57Bl/6 mice subjected to voluntary wheel running for 43–49 days displayed promoted neurogenesis; meanwhile, LTP in the CA1 and their learning performance in the MWM task were both improved. Contrary to these results, we found no link between neurogenesis and learning associated GM swelling in LEnt. To access neurogenesis, the rats were injected with 5′-Bromodeoxyuridine (BrdU) immediately after MD and no alternation in the number of newly born cells was seen (Fig. 23). A possible explanation would be that previous studies focused on hippocampal-dependent learning that is distinctly influenced by newly born neurons (Cameron and Glover, 2015; Kee et al., 2007; Lemaire et al., 2000) while MD associated perceptual learning might not be dependent on hippocampus (as we did not found any structural changes in the hippocampus following MD) and hence showed no correlation with neurogenesis as already analyzed by Gould et al. (1999a) for hippocampal independent learning task. Rats were trained on a cue test in the water maze that does not require the hippocampus, showed no change in the number of newly born cells while a significant increase in the numbers of newly generated neurons was seen for rats subjected to place test in the water maze that requires the hippocampus. Additionally, we observed a trend towards reduction in the density of newly born cells in MD rats during GM swelling. Synonymous results were seen for the density of S100ß stained astrocytes (Fig. 24). Overall, we found a ≈5-6% reduction in the density of BrdU and S100ß stained cells during ≈6% GM swelling in LEnt. Moreover, the variation in the density of S100ß stained cells was reversed along with structural changes in GM. As

previously described, macrostructural brain plasticity correlates with an alternation in the astrocyte density (Vernon et al., 2014), and hence it is reasonable to postulate that the reduction in the cell density represents morphometry based GM structural changes at the histological level.

Learning is a physical phenomenon (Zull, 2002) and is accompanied by a chemical change at the synapse level (Black et al., 1990; Kleim et al., 2002) to reorganize the brain circuits and this remodeling encodes new experiences and enables behavioral change. With advancement in MRI (MRI) and morphometric analysis, it is possible to analyze the learning specific structural reorganization in the brain. People with different expertise and experiences undergo changes in the different areas of brain (Aydin et al., 2007; Gaser and Schlaug, 2003; Maguire et al., 2000; Maguire et al., 2006; Mechelli et al., 2004). Studies with longitudinal morphometry have shown that learning related GM changes can be seen within short duration after initiating the learning and only persist during the period of training (Boyke et al., 2008; Draganski et al., 2004; Draganski et al., 2006; Driemeyer et al., 2008) and confirmed the functional importance of the distinct brain regions during the different phases of learning (Taubert et al., 2010). The learning curve represents an improvement in one's skills and response over the time (Keifer et al., 2015; Kleim et al., 2007; Taubert et al., 2010). We used MD to analyze reorganization in the brain during visual perceptual learning and learning outcome was observed as an enhanced functioning of un-deprived right eye indicated by increased visual acuity and contrast sensitivity (OKR sensitivity) through undeprived eye as reported in the literature (Greifzu et al., 2011; Lehmann and Löwel, 2008; Prusky et al., 2006). Our longitudinal as well as cross-sectional analyses present maximum increase in the OKR sensitivity immediately after MD indicating the importance of the initial phase of MD for the OKR sensitivity enhancement (Fig. 15, 16, 20, 21). Further, it was observed that daily testing with an optometer amplified the VA increase following MD and the increase in VA was significantly more when MD was coupled with daily optometry (Fig. 18) confirming that repetitive exposure to visual stimulus enhanced perceptual learning (Saarinen and Levi, 1995). However, optometry could not induce any change in the OKR sensitivity in the absence of MD (Fig. 19).

The previous studies indicate the role of visual cortex in the OKR plasticity following MD (Greifzu et al., 2011; Lunghi et al., 2015; Prusky et al., 2006).

However, Prusky et al. (2006) removed the visual cortex bilaterally and still observed a slight increase in VA for the initial 2 days following MD, pointing out the role of another brain network specifically for initiating the OKR sensitivity enhancement immediately after MD. We observed temporal volume changes in the visual cortex (V1B, V2L), medial temporal lobe (Lateral entorhinal cortex [LEnt]) and cerebellum (paramedian lobule [PML]) (Fig. 22) According to Zull (2002), learning starts with the gathering of sensory experiences through the sensory cortices which receive input from the surrounding world in the form of vision, hearing, touch, position, smell and taste. The next phase is reflection which involves the integration of the sensory information received during the gathering phase. The reflection phase engages the temporal lobe and without reflection learning will be severed and shallow. The last stage of learning is active testing which is a physical process that allows the brain to make intellectual concrete by translating mental ideas into actions and depends on motor areas (Zull, 2002). MD of the left eye blocked its visual input to the brain and only source for visual stimulus was then right eye, as a result, the corresponding ipsilateral binocular visual cortex (V1B) became activated and this activation was recorded as temporal structural plasticity. The importance of visual cortex in MD-based plasticity has been well-established (Greifzu et al., 2011; Lunghi et al., 2015; Prusky et al., 2006). Subsequently, the brain started reflecting and concentrating on the right eye as a sole source of gathering visual perception from the outside world by engaging the LEnt. This resulted in the transient swelling that was mainly contributed by the astrocytic enlargement; consequently, the OKR sensitivity of right eye increased. LEnt is a key component of the medial temporal lobe (MTL) that was previously studied crucial for learning and memory (Draganski et al., 2006; Ferbinteanu et al., 1999; Murray et al., 2007; Squire et al., 2004). Given from literature evidence, the stimulation of the entorhinal cortex enhanced spatial learning (Suthana et al., 2012). Besides, the entorhinal cortex is a chief gateway to the hippocampus and has been known to play a crucial role in cognition and navigation (Deshmukh and Knierim, 2011; Ferbinteanu et al., 1999; Hafting et al., 2005; Zhu et al., 1995). When the reflection was over and OKR sensitivity became stable, the brain might have decided to restrict itself to the right eye as the visual source, and as a result, the projections from the left eye started deteriorating and resulted in the shrinkage in visual cortices corresponding to the left eye. The next phase was to translate this decision (using right eye to perceive visual stimulus) into

actions and modify the behavior according to monocular vision by initiating reorganization as swelling in PML of cerebellum that has already been found to be important for the motor learning and balancing (Boyden et al., 2004; Christian and Thompson, 2003; Kleim et al., 2007).

6. Conclusion and Outlook

Overall our study established first evidence regarding the complete profile of macrostructural neuroplasticity associated with MD-based visual perceptual learning and showed glial hypertrophy as the major cellular mechanism underlying these structural changes. In summary, over a period of 10 days MD, we found temporal volume changes in the visual cortex (V1B, V2L) medial temporal lobe (Lateral entorhinal cortex [LEnt]) and cerebellum (paramedian lobule [PML]). The enhanced functioning of the un-deprived eye was monitored by measuring the visual acuity and contrast sensitivity and we observed that the learning curve (increase in VA/day) correlated positively only with the time course of volume changes in LEnt at all-time points, on this basis we selected LEnt for elucidating the cellular substrates of GM volumetric changes. Using cross-sectional microscopic analyses, we observed elevated Arc expression, an enhanced spine pool (both immatured and matured spines) and significantly enlarged but morphologically simple astrocytes during GM swelling at the 3rd day of MD that was further accompanied by a reduced density of astrocytes and newly born nuclei. The swelling in LEnt was reversed towards the baseline until the 10th day of MD. The Arc expression, density and hypertrophy of astrocytes also reversed to baseline along with GM but the spine pool of matured spines persisted. Besides, we observed that volume changes in astrocytes went parallel to GM and explained 60% contribution, signifying astrocytic hypertrophy underlie the main factor for the morphometry based GM swelling. Moreover, we did not see any increase in the density of newly born nuclei and astrocytes, representing that angio as well as neuronal and glial genesis did not contribute in DBM based swelling. In addition, analysis of the primary auditory cortex (Au1), which was selected as the control region, showed no significant difference in the microscopic analyses, signifying the observed structural and functional alternations were learning specific. Therefore, by showing a significant correlation between the Arc expression, astrocytic enlargement, and DBM signal in the LEnt, these results fill the huge gap in our current understanding of cellular substrates of morphometry based structural changes.

Additionally, our data allows us to present a theoretical model of the microscopic basis of learning based macroscopic structural rearrangements. MD (External sensory stimulus) invokes perceptual learning in rats that stimulates LEnt. This

stimulation induces neuronal firing and synaptic plasticity (represented by Arc expression) that enhances the spine pool and also demand counter-morphological changes in astrocytes. Consequently, astrocytes become plastic and enlarged and result in the expansion of LEnt (seen via morphometry). When learning is ended, neurons return to baseline activity and the synaptic and spine rearrangement is also over. As a result, astrocytes retain their original volume with increased structural complexity that ultimately leads to a tendency of increased volume of LEnt in MD rats relative to controls (Fig. 35).
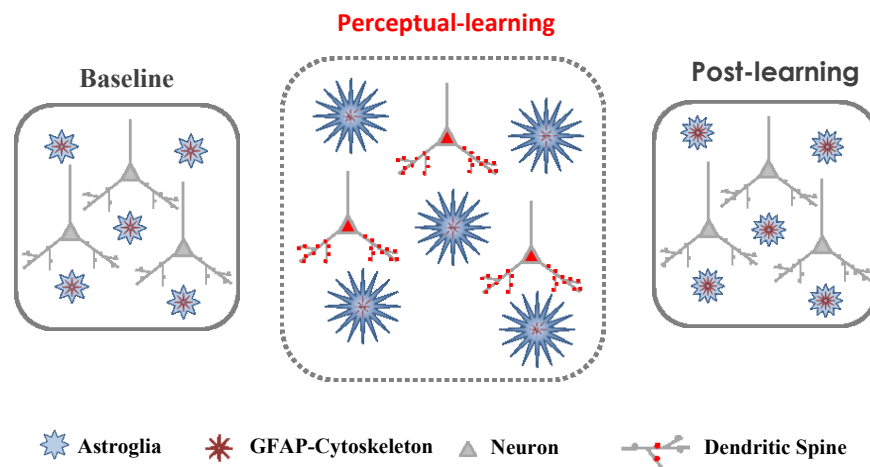

Fig. 35: A proposed theoretical model for cellular underpinnings of the volume changes during monocular deprivation based (MD) perceptual learning.

A schematic representation of cellular structures before MD (Baseline). MD induces sensory learning through the undeprived eye which stimulates LEnt. This stimulation results in neuronal firing and synaptic plasticity. Subsequently spine rearrangement and counter morphological changes in astrocytes take place. Astrocytes swell and results in expansion of LEnt (perceptual learning). When learning through the undeprived eye ends, neurons return to baseline activity, spine and synaptic rearrangement is also over. Consequently, astrocytes retain their original volume with an increased complexity (Post-learning).

Our data present astrocytic enlargement as the major underlying mechanism of transient brain structural plasticity that is detected by MRI and DBM; and swelling of astrocytic soma explains a small proportion of that enlargement, signifying the future elucidation of rearrangement of fine astrocytic processes using super-resolution microscopy (dSTORM) to understand their possible contribution. Simultaneous variations in GM volume, Arc expression (neuronal activation and synaptic plasticity) and astrocytic volume and morphology may explicate a plausible mechanism; follow-up work should focus on providing further evidence for this

correlation, including experimental manipulations to establish causality. Importantly, shift in the astrocytic volume accounts 60% of the story and further attention must be paid towards other possible structural changes that can co-occur, most likely blood vessels dilatation. It is worthy to note that vessels dilate during neuronal firing (Filosa et al., 2006). Understanding of the precise mechanisms of learning associated structural plasticity and its functional correlates leads to the development better strategies to enhance learning capabilities of patients suffering from learning and cognitive defects and hopefully to translate these into improved quality of life.

7. References

al-Ali SY, al-Hussain SM. An ultrastructural study of the phagocytic activity of astrocytes in adult rat brain. Journal of Anatomy, 1996; 188: 257-62.

Allen NJ, Bennett ML, Foo LC, Wang GX, Chakraborty C, Smith SJ, Barres BA. Astrocyte glypicans 4 and 6 promote formation of excitatory synapses via GluA1 AMPA receptors. Nature, 2012; 486: 410-4.

Altman J, Das GD. AUTORADIOGRAPHIC EXAMINATION OF THE EFFECTS OF ENRICHED ENVIRONMENT ON THE RATE OF GLIAL MULTIPLICATION IN THE ADULT RAT BRAIN. Nature, 1964; 204: 1161-3.

Anderson BJ, Li X, Alcantara AA, Isaacs KR, Black JE, Greenough WT. Glial hypertrophy is associated with synaptogenesis following motor-skill learning, but not with angiogenesis following exercise. Glia, 1994; 11: 73-80.

Andrew RD, Labron MW, Boehnke SE, Carnduff L, Kirov SA. Physiological evidence that pyramidal neurons lack functional water channels. Cerebral Cortex, 2007; 17: 787-802.

Aydin K, Ucar A, Oguz KK, Okur OO, Agayev A, Unal Z, Yilmaz S, Ozturk C. Increased gray matter density in the parietal cortex of mathematicians: a voxel-based morphometry study. AJNR. American journal of neuroradiology, 2007; 28: 1859-64.

Ballanyi K, Grafe P, ten Bruggencate G. Ion activities and potassium uptake mechanisms of glial cells in guinea-pig olfactory cortex slices. The Journal of Physiology, 1987; 382: 159-74.

Barnea A, Nottebohm F. Seasonal Recruitment of Hippocampal-Neurons in Adult Free-Ranging Black-Capped Chickadees. P Natl Acad Sci USA, 1994; 91: 11217-21.

Barot SK, Chung A, Kim JJ, Bernstein IL. Functional imaging of stimulus convergence in amygdalar neurons during Pavlovian fear conditioning. PloS one, 2009; 4: e6156.

Bayer SA. Changes in the total number of dentate granule cells in juvenile and adult rats: a correlated volumetric and 3H-thymidine autoradiographic study. Experimental brain research, 1982; 46: 315-23.

Bechmann I, Nitsch R. Astrocytes and microglial cells incorporate degenerating fibers following entorhinal lesion: A light, confocal, and electron microscopical study using a phagocytosis-dependent labeling technique. Glia, 1997; 20: 145-54.

Berbel P, Innocenti GM. The development of the corpus callosum in cats: A light- and electron- microscopic study. The Journal of comparative neurology, 1988; 276: 132-56.

Bernardinelli Y, Randall J, Janett E, Nikonenko I, Konig S, Jones EV, Flores CE, Murai KK, Bochet CG, Holtmaat A, Muller D. Activity-dependent structural plasticity of perisynaptic astrocytic domains promotes excitatory synapse stability. Current biology : CB, 2014; 24: 1679-88.

Bignami A, Eng LF, Dahl D, Uyeda CT. Localization of the glial fibrillary acidic protein in astrocytes by immunofluorescence. Brain Research, 1972; 43: 429-35.

Black JE, Isaacs KR, Anderson BJ, Alcantara AA, Greenough WT. Learning causes synaptogenesis, whereas motor activity causes angiogenesis, in cerebellar cortex of adult rats. Proc Natl Acad Sci U S A, 1990; 87: 5568-72.

Boyden ES, Katoh A, Raymond JL. Cerebellum-dependent learning: the role of multiple plasticity mechanisms. Annual review of neuroscience, 2004; 27: 581-609.

Boyke J, Driemeyer J, Gaser C, Buchel C, May A. Training-induced brain structure changes in the elderly. J Neurosci, 2008; 28: 7031-5.

Briones TL, Klintsova AY, Greenough WT. Stability of synaptic plasticity in the adult rat visual cortex induced by complex environment exposure. Brain Research, 2004; 1018: 130-5.

Bruel-Jungerman E, Laroche S, Rampon C. New neurons in the dentate gyrus are involved in the expression of enhanced long-term memory following environmental enrichment. Eur J Neurosci, 2005; 21: 513-21.

Cameron HA, Glover LR. Adult neurogenesis: beyond learning and memory. Annual review of psychology, 2015; 66: 53-81.

Carpenter-Hyland EP, Plummer TK, VazdarjANOVA A, Blake DT. Arc expression and neuroplasticity in primary auditory cortex during initial learning are inversely related to neural activity. Proc Natl Acad Sci U S A, 2010; 107: 14828-32.

Chklovskii DB, Mel BW, Svoboda K. Cortical rewiring and information storage. Nature, 2004; 431: 782-8.

Christian KM, Thompson RF. Neural substrates of eyeblink conditioning: acquisition and retention. Learning & memory (Cold Spring Harbor, N.Y.), 2003; 10: 427-55.

Christopherson KS, Ullian EM, Stokes CCA, Mullowney CE, Hell JW, Agah A, Lawler J, Mosher DF, Bornstein P, Barres BA. Thrombospondins Are Astrocyte-Secreted Proteins that Promote CNS Synaptogenesis. Cell, 2005; 120: 421-33.

Clarke LE, Barres BA. Emerging roles of astrocytes in neural circuit development. Nature reviews. Neuroscience, 2013; 14: 311-21.

Comery TA, Stamoudis CX, Irwin SA, Greenough WT. Increased density of multiple-head dendritic spines on medium-sized spiny neurons of the striatum in rats reared in a complex environment. Neurobiology of learning and memory, 1996; 66: 93-6.

Cooper SJ. Donald O. Hebb's synapse and learning rule: a history and commentary. Neuroscience and biobehavioral reviews, 2005; 28: 851-74.

Cummings BJ, Uchida N, Tamaki SJ, Salazar DL, Hooshmand M, Summers R, Gage FH, Anderson AJ. Human neural stem cells differentiate and promote locomotor recovery in spinal cord-injured mice. P Natl Acad Sci USA, 2005; 102: 14069-74.

Dall'Oglio A, Gehlen G, Achaval M, Rasia-Filho AA. Dendritic branching features of Golgi-impregnated neurons from the "ventral" medial amygdala subnuclei of adult male and female rats. Neuroscience letters, 2008; 439: 287-92.

De Roo M, Klauser P, Muller D. LTP Promotes a Selective Long-Term Stabilization and Clustering of Dendritic Spines. PLoS Biology, 2008; 6: e219.

Desgranges B, Ramirez-Amaya V, Ricaño-Cornejo I, Lévy F, Ferreira G. Flavor Preference Learning Increases Olfactory and Gustatory Convergence onto

Single Neurons in the Basolateral Amygdala but Not in the Insular Cortex in Rats. PloS one, 2010; 5: e10097.

Deshmukh SS, Knierim JJ. Representation of non-spatial and spatial information in the lateral entorhinal cortex. Front Behav Neurosci, 2011; 5.

Dietzel I, Heinemann U, Lux HD. Relations between slow extracellular potential changes, glial potassium buffering, and electrolyte and cellular volume changes during neuronal hyperactivity in cat brain. Glia, 1989; 2: 25-44.

Draganski B, Gaser C, Busch V, Schuierer G, Bogdahn U, May A. Neuroplasticity: changes in grey matter induced by training. Nature, 2004; 427: 311-2.

Draganski B, Gaser C, Kempermann G, Kuhn HG, Winkler J, Buchel C, May A. Temporal and spatial dynamics of brain structure changes during extensive learning. J Neurosci, 2006; 26: 6314-7.

Driemeyer J, Boyke J, Gaser C, Buchel C, May A. Changes in gray matter induced by learning--revisited. PloS one, 2008; 3: e2669.

Eliasson C, Sahlgren C, Berthold CH, Stakeberg J, Celis JE, Betsholtz C, Eriksson JE, Pekny M. Intermediate filament protein partnership in astrocytes. Journal of Biological Chemistry, 1999a; 274: 23996-4006.

Eliasson C, Sahlgren C, Berthold CH, Stakeberg J, Celis JE, Betsholtz C, Eriksson JE, Pekny M. Intermediate filament protein partnership in astrocytes. The Journal of biological chemistry, 1999b; 274: 23996-4006.

Eng LF, Vanderhaeghen JJ, Bignami A, Gerstl B. An acidic protein isolated from fibrous astrocytes. Brain Research, 1971; 28: 351-4.

Engert F, Bonhoeffer T. Dendritic spine changes associated with hippocampal long-term synaptic plasticity. Nature, 1999; 399: 66-70.

Eroglu C, Barres BA. Regulation of synaptic connectivity by glia. Nature, 2010; 468: 223-31.

Feng R, Rampon C, Tang YP, Shrom D, Jin J, Kyin M, Sopher B, Martin GM, Kim SH, Langdon RB, Sisodia SS, Tsien JZ. Deficient neurogenesis in forebrain-specific presenilin-1 knockout mice is associated with reduced clearance of hippocampal memory traces. Neuron, 2001; 32: 911-26.

Ferbinteanu J, Holsinger RMD, McDonald RJ. Lesions of the medial or lateral perforant path have different effects on hippocampal contributions to place learning and on fear conditioning to context. Behav Brain Res, 1999; 101: 65-84.

Filosa JA, Bonev AD, Straub SV, Meredith AL, Wilkerson MK, Aldrich RW, Nelson MT. Local potassium signaling couples neuronal activity to vasodilation in the brain. Nature Neuroscience, 2006; 9: 1397-403.

Fu M, Zuo Y. Experience-dependent structural plasticity in the cortex. Trends in neurosciences, 2011; 34: 177-87.

Gao M, Sossa K, Song L, Errington L, Cummings L, Hwang H, Kuhl D, Worley P, Lee HK. A specific requirement of Arc/Arg3.1 for visual experience-induced homeostatic synaptic plasticity in mouse primary visual cortex. J Neurosci, 2010; 30: 7168-78.

Gaser C, Nenadic I, Buchsbaum BR, Hazlett EA, Buchsbaum MS. Deformation-based morphometry and its relation to conventional volumetry of brain lateral ventricles in MRI. Neuroimage, 2001; 13: 1140-5.

Gaser C, Schlaug G. Brain structures differ between musicians and non-musicians. J Neurosci, 2003; 23: 9240-5.

Gaser C, Schmidt S, Metzler M, Herrmann KH, Krumbein I, Reichenbach JR, Witte OW. Deformation-based brain morphometry in rats. Neuroimage, 2012; 63: 47-53.

Genoud C, Quairiaux C, Steiner P, Hirling H, Welker E, Knott GW. Plasticity of Astrocytic Coverage and Glutamate Transporter Expression in Adult Mouse Cortex. PLoS Biology, 2006; 4: e343.

Goritz C, Mauch DH, Pfrieger FW. Multiple mechanisms mediate cholesterol-induced synaptogenesis in a CNS neuron. Molecular and cellular neurosciences, 2005; 29: 190-201.

Gould E, Beylin A, Tanapat P, Reeves A, Shors TJ. Learning enhances adult neurogenesis in the hippocampal formation. Nature Neuroscience, 1999a; 2: 260-5.

Gould E, McEwen BS, Tanapat P, Galea LA, Fuchs E. Neurogenesis in the dentate gyrus of the adult tree shrew is regulated by psychosocial stress and NMDA receptor activation. J Neurosci, 1997; 17: 2492-8.

Gould E, Tanapat P, Hastings NB, Shors TJ. Neurogenesis in adulthood: a possible role in learning. Trends in cognitive sciences, 1999b; 3: 186-92.

Greifzu F, Schmidt S, Schmidt KF, Kreikemeier K, Witte OW, Lowel S. Global impairment and therapeutic restoration of visual plasticity mechanisms after a localized cortical stroke. Proc Natl Acad Sci U S A, 2011; 108: 15450-5.

Grosche A, Grosche J, Tackenberg M, Scheller D, Gerstner G, Gumprecht A, Pannicke T, Hirrlinger PG, Wilhelmsson U, Huttmann K, Hartig W, Steinhauser C, Pekny M, Reichenbach A. Versatile and simple approach to determine astrocyte territories in mouse neocortex and hippocampus. PloS one, 2013; 8: e69143.

Gull S, Ingrisch I, Tausch S, Witte OW, Schmidt S. Consistent and reproducible staining of glia by a modified Golgi-Cox method. J Neurosci Methods, 2015; 256: 141-50.

Gusev PA, Cui C, Alkon DL, Gubin AN. Topography of Arc/Arg3.1 mRNA expression in the dorsal and ventral hippocampus induced by recent and remote spatial memory recall: dissociation of CA3 and CA1 activation. J Neurosci, 2005; 25: 9384-97.

Guzowski JF, McNaughton BL, Barnes CA, Worley PF. Environment-specific expression of the immediate-early gene Arc in hippocampal neuronal ensembles. Nat Neurosci, 1999; 2: 1120-4.

Guzowski JF, Setlow B, Wagner EK, McGaugh JL. Experience-dependent gene expression in the rat hippocampus after spatial learning: a comparison of the immediate-early genes Arc, c-fos, and zif268. J Neurosci, 2001; 21: 5089-98.

Hafting T, Fyhn M, Molden S, Moser MB, Moser EI. Microstructure of a spatial map in the entorhinal cortex. Nature, 2005; 436: 801-6.

Haseleu J, Anlauf E, Blaess S, Endl E, Derouiche A. Studying subcellular detail in fixed astrocytes: dissociation of morphologically intact glial cells (DIMIGs). Front Cell Neurosci, 2013; 7.

Hawrylak N, Chang FL, Greenough WT. Astrocytic and synaptic response to kindling in hippocampal subfield CA1. II. Synaptogenesis and astrocytic process increases to in vivo kindling. Brain Res, 1993; 603: 309-16.

Hayashi Y, Okamoto K-i, Bosch M, Futai K. Roles of Neuronal Activity-Induced Gene Products in Hebbian and Homeostatic Synaptic Plasticity, Tagging, and Capture. In Kreutz MR, Sala C, editors. Synaptic Plasticity. Springer Vienna, 2012: 335-54.

Hebb DO. The organization of behavior: A neuropsychological theory. Science Education, 1949; 34: 336-7.

Herrmann KH, Schmidt S, Kretz A, Haenold R, Krumbein I, Metzler M, Gaser C, Witte OW, Reichenbach JR. Possibilities and limitations for high resolution small animal MRI on a clinical whole-body 3T scanner. Magma (New York, N.Y.), 2012; 25: 233-44.

Hirrlinger J, Hulsmann S, Kirchhoff F. Astroglial processes show spontaneous motility at active synaptic terminals in situ. Eur J Neurosci, 2004; 20: 2235-9.

Ho VM, Lee JA, Martin KC. The Cell Biology of Synaptic Plasticity. Science, 2011; 334: 623-8.

Hofer SB, Mrsic-Flogel TD, Bonhoeffer T, Hubener M. Experience leaves a lasting structural trace in cortical circuits. Nature, 2009; 457: 313-U4.

Holtmaat A, Svoboda K. Experience-dependent structural synaptic plasticity in the mammalian brain. Nature Reviews Neuroscience, 2009; 10: 647-58.

Holtmaat AJGD, Trachtenberg JT, Wilbrecht L, Shepherd GM, Zhang X, Knott GW, Svoboda K. Transient and Persistent Dendritic Spines in the Neocortex In Vivo. Neuron, 2005; 45: 279-91.

Huerta PT, Lisman JE. Heightened Synaptic Plasticity of Hippocampal Ca1 Neurons during a Cholinergically Induced Rhythmic State. Nature, 1993; 364: 723-5.

Iso H, Simoda S, Matsuyama T. Environmental change during postnatal development alters behaviour, cognitions and neurogenesis of mice. Behav Brain Res, 2007; 179: 90-8.

Jacobson M. Developmental Neurobiology, Third ed. Springer science +Business media,LLC: New York, 1993.

Johansen-Berg H, Baptista CS, Thomas AG. Human Structural Plasticity at Record Speed. Neuron, 2012; 73: 1058-60.

Jones TA, Greenough WT. Ultrastructural evidence for increased contact between astrocytes and synapses in rats reared in a complex environment. Neurobiology of learning and memory, 1996; 65: 48-56.

Jones TA, Hawrylak N, Greenough WT. Rapid laminar-dependent changes in GFAP immunoreactive astrocytes in the visual cortex of rats reared in a complex environment. Psychoneuroendocrinology, 1996; 21: 189-201.

Jones TA, Klintsova AY, Kilman VL, Sirevaag AM, Greenough WT. Induction of multiple synapses by experience in the visual cortex of adult rats. Neurobiology of learning and memory, 1997; 68: 13-20.

Kandel ER. The molecular biology of memory storage: a dialogue between genes and synapses. Science, 2001; 294: 1030-8.

Kasai H, Hayama T, Ishikawa M, Watanabe S, Yagishita S, Noguchi J. Learning rules and persistence of dendritic spines. Eur J Neurosci, 2010; 32: 241-9.

Kassem MS, Lagopoulos J, Stait-Gardner T, Price WS, Chohan TW, Arnold JC, Hatton SN, Bennett MR. Stress-induced grey matter loss determined by MRI is primarily due to loss of dendrites and their synapses. Molecular neurobiology, 2013; 47: 645-61.

Kee N, Teixeira CM, Wang AH, Frankland PW. Preferential incorporation of adult-generated granule cells into spatial memory networks in the dentate gyrus. Nat Neurosci, 2007; 10: 355-62.

Keifer OP, Jr., Hurt RC, Gutman DA, Keilholz SD, Gourley SL, Ressler KJ. Voxel-based morphometry predicts shifts in dendritic spine density and morphology with auditory fear conditioning. Nature communications, 2015; 6: 7582.

Kelly MP, Deadwyler SA. Experience-dependent regulation of the immediate-early gene arc differs across brain regions. J Neurosci, 2003; 23: 6443-51.

Kempermann G, Gage FH. Genetic determinants of adult hippocampal neurogenesis correlate with acquisition, but not probe trial performance, in the water maze task. Eur J Neurosci, 2002; 16: 129-36.

Kempermann G, Kuhn HG, Gage FH. More hippocampal neurons in adult mice living in an enriched environment. Nature, 1997; 386: 493-5.

Kleim JA, Barbay S, Cooper NR, Hogg TM, Reidel CN, Remple MS, Nudo RJ. Motor learning-dependent synaptogenesis is localized to functionally reorganized motor cortex. Neurobiology of learning and memory, 2002; 77: 63-77.

Kleim JA, Lussnig E, Schwarz ER, Comery TA, Greenough WT. Synaptogenesis and FOS expression in the motor cortex of the adult rat after motor skill learning. J Neurosci, 1996; 16: 4529-35.

Kleim JA, Markham JA, Vij K, Freese JL, Ballard DH, Greenough WT. Motor learning induces astrocytic hypertrophy in the cerebellar cortex. Behav Brain Res, 2007; 178: 244-9.

Kleim JA, Swain RA, Armstrong KA, Napper RMA, Jones TA, Greenough WT. Selective synaptic plasticity within the cerebellar cortex following complex motor skill learning. Neurobiology of learning and memory, 1998; 69: 274-89.

Kleim JA, Vij K, Ballard DH, Greenough WT. Learning-dependent synaptic modifications in the cerebellar cortex of the adult rat persist for at least four weeks. J Neurosci, 1997; 17: 717-21.

Klintsova A, Levy WB, Desmond NL. Astrocytic Volume Fluctuates in the Hippocampal Ca1 Region across the Estrous-Cycle. Brain Research, 1995; 690: 269-74.

Knott GW, Holtmaat A, Wilbrecht L, Welker E, Svoboda K. Spine growth precedes synapse formation in the adult neocortex in vivo. Nat Neurosci, 2006; 9: 1117-24.

Kozorovitskiy Y, Gross CG, Kopil C, Battaglia L, McBreen M, Stranahan AM, Gould E. Experience induces structural and biochemical changes in the adult primate brain. P Natl Acad Sci USA, 2005; 102: 17478-82.

Kucukdereli H, Allen NJ, Lee AT, Feng A, Ozlu MI, Conatser LM, Chakraborty C, Workman G, Weaver M, Sage EH, Barres BA, Eroglu C. Control of excitatory CNS synaptogenesis by astrocyte-secreted proteins Hevin and SPARC. Proc Natl Acad Sci U S A, 2011; 108: E440-9.

Lamprecht R, Farb CR, Rodrigues SM, LeDoux JE. Fear conditioning drives profilin into amygdala dendritic spines. Nat Neurosci, 2006; 9: 481-3.

Lang C, Barco A, Zablow L, Kandel ER, Siegelbaum SA, Zakharenko SS. Transient expansion of synaptically connected dendritic spines upon induction of hippocampal long-term potentiation. P Natl Acad Sci USA, 2004; 101: 16665-70.

Lantos PL. An electron microscope study of reacting astrocytes in gliomas induced by N-ethyl-N-nitrosourea in rats. Acta neuropathologica, 1974; 30: 175-81.

Lee KJ, Jung JG, Arii T, Imoto K, Rhyu IJ. Morphological changes in dendritic spines of Purkinje cells associated with motor learning. Neurobiology of learning and memory, 2007; 88: 445-50.

Lehmann K, Löwel S. Age-Dependent Ocular Dominance Plasticity in Adult Mice. PloS one, 2008; 3: e3120.

Lemaire V, Koehl M, Le Moal M, Abrous DN. Prenatal stress produces learning deficits associated with an inhibition of neurogenesis in the hippocampus. Proc Natl Acad Sci U S A, 2000; 97: 11032-7.

Lerch JP, Yiu AP, Martinez-Canabal A, Pekar T, Bohbot VD, Frankland PW, Henkelman RM, Josselyn SA, Sled JG. Maze training in mice induces MRI-detectable brain shape changes specific to the type of learning. Neuroimage, 2011; 54: 2086-95.

Leuner B, Falduto J, Shors TJ. Associative memory formation increases the observation of dendritic spines in the hippocampus. J Neurosci, 2003; 23: 659-65.

Luders E, Toga AW, Lepore N, Gaser C. The underlying anatomical correlates of long-term meditation: larger hippocampal and frontal volumes of gray matter. Neuroimage, 2009; 45: 672-8.

Lunghi C, Emir UE, Morrone MC, Bridge H. Short-term monocular deprivation alters GABA in the adult human visual cortex. Current biology : CB, 2015; 25: 1496-501.

Lux HD, Heinemann U, Dietzel I. Ionic changes and alterations in the size of the extracellular space during epileptic activity. Advances in neurology, 1986; 44: 619-39.

Macvicar BA, Feighan D, Brown A, Ransom B. Intrinsic optical signals in the rat optic nerve: Role for K+ uptake via NKCC1 and swelling of astrocytes. Glia, 2002; 37: 114-23.

Maguire EA, Gadian DG, Johnsrude IS, Good CD, Ashburner J, Frackowiak RS, Frith CD. Navigation-related structural change in the hippocampi of taxi drivers. Proc Natl Acad Sci U S A, 2000; 97: 4398-403.

Maguire EA, Woollett K, Spiers HJ. London taxi drivers and bus drivers: A structural MRI and neuropsychological analysis. Hippocampus, 2006; 16: 1091-101.

Maletic-Savatic M, Malinow R, Svoboda K. Rapid dendritic morphogenesis in CA1 hippocampal dendrites induced by synaptic activity. Science, 1999; 283: 1923-7.

Matsumoto-Miyai K, Sokolowska E, Zurlinden A, Gee CE, Luscher D, Hettwer S, Wolfel J, Ladner AP, Ster J, Gerber U, Rulicke T, Kunz B, Sonderegger P. Coincident pre- and postsynaptic activation induces dendritic filopodia via neurotrypsin-dependent agrin cleavage. Cell, 2009; 136: 1161-71.

Mauch DH, Nagler K, Schumacher S, Goritz C, Muller EC, Otto A, Pfrieger FW. CNS synaptogenesis promoted by glia-derived cholesterol. Science, 2001; 294: 1354-7.

May A. Experience-dependent structural plasticity in the adult human brain. Trends in cognitive sciences, 2011; 15: 475-82.

May A, Hajak G, Ganssbauer S, Steffens T, Langguth B, Kleinjung T, Eichhammer P. Structural brain alterations following 5 days of intervention: dynamic aspects of neuroplasticity. Cerebral cortex (New York, N.Y. : 1991), 2007; 17: 205-10.

Mechelli A, Crinion JT, Noppeney U, O'Doherty J, Ashburner J, Frackowiak RS, Price CJ. Neurolinguistics: structural plasticity in the bilingual brain. Nature, 2004; 431: 757.

Middeldorp J, Hol EM. GFAP in health and disease. Prog Neurobiol, 2011; 93: 421-43.

Mietchen D, Gaser C. Computational Morphometry for Detecting Changes in Brain Structure Due to Development, Aging, Learning, Disease and Evolution. Frontiers in Neuroinformatics, 2009; 3: 25.

Missler M, Eins S, Bottcher H, Wolff JR. Postnatal-Development of Glial Fibrillary Acidic Protein, Vimentin and S100 Protein in Monkey Visual-Cortex - Evidence for a Transient Reduction of Gfap Immunoreactivity. Dev Brain Res, 1994; 82: 103-17.

Murray EA, Bussey TJ, Saksida LM. Visual perception and memory: a new view of medial temporal lobe function in primates and rodents. Annual review of neuroscience, 2007; 30: 99-122.

Nagerl UV, Eberhorn N, Cambridge SB, Bonhoeffer T. Bidirectional activity-dependent morphological plasticity in hippocampal neurons. Neuron, 2004; 44: 759-67.

Nagerl UV, Kostinger G, Anderson JC, Martin KAC, Bonhoeffer T. Protracted synaptogenesis after activity-dependent spinogenesis in hippocampal neurons. J Neurosci, 2007; 27: 8149-56.

Nilsson M, Perfilieva E, Johansson U, Orwar O, Eriksson PS. Enriched environment increases neurogenesis in the adult rat dentate gyrus and improves spatial memory. Journal of neurobiology, 1999; 39: 569-78.

O'Malley A, O'Connell C, Murphy KJ, Regan CM. Transient spine density increases in the mid-molecular layer of hippocampal dentate gyrus accompany consolidation of a spatial learning task in the rodent. Neuroscience, 2000; 99: 229-32.

Ogata K, Kosaka T. Structural and quantitative analysis of astrocytes in the mouse hippocampus. Neuroscience, 2002; 113: 221-33.

Okabe S, Miwa A, Okado H. Spine formation and correlated assembly of presynaptic and postsynaptic molecules. J Neurosci, 2001; 21: 6105-14.

Okamoto KI, Nagai T, Miyawaki A, Hayashi Y. Rapid and persistent modulation of actin dynamics regulates postsynaptic reorganization underlying bidirectional plasticity. Nature Neuroscience, 2004; 7: 1104-12.

Okuno H. Regulation and function of immediate-early genes in the brain: beyond neuronal activity markers. Neuroscience research, 2011; 69: 175-86.

Olude MA, Mustapha OA, Aderounmu OA, Olopade JO, Ihunwo AO. Astrocyte morphology, heterogeneity, and density in the developing African giant rat (Cricetomys gambianus). Frontiers in neuroanatomy, 2015; 9: 67.

Ostby I, Oyehaug L, Einevoll GT, Nagelhus EA, Plahte E, Zeuthen T, Lloyd CM, Ottersen OP, Omholt SW. Astrocytic mechanisms explaining neural-activity-induced shrinkage of extraneuronal space. PLoS computational biology, 2009; 5: e1000272.

Paxinos G, Watson C. The rat brain in stereotaxic coordinates London : Elsevier Academic, 2004.

Pekny M, Johansson CB, Eliasson C, Stakeberg J, Wallen A, Perlmann T, Lendahl U, Betsholtz C, Berthold CH, Frisen J. Abnormal reaction to central nervous system injury in mice lacking glial fibrillary acidic protein and vimentin. The Journal of cell biology, 1999; 145: 503-14.

Pekny M, Wilhelmsson U. Intermediate Filaments in Astrocytes in Health and Disease. Intermediate Filaments. Springer US, 2006: 10-34.

Pellerin L. How astrocytes feed hungry neurons. Molecular neurobiology, 2005; 32: 59-72.

Perea G, Araque A. Glial calcium signaling and neuron–glia communication. Cell Calcium, 2005; 38: 375-82.

Perez-Alvarez A, Navarrete M, Covelo A, Martin ED, Araque A. Structural and functional plasticity of astrocyte processes and dendritic spine interactions. J Neurosci, 2014; 34: 12738-44.

Prusky GT, Alam NM, Beekman S, Douglas RM. Rapid quantification of adult and developing mouse spatial vision using a virtual optomotor system. Investigative ophthalmology & visual science, 2004; 45: 4611-6.

Prusky GT, Alam NM, Douglas RM. Enhancement of vision by monocular deprivation in adult mice. J Neurosci, 2006; 26: 11554-61.

Quallo MM, Price CJ, Ueno K, Asamizuya T, Cheng K, Lemon RN, Iriki A. Gray and white matter changes associated with tool-use learning in macaque monkeys. P Natl Acad Sci USA, 2009; 106: 18379-84.

Ramirez-Amaya V, Vazdarjanova A, Mikhael D, Rosi S, Worley PF, Barnes CA. Spatial exploration-induced Arc mRNA and protein expression: evidence for selective, network-specific reactivation. J Neurosci, 2005; 25: 1761-8.

Ranjan A, Mallick BN. Differential staining of glia and neurons by modified Golgi-Cox method. J Neurosci Meth, 2012; 209: 269-79.

Ransom BR, Yamate CL, Connors BW. Activity-dependent shrinkage of extracellular space in rat optic nerve: a developmental study. J Neurosci, 1985; 5: 532-5.

Rapanelli M, Lew SE, Frick LR, Zanutto BS. Plasticity in the rat prefrontal cortex: linking gene expression and an operant learning with a computational theory. PloS one, 2010; 5: e8656.

Raslan A, Ernst P, Werle M, Thieme H, Szameit K, Finkensieper M, Guntinas-Lichius O, Irintchev A. Reduced cholinergic and glutamatergic synaptic input to regenerated motoneurons after facial nerve repair in rats: potential implications for recovery of motor function. Brain structure & function, 2014; 219: 891-909.

Richards DA, Mateos JM, Hugel S, de Paola V, Caroni P, Gahwiler BH, McKinney RA. Glutamate induces the rapid formation of spine head protrusions in hippocampal slice cultures. P Natl Acad Sci USA, 2005; 102: 6166-71.

Risher WC, Eroglu C. Thrombospondins as key regulators of synaptogenesis in the central nervous system. Matrix Biology, 2012; 31: 170-7.

Rodnight R, Goncalves CA, Wofchuk ST, Leal R. Control of the phosphorylation of the astrocyte marker glial fibrillary acidic protein (GFAP) in the immature rat hippocampus by glutamate and calcium ions: possible key factor in astrocytic plasticity. Brazilian journal of medical and biological research = Revista

brasileira de pesquisas medicas e biologicas / Sociedade Brasileira de Biofisica … [et al.], 1997; 30: 325-38.

Saarinen J, Levi DM. Perceptual learning in vernier acuity: What is learned? Vision Research, 1995; 35: 519-27.

Shepherd JD, Rumbaugh G, Wu J, Chowdhury S, Plath N, Kuhl D, Huganir RL, Worley PF. Arc/Arg3.1 mediates homeostatic synaptic scaling of AMPA receptors. Neuron, 2006; 52: 475-84.

Sholl DA. Dendritic organization in the neurons of the visual and motor cortices of the cat. J Anat, 1953; 87: 387-406.

Shors TJ, Townsend DA, Zhao M, Kozorovitskiy Y, Gould E. Neurogenesis may relate to some but not all types of hippocampal-dependent learning. Hippocampus, 2002; 12: 578-84.

Simard M, Nedergaard M. The neurobiology of glia in the context of water and ion homeostasis. Neuroscience, 2004; 129: 877-96.

Sirevaag AM, Greenough WT. Plasticity of GFAP-immunoreactive astrocyte size and number in visual cortex of rats reared in complex environments. Brain Res, 1991; 540: 273-8.

Somjen GG. Ions in the Brain. Oxford University Press. New York, 2004.

Squire LR, Stark CE, Clark RE. The medial temporal lobe. Annual review of neuroscience, 2004; 27: 279-306.

Suthana N, Haneef Z, Stern J, Mukamel R, Behnke E, Knowlton B, Fried I. Memory enhancement and deep-brain stimulation of the entorhinal area. The New England journal of medicine, 2012; 366: 502-10.

Takemura M, Gomi H, Colucci-Guyon E, Itohara S. Protective role of phosphorylation in turnover of glial fibrillary acidic protein in mice. J Neurosci, 2002; 22: 6972-9.

Taubert M, Draganski B, Anwander A, Muller K, Horstmann A, Villringer A, Ragert P. Dynamic properties of human brain structure: learning-related changes in cortical areas and associated fiber connections. J Neurosci, 2010; 30: 11670-7.

Theodosis DT, Poulain DA, Oliet SH. Activity-dependent structural and functional plasticity of astrocyte-neuron interactions. Physiological reviews, 2008; 88: 983-1008.

Thomas AG, Dennis A, Bandettini PA, Johansen-Berg H. The Effects of Aerobic Activity on Brain Structure. Frontiers in Psychology, 2012; 3: 86.

van Praag H, Christie BR, Sejnowski TJ, Gage FH. Running enhances neurogenesis, learning, and long-term potentiation in mice. Proc Natl Acad Sci U S A, 1999; 96: 13427-31.

Vernon AC, Crum WR, Lerch JP, Chege W, Natesan S, Modo M, Cooper JD, Williams SC, Kapur S. Reduced cortical volume and elevated astrocyte density in rats chronically treated with antipsychotic drugs-linking magnetic resonance imaging findings to cellular pathology. Biological psychiatry, 2014; 75: 982-90.

Vinade L, Goncalves CA, Wofchuk S, Gottfried C, Rodnight R. Evidence for a role for calcium ions in the dephosphorylation of glial fibrillary acidic protein (GFAP) in immature hippocampal slices and in astrocyte cultures from the rat. Brain research. Developmental brain research, 1997; 104: 11-7.

Viola GG, Rodrigues L, Americo JC, Hansel G, Vargas RS, Biasibetti R, Swarowsky A, Goncalves CA, Xavier LL, Achaval M, Souza DO, Amaral OB. Morphological

changes in hippocampal astrocytes induced by environmental enrichment in mice. Brain Res, 2009; 1274: 47-54.

Walz W, Hertz L. Intracellular ion changes of astrocytes in response to extracellular potassium. Journal of neuroscience research, 1983; 10: 411-23.

Walz W, Hinks EC. Carrier-mediated KCl accumulation accompanied by water movements is involved in the control of physiological K+ levels by astrocytes. Brain Res, 1985; 343: 44-51.

Weibel ER, Taylor CR, Hoppeler H. The concept of symmorphosis: a testable hypothesis of structure-function relationship. P Natl Acad Sci USA, 1991; 88: 10357-61.

Whitlock JR, Heynen AJ, Shuler MG, Bear MF. Learning induces long-term potentiation in the hippocampus. Science, 2006; 313: 1093-7.

Wiesel TN, Hubel DH. Comparison of the effects of unilateral and bilateral eye closure on cortical unit responses in kittens. Journal of neurophysiology, 1965; 28: 1029-40.

Witter MP, Amaral DG. Chapter 21 - Hippocampal Formation. In Paxinos G, editor. The Rat Nervous System (Third Edition). Academic Press: Burlington, 2004: 635-704.

Wolff J CT. Cytoarchitectonics of nonneuronal cells in the central nervous system. Non-neuronal Cells of the Nervous System: Function and Dysfunction. Amsterdam ; London : Elsevier, 2004: 1–52.

Yasumatsu N, Matsuzaki M, Miyazaki T, Noguchi J, Kasai H. Principles of Long-Term Dynamics of Dendritic Spines. J Neurosci, 2008; 28: 13592-608.

Yuste R, Bonhoeffer T. Morphological changes in dendritic spines associated with long-term synaptic plasticity. Annual review of neuroscience, 2001; 24: 1071-89.

Zagami CJ, O'Shea RD, Lau CL, Cheema SS, Beart PM. Regulation of glutamate transporters in astrocytes: Evidence for a relationship between transporter expression and astrocytic phenotype. Neurotox Res, 2005; 7: 143-9.

Zhou Q, Homma KJ, Poo MM. Shrinkage of dendritic spines associated with long-term depression of hippocampal synapses. Neuron, 2004; 44: 749-57.

Zhu XO, Brown MW, Aggleton JP. Neuronal Signaling of Information Important to Visual Recognition Memory in Rat Rhinal and Neighboring Cortices. Eur J Neurosci, 1995; 7: 753-65.

Zille K. The cortex of the Rat: A Stereotaxic Atlas, 1st ed. Springer-Verlag Berlin, Heidelberg, New York, Tokyo 1985

Zito K, Scheuss V, Knott G, Hill T, Svoboda K. Rapid Functional Maturation of Nascent Dendritic Spines. Neuron, 2009; 61: 247-58.

Ziv NE, Smith SJ. Evidence for a role of dendritic filopodia in synaptogenesis and spine formation. Neuron, 1996; 17: 91-102.

Zull JE. THE ART OF CHANGING THE BRAIN, First ed. Stylus Publishing, LLC 22883 Quicksilver Drive Sterling, Virginia 20166, 2002.

8. Appendix

Tab.5: Summary of major results for visual acuity change and statistical significance.

Group	Study	N	Baseline	Maximum	%	Days	*p*	Figure
Test study	T	5	0.222 ± 0.0028	0.286 ± 0.0056	29	7	<0.05	15A
MD-OPT-MRI	L	24	0.208 ± 0.0022	0.285 ± 0.0032	37	9	<0.05	16A
MD-MRI	L	10	0.230 ± 0.0005	0.286 ± 0.0013	24	10	<0.05	17
OPT-MRI	L	20	0.230 ± 0.0004	0.230 ± 0.0004	0	9		19A
MD-3d	C.S	20	0.217 ± 0.0037	0.266 ± 0.0039	23	3	<0.05	20A
MD-10d	C.S	5	0.196 ± 0.0043	0.258 ± 0.0071	31	10	<0.05	21A

Groups are listed (left column) and arranged according to study: Test (T), Longitudinal (L), and Cross-sectional (C.S). The number of animals in a group (*N*), the baseline spatial frequency sensitivity with SEM (Baseline), the maximum sensitivity over the course of the experiment with SEM (Maximum), the percentage change between baseline and maximum sensitivity (%), the number of days after MD and baseline MRI (Days), *p* values of repeated-measures ANOVAs on ranks for the group (*p*), to figure number and panel of the experiment (Figures) are listed for each group in columns.

Tab. 6: Summary of major results for contrast sensitivity change and statistical significance.

Group	Study	N	Baseline at 0.044	Maximum at 0.044	%	Days	*p*	Figure
Test study	T	5	1.97 ± 0.0081	2.22 ± 0.0434	12	7	<0.05	15B
MD-OPT-MRI	L	24	1.96 ± 0.0143	2.14 ± 0.0205	9	9	<0.05	16B
OPT-MRI	L	20	2.06 ± 0.0021	2.06 ± 0.0021	0	9		19B
MD-3d	C.S	20	1.97 ± 0.0159	2.13 ± .0261	8	3	<0.05	20B
MD-10d	C.S	5	1.85 ± 0.0134	2.02 ± 0.0197	9	10	<0.05	21B
Group	**Study**	**N**	**Baseline at 0.061**	**Maximum at 0.061**	**%**	**Days**	***p***	**Figure**
Test study	T	5	2.97 ± 0.0204	3.5 ± 0.0769	18	7	<0.05	15B
MD-OPT-MRI	L	24	2.84 ± 0.0266	3.25 ± 0.0348	14	9	<0.05	16B
OPT-MRI	L	20	2.95 ± 0.0042	2.95 ± 0.0042	0	9		19B
MD-3d	C.S	20	2.89 ± 0.0282	3.20± 0.0475	11	3	<0.05	20B
MD-10d	C.S	5	2.72 ± 0.0193	3.12 ± 0.0486	15	10	<0.05	21B
Group	**Study**	**N**	**Baseline at 0.089**	**Maximum at 0.089**	**%**	**Days**	***p***	**Figure**
Test study	T	5	2.74 ± 0.0170	3.20 ± 0.0648	17	7	<0.05	15B
MD-OPT-MRI	L	24	2.67 ± 0.0185	3.04 ± 0.0233	13.8	9	<0.05	16B
OPT-MRI	L	20	2.71 ± 0.0043	2.71 ± 0.0043	0	9		19B
MD-3d	C.S	20	2.68 ± 0.0201	2.98 ± 0.0397	11	3	<0.05	20B
MD-10d	C.S	5	2.56 ± 0.0161	2.87 ± 0.0380	12	10	<0.05	21B
Group	**Study**	**N**	**Baseline at 0.119**	**Maximum at 0.119**	**%**	**Days**	***p***	**Figure**
Test study	T	5	2.44 ± 0.0186	2.85 ± 0.0620	17	7	<0.05	15B
MD-OPT-MRI	L	24	2.46 ± 0.0109	2.79 ± 0.0164	13.4	9	<0.05	16B
OPT-MRI	L	20	2.45 ± 0.0026	2.45 ± 0.0026	0	9		19B
MD-3d	C.S	20	2.43 ± 0.0127	2.66 ± 0.0203	9.4	3	<0.05	20B
MD-10d	C.S	5	2.39 ± 0.0292	2.70 ± 0.0404	13	10	<0.05	21B
Group	**Study**	**N**	**Baseline at 0.150**	**Maximum at 0.150**	**%**	**Days**	***p***	**Figure**
Test study	T	5	2.11 ± 0.0238	2.42 ± 0.0160	13	7	<0.05	15B
MD-OPT-MRI	L	24	2.12 ± 0.0055	2.35 ± 0.0120	11	9	<0.05	16B
OPT-MRI	L	20	2.10 ± 0.0016	2.10± 0.0016	0	9		19B
MD-3d	C.S	20	2.10 ± 0.0069	2.29 ± 0.0045	8.3	3	<0.05	20B
MD-10d	C.S	5	2.13 ± 0.0115	2.39 ± 0.0273	12.2	10	<0.05	21B

Tab.6: Groups are listed (left column) and arranged according to study: Test (T), Longitudinal (L), and Cross-sectional (C.S). The number of animals in a group (*N*), the baseline contrast sensitivity with SEM (Baseline), the maximum sensitivity over the course of the experiment with SEM (Maximum), the percentage change between baseline and maximum sensitivity (%), the number of days after MD and baseline MRI (Days), *p* values of repeated-measures ANOVAs on ranks for the group (*p*), to figure number and panel of the experiment (Figures) are listed for each group in columns.

Tab. 7: DBM analysis and statistical significance.

| Area | Hemisphere | Coordinates | | | p <0.05(FWE) | | p <0.001(uncorr) | |
		X	Y	Z	p value	cluster size	p value	cluster size
LEnt*	L	-6.7	-8.4	-5.4	0.011	3	0.006	82
V1B*	L	-4.5	-2.0	-7.0	0.011	3	0.004	95
V2L*	R	6.1	-2.9	-7.2	ns		0.011	70
PM**	L	-5.1	-6.4	-12.6	ns		0.032	46

* Initial swelling (MD3d > MD10d vs. CTR3d<CTR10d)
** Late swelling (MD3d < MD10d vs. CTR3d > CTR10d)
FWE: Familywise error test, ns: non-significant, uncorr.: uncorrected.

Tab. 8: Density of BrdU$^+$ cells and statistical significance.

LEnt	Left	Right	Left vs Right (Paired t-test)
Control	6653.2 ± 332.47	6650.5 ± 231.96	0.737
MD-3d	6208.7 ± 251.17	6678.2 ± 363.71	0.527
p **(Between the groups) Student t-test**	C vs 3d : 0.16	C vs 3d : 0.4	
Au1	**Left**	**Right**	**Left vs Right (Paired t-test)**
Control	3212.1 ± 233	3313.13 ± 257.12	0.672
MD-3d	3319 ± 316	3306.4 ± 246.74	0.726
p **(Between the groups) Student t-test**	C vs 3d : 0.39	C vs 3d : 0.493	

Abbreviations: MD: monocular deprivation, d: days, LEnt: Lateral entorhinal cortex, Au1: Primary auditory cortex.

Tab. 9: Density of S100ß$^+$ astrocytes and statistical significance.

LEnt	Left	Right	Left vs Right (Paired t-test)
Control	35309.3 ± 516.6	35072.6 ± 957	0.816
MD-3d	33566.4 ± 920.4	35287.8 ± 722.2	0.149
MD-10d	35431.2 ± 492.7	35502.9 ± 588	0.931
***p* (Among the groups) 1 way Anova (Turkey HSD)**	C vs 3d vs 10d : 0.131 C vs 3d : 0.155 C vs 10d : 0.989 3d vs 10d : 0.173	C vs 3d vs 10d : 0.94 C vs 3d : 0.983 C vs 10d : 0.935 3d vs 10d : 0.987	
***p* (Between the groups) Student t-test**	C vs 3d : 0.048 C vs 10d : 0.438 3d vs 10d : 0.047	C vs 3d : 0.439 C vs 10d : 0.375 3d vs 10d : 0.411	
Au1	**Left**	**Right**	**Left vs Right (Paired t-test)**
Control	21420.4 ± 1028.6	22230.1 ± 1534.8	0.983
MD-3d	21732.9 ± 922.7	22642 ± 901.2	0.405
MD-10d	21804 ± 1163.4	23331 ± 1107	0.153
***p* (Among the groups) 1 way Anova (Turkey HSD)**	C vs 3d vs 10d : 0.840 C vs 3d : 0.976 C vs 10d : 0.828 3d vs 10d : 0.931	C vs 3d vs 10d : 0.819 C vs 3d : 0.990 C vs 10d : 0.819 3d vs 10d : 0.886	
***p* (Between the groups) Student t-test**	C vs 3d : 0.048 C vs 10d : 0.438 3d vs 10d : 0.481	C vs 3d : 0.407 C vs 10d : 0.291 3d vs 10d : 0.411	

Abbreviations: MD: monocular deprivation, d: days, LEnt: Lateral entorhinal cortex, Au1: Primary auditory cortex.

Tab. 10: Density of different types of spines on basal dendrites of pyramidal neurons and statistical significance in LEnt.

LEnt	Left						Right					
Spine Types	**Small**	**Medium**	**Large**	**Mushroom**	**Spiny**	**Sum**	**Small**	**Medium**	**Large**	**Mushroom**	**Spiny**	**Sum**
Control (C)	35 ± 1.2	11.4 ± 0.4	5.1 ± 0.3	4.3 ± 0.3	4.3 ± 0.2	60 ± 1.1	38.3 ± 1.1	12.9 ± 0.4	5.8 ± 0.6	4.2 ± 0.3	4.1 ± 0.3	65.2 ± 1.4
MD-3d (3d)	51 ± 2.1	19.6 ± 1.1	9.9 ± 1.1	7.6 ± 0.5	7 ± 0.6	94.8 ± 2.7	38 ± 2.0	12.1 ± 0.8	6.8 ± 0.7	4.3 ± 0.3	4.8 ± 0.5	66 ± 3.1
MD-10d (10d)	38.8 ± 0.5	16.6 ± 0.9	8.4 ± 0.7	7.6 ± 0.3	7 ± 0.6	78.3 ± 2.1	37 ± 1.9	13.3 ± 0.9	5.3 ± 0.6	4.8 ± 0.5	4 ± 0.4	64.3 ± 3
1 way Anova (Turkey HSD)												
p: C vs 3d vs 10d	<0.001	<0.001	<0.001	<0.001	<0.001	<0.001	0.801	0.572	0.425	0.479	0.314	0.892
p: C vs 3d	<0.001	<0.001	<0.001	<0.001	<0.001	<0.001	0.995	0.76	0.626	0.988	0.412	0.972
p C vs 10d	0.141	<0.001	0.005	<0.001	<0.001	<0.001	0.792	0.876	0.845	0.467	0.937	0.948
p : 3d vs 10d	<0.001	0.042	0.321	0.996	0.998	<0.001	0.895	0.542	0.394	0.68	0.31	0.886

Abbreviations: MD: monocular deprivation, d: days, LEnt: Lateral Entorhinal cortex.

Tab. 11: Density of different types of spines on basal dendrites of pyramidal neurons and statistical significance in Au1.

Au1	Left						Right					
Spine Types	**Small**	**Medium**	**Large**	**Mushroom**	**Spiny**	**Sum**	**Small**	**Medium**	**Large**	**Mushroom**	**Spiny**	**Sum**
Control (C)	39.4 ± 1.4	14.1 ± 0.7	6.2 ± 0.2	5.5 ± 0.4	4.8 ± 0.3	70.0 ± 0.4	38.3 ± 1.1	13.3 ± 0.9	5.9 ± 0.2	5.2 ± 0.2	4.8 ± 0.1	67.6 ± 1.2
MD-3d (3d)	41.1 ± 1.4	15.5 ± 0.8	6.3 ± 0.3	5.5 ± 0.2	4.3 ± 0.5	70.0 ± 2.1	37.7 ± 1.2	15.4 ± 0.8	7.1 ± 0.6	5.5 ± 0.2	4.3 ± 0.5	70.0 ± 2.1
MD-10d (10d)	39.7 ± 1.9	16.0 ± 0.8	6.9 ± 0.7	5.4 ± 0.1	5.1 ± 0.6	73.0 ± 2.9	37.7 ± 1.3	15.2 ± 1.4	6.2 ± 0.5	5.2 ± 0.7	5.3 ± 0.7	69.5 ± 3.7
1 way Anova (Turkey HSD)												
p: C vs 3d vs 10d	0.768	0.2	0.518	0.867	0.456	0.566	0.933	0.070	0.203	0.814	0.258	0.448
p: C vs 3d	0.761	0.352	0.987	0.856	0.727	0.692	0.997	0.111	0.183	0.811	0.738	0.465
p C vs 10d	0.988	0.228	0.520	0.955	0.424	0.593	0.927	0.130	0.861	0.994	0.563	0.619
p : 3d vs 10d	0.855	0.973	0.659	0.969	0.831	0.991	0.979	0.992	0.444	0.877	0.232	0.963

Abbreviations: MD: monocular deprivation, d: days, Au1: Primary auditory cortex.

Tab. 12: Statistical significance of different types of spines between the hemispheres.

LEnt	Left vs Right (Paired t-test)					
Spine Types	Small	Medium	Large	Mushroom	Spiny	Sum
Control	0.134	0.051	0.159	0.591	0.726	0.015
MD-3d	<0.001	0.007	0.018	0.003	0.018	<0.001
MD-10d	0.172	0.03	0.023	0.002	0.001	0.002
Au1	Left vs Right (Paired t-test)					
Spine Types	Small	Medium	Large	Mushroom	Spiny	Sum
Control	0.538	0.404	0.553	0.390	0.978	0.262
MD-3d	0.184	0.737	0.245	0.627	0.947	0.330
MD-10d	0.428	0.507	0.231	0.739	0.742	0.310

Abbreviations: MD: monocular deprivation, d: days, LEnt: Lateral entorhinal cortex, Au1: Primary auditory cortex.

Tab. 13: Mean number of astrocytic intersections and statistical significance.

LEnt	Left	Right	Left vs Right (Paired t-test)
Control	18.8 ± 0.4	17.7 ± 0.4	0.089
MD-3d	16.1 ± 0.4	18.8 ± 0.3	<0.001
MD-10d	21.4 ± 0.5	18.2 ± 0.5	<0.001
p **(Among the groups) 1 way Anova (Turkey HSD)**	C vs 3d vs 10d : < 0.001 C vs 3d : < 0.001 C vs 10d : < 0.001 3d vs 10d : < 0.001	C vs 3d vs 10d : 0.171 C vs 3d : 0.147 C vs 10d : 0.702 3d vs 10d : 0.523	
Au1	**Left**	**Right**	**Left vs Right (Paired t-test)**
Control	19.3 ± 0.43	20 ± 0.55	0.289
MD-3d	19.1 ± 0.53	19.3 ± 0.6	0.779
MD-10d	19.7 ± 0.65	19.8 ± 0.53	0.863
p **(Among the groups) 1 way Anova (Turkey HSD)**	C vs 3d vs 10d : 0.770 C vs 3d : 0.951 C vs 10d : 0.908 3d vs 10d : 0.752	C vs 3d vs 10d : 0.396 C vs 3d : 0.657 C vs 10d : 0.981 3d vs 10d : 0.787	

Abbreviations: MD: monocular deprivation, d: days, LEnt: Lateral entorhinal cortex, Au1: Primary auditory cortex.

Tab. 14: Number of primary processes of astrocytes and statistical significance.

LEnt	Left	Right	Left vs Right (Paired t-test)
Control	9.1 ± 0.2	9.1 ± 0.3	0.887
MD-3d	9.1 ± 0.3	9.0 ± 0.3	0.773
MD-10d	9.6 ± 0.3	9.3 ± 0.2	0.558
p **(Among the groups) 1 way Anova (Turkey HSD)**	C vs 3d vs 10d : 0.343 C vs 3d : 0.991 C vs 10d : 0.381 3d vs 10d : 0.453	C vs 3d vs 10d : 0.633 C vs 3d : 0.955 C vs 10d : 0.794 3d vs 10d : 0.619	
Au1	**Left**	**Right**	**Left vs Right (Paired t-test)**
Control	8.2 ± 0.3	8.2 ± 0.24	0.897
MD-3d	8.2 ± 0.24	8.1 ± 0.2	0.832
MD-10d	8.4 ± 0.23	8.0 ± 0.22	0.293
p **(Among the groups) 1 way Anova (Turkey HSD)**	C vs 3d vs 10d : 0.824 C vs 3d : 0.990 C vs 10d : 0.889 3d vs 10d : 0.824	C vs 3d vs 10d : 0.899 C vs 3d : 0.987 C vs 10d : 0.893 3d vs 10d : 0.951	

Abbreviations: MD: monocular deprivation, d: days, LEnt: Lateral entorhinal cortex, Au1: Primary auditory cortex.

Tab. 15: Volume of astrocytes and statistical significance.

LEnt	Left	Right	Left vs Right (Paired t-test)
Control	1534.7 ± 65.8	1492.4 ± 21.5	0.861
MD-3d	2305.2 ± 50.2	1483.2 ± 21.1	< 0.001
MD-10d	1706.7 ± 36	1436 ± 47.7	0.001
p (Among the groups) 1 way Anova (Turkey HSD)	C vs 3d vs 10d : < 0.001 C vs 3d : < 0.001 C vs 10d : 0.075 3d vs 10d : < 0.001	C vs 3d vs 10d : 0.516 C vs 3d : 0.985 C vs 10d : 0.560 3d vs 10d : 0.628	
Au1	**Left**	**Right**	**Left vs Right (Paired t-test)**
Control	1132.3 ± 10	1166.4 ± 16.6	0.233
MD-3d	1086.6 ± 30.3	1116.9 ± 18.3	0.833
MD-10d	1084.6 ± 26	1097.6 ± 30	0.722
p (Among the groups) 1 way Anova (Turkey HSD)	C vs 3d vs 10d : 0.461 C vs 3d : 0.526 C vs 10d : 0.478 3d vs 10d : 0.998	C vs 3d vs 10d : 0.194 C vs 3d : 0.383 C vs 10d : 0.175 3d vs 10d : 0.822	

Abbreviations: MD: monocular deprivation, d: days, LEnt: Lateral entorhinal cortex, Au1: Primary auditory cortex.

Tab. 16: Volume of astrocytic soma and statistical significance.

LEnt	Left	Right	Left vs Right (Paired t-test)
Control	330.81 ± 6.31	332.37 ± 5.57	0.544
MD-3d	383.94 ± 16.59	338.54 ± 5.74	0.001
MD-10d	327.20 ± 9.57	348.46 ± 6.88	0.758
***p* (Among the groups) 1 way Anova (Turkey HSD)**	C vs 3d vs 10d : < 0.001 C vs 3d : < 0.001 C vs 10d : 0.559 3d vs 10d : 0.002	C vs 3d vs 10d : 0.195 C vs 3d : 0.775 C vs 10d : 0.169 3d vs 10d : 0.589	
Au1	**Left**	**Right**	**Left vs Right (Paired t-test)**
Control	425.8 ± 11.2	414.94 ± 12.83	0.456
MD-3d	427.4 ± 12.82	433.8 ± 22.04	0.833
MD-10d	426.5 ± 11.31	419.5 ± 22.3	0.666
***p* (Among the groups) 1 way Anova (Turkey HSD)**	C vs 3d vs 10d : 0.995 C vs 3d : < 0.995 C vs 10d : 0.999 3d vs 10d : 0.999	C vs 3d vs 10d : 0.750 C vs 3d : 0.734 C vs 10d : 0.982 3d vs 10d : 0.866	

Abbreviations: MD: monocular deprivation, d: days, LEnt: Lateral entorhinal cortex, Au1: Primary auditory cortex.

Tab. 17: Density of Arc$^+$ cells and statistical significance.

LEnt	Left	Right	Left vs Right (Paired t-test)
Control	90454.5 ± 5409.1	90235.7 ± 5055.6	0.391
MD-3d	114520.2 ± 2717.3	98021.9 ± 5243.5	0.036
MD-10d	93013.5 ± 4352.3	85858.6 ± 2996.4	0.034
***p* (Among the groups) 1 way Anova (Turkey HSD)**	C vs 3d vs 10d : 0.007 C vs 3d : 0.007 C vs 10d : 0.928 3d vs 10d : 0.031	C vs 3d vs 10d : 0.303 C vs 3d : 0.502 C vs 10d : 0.818 3d vs 10d : 0.292	
Au1	**Left**	**Right**	**Left vs Right (Paired t-test)**
Control	139671.7 ± 7166.2	139494.9 ± 6934.2	0.973
MD-3d	139343.4 ± 10437	143139.7 ± 11346.9	0.237
MD-10d	142382.1 ± 10382.5	136363.6 ± 10159.8	0.501
***p* (Among the groups) 1 way Anova (Turkey HSD)**	C vs 3d vs 10d : 0.970 C vs 3d : 1 C vs 10d : 0.973 3d vs 10d : 0.975	C vs 3d vs 10d : 0.891 C vs 3d : 0.955 C vs 10d : 0.967 3d vs 10d : 0.881	

Abbreviations: MD: monocular deprivation, d: days, LEnt: Lateral entorhinal cortex, Au1: Primary auditory cortex.

Tab. 18: List of chemicals.

Chemicals	Cat #	Company
Bovine serum albumin	11930.03	SERVA, Germany
DAB Tablet	D-4293	Sigma, USA, Germany
Gelatine	1.040780500	Merck, Germany
Entellen	1.07961.0100	Merck, Germany
HCL	H1758	Sigma, USA
H_2O_2 Tablet	U-1380	Sigma, USA
30% H_2O_2	1.07209.0250	Merck, Germany
KCl	1049361000	Merck, Germany
KH_2PO_4	1.04873.1000	Merck, Germany
Milk powder	T145.2	Roth, Germany
NaCl	3957.1	Roth, Germany
Normal donkey serum	S30-100ML	Chemicon, USA
$Na_3C_6H_5O_7$	71404-250G	Sigma, USA
PFA	16005	Riedel de Häen, Germany
Tris-hydrochlorid	9090.3	Roth, Germany
Tris-Ultra	5429.3	Roth, Germany
Triton X-100	T9284	Sigma, USA
Tween 20	9127.1	Roth, Germany

Tab. 19: Kits used for staining

Kit	Cat #	Company
FD Rapid Golgi Stain™	PK401	FD Neurotechnologies, USA
Vectastain Elite ABC-Kit	PK-6100	Vectorlab, USA

Abbreviations: ABC: Avidin-Biotin-Peroxidase-complex.

List of Figures

List of Tables

87

Curriculum Vitae

Personal Information

Name: Sidra Gull

Date of Birth: 22.03.1983

Nationality: Pakistani

Education

2011-2015	PhD: Neurosciences Hans Berger Department of Neurology, Jena University Hospital, Jena, Germany.
2006-2008	MS: Biotechnology University of the Punjab, Lahore, Pakistan.
2002-2006	B.Sc (Hons): Biotechnology University of the Punjab, Lahore, Pakistan.

Research Experience

2011-2015	Doctrol Research Fellow Hans Berger Department of Neurology, Jena University Hospital, Jena, Germany.
2009-2010	Research Associate Shaukat Khanum Memorial Cancer Hospital and Research Center-Lahore Pakistan.
2007	Research Student Shaukat Khanum Memorial Cancer Hospital and Research Center-Lahore Pakistan.

Poster Presentation

- Gull S., Schmidt S., Herrmann K. H., Reichenbach J., Gaser C. and Witte O.W. Experience-dependent structural plasticity in in entorhinal cortex following monocular deprivation the adult rat brain. Presented at: Society for

Neuroscience (SFN); 2014 November 15-19; Washington D.C., United States.

- Schmidt S., Gull S., Reichenbach J., Gaser C. and Witte O.W. Experience-dependent structural plasticity in the adult rat brain. Presented at: 30th International Congress on Clinical Neurophysiology (ICCN) of the IFCN; 2014 March 19-23; Berlin, Germany

Publications and Conference Papers

Publications

- **<u>Gull S.</u>**, Ingrisch I., Tausch S., Witte O. W., Schmidt S. Consistent and reproducible staining of glia by a modified Golgi-Cox method. (2015) J Neurosci Methods.

- Rashid M. U., **<u>Gull S.</u>**, Asghar K., Muhammad N., Amin A., Hamann U. Prevalence of *TP53* germ line mutations in young Pakistani breast cancer patients. (2012) Fam Cancer. Pg: 307-3011.

- Rashid M. U., **<u>Gull S</u>**, Faisal S., Khaliq S., Asghar K., Siddiqui N., Amin A., Hamann U. Identification of the deleterious 2080insA BRCA1 mutation in a male renal cell carcinoma patient from a family with multiple cancer diagnoses from Pakistan. (2011) Fam Cancer. Pg: 709-712.

Conference Paper

- Schmidt S., **<u>Gull S</u>**., Reichenbach J., Gaser C. and Witte O.W. Experience-dependent structural plasticity in the adult rat brain. Volume 125, Supplement 1, June 2014, Pages S230-S231 DOI: 10.1016/S1388-2457(14) 50755-9 (IF: 3.144).

Acknowledgement

Firstly I would like to thank Almighty God for giving me an opportunity to work on this project and then for giving me strenghts to fulfill my responsibilities and achieve the aims of this work.

I am exceedingly thankful to Prof. Dr. Otto W. Witte for appointing me to work on this interesting project and for providing me excellent working conditions. I am also very grateful to him for the patience he showed me as well as for the time he spared for the innumerable discussions and for his continuous interest in the progress of my work. His insightful comments and encouragement gave me incentive to widen my research and look at it from various perspectives. Lastly, his ongoing guidance helped me during my time in his lab and during the writing of this thesis. I would also like to express my sincere gratitude to Dr. Silvio Schmidt for his patience, motivation, continual guidance and support during the planning and performing of the experimental work, data analysis, preparation of results and thesis writing. I could not have imagined having better advisors and mentors for my Ph.D work.

I am deeply thankful to Prof. Dr. Regine Heller for her helpful suggestions, and moral support as well as for all her efforts towards including me in social activities and for providing me with a wonderful time outside the laboratory.

I furthermore would like to thank all technical assistants in the "Department of Neurology" especially Ina Ingrisch for her constant and valuable support.

I thank my fellow labmates for the stimulating discussions and support in experimental work especially Dr. Anja Urbach, Dr. Knut Kirmse, Dr. Christian Schmeer, Anne Ansorg, Katja Krempler and Iwa Antonow. In particular, I thank Marcus Böhme for his invaluable support during the many years in which we worked, discussed and also had some fun. I am also thankful to Nasim Kroegel, our project manager for her support with regard to administrative matters during my time in the Department. I am also grateful for her help with language editing. .

I also thank my friends Ndirem, Manmeet, Quratul Ain, Seerat, Varunika, Amama, Fatima and Henna for the wonderful time we spent together during the last five years.

Last but not the least, I would like to give special thanks to my family in particular my parents, my siblings and my husband for supporting me spiritually throughout my research and my life in general.

Ehrenwörtliche Erklärung

Hiermit erkläre ich, dass mir die Promotionsordnung der Medizinischen Fakultät der Friedrich-Schiller-Universität bekannt ist,

ich die Dissertation selbst angefertigt habe und alle von mir benutzten Hilfsmittel, persönlichen Mitteilungen und Quellen in meiner Arbeit angegeben sind,

mich folgende Personen bei der Auswahl und Auswertung des Materials sowie bei der

Herstellung des Manuskripts unterstützt haben: Dr. Silvio Schmidt, Prof. Dr. Otto W. Witte

die Hilfe eines Promotionsberaters nicht in Anspruch genommen wurde und dass Dritte weder unmittelbar noch mittelbar geldwerte Leistungen von mir für Arbeiten erhalten haben, die im Zusammenhang mit dem Inhalt der vorgelegten Dissertation stehen,

dass ich die Dissertation noch nicht als Prüfungsarbeit für eine staatliche oder andere

wissenschaftliche Prüfung eingereicht habe und

dass ich die gleiche, eine in wesentlichen Teilen ähnliche oder eine andere Abhandlung nicht

bei einer anderen Hochschule als Dissertation eingereicht habe.

Jena, den 28.04.2016 _____

Sidra Gull